1-1-2015

On The Nature Of Excited States In Ruthenium Complexes: Towards Renewable Energy

Ryan A. Thomas
Wayne State University,

ON THE NATURE OF EXCITED STATES IN RUTHENIUM COMPLEXES: TOWARDS RENEWABLE ENERGY

by

RYAN ANTONIO THOMAS

DISSERTATION

Submitted to the Graduate School

of Wayne State University,

Detroit, Michigan

in partial fulfillment of the requirements

for the degree of

DOCTOR OF PHILOSOPHY

2015

MAJOR: CHEMISTRY (Analytical)

Approved by:

_____

Advisor Date

_____

Advisor Date

_____

_____

_____

DEDICATION

My dissertation is dedicated to Mason, Toni and Mom

ACKNOWLEDGMENTS

My deepest gratitude goes to Professor John F. Endicott for his encouragement, guidance and patience through this process. I also would like to thank Professor Cláudio N. Verani for his generosity and continuous support.

Thanks to current and past Endicott lab members Professor Yuan-Jang Chen, Marco Allard, Rick Van Camp and Marim Alnaed for helping to create a pleasurable lab experience. Additional thanks to the current Verani lab members Debashis Basu, Habib Baydoun, Danushka Ekanayake, Pavithra Kankanamalage, Sunalee Gonawala, Kenneth Kpogo and Brittany Venglarcik for their kind attention during group meetings and useful suggestions.

I am grateful for my graduate committee members, Professor H. Bernhard Schlegel, Professor Parastoo Hashemi and Professor Christopher Kelly for their precious time and comments.

A special thanks goes to my family, specifically my wife Toni for her extreme patience and motivation, Madeline for her help and understanding, my mother Tracy for her wisdom, guidance and inspiration and my son Mason for making the inevitable obstacles worth overcoming.

TABLE OF CONTENTS

LIST OF TABLES

LIST OF FIGURES

CHAPTER I: Introduction

Numerous issues are associated with the current societal dependency on fossil fuels.[1] From environmental thermal degradation to the inevitable depletion of resources, the concerns on meeting global energy demand has gained the attention of scientists for many years. As a result, alternative and renewable energy sources have emerged as top contenders to address the energy crisis. Of all of the renewable energy sources, solar energy conversion is the most abundant being from the radiation of the sun. The basic science behind the conversion of solar radiation into useable sources is non-trivial. Furthermore, the solar radiation conversion needs to be maximized for more efficiency from the process.

Intramolecular (within a molecule) excited state electron transfer reactions of transition metal complexes are often useful for solar energy conversion processes.[1-5] For these complexes to be efficient for photo-processes, it is important to know the nature of the lowest energy excited states (such as ^{3}MLCT-metal-to-ligand charge-transfer and/or ^{3}MC-metal centered) and their physical properties since the properties of these states generally determine the overall electron transfer reactivity. The general characteristics of excited states change among different complexes as a result of differences in ground state and excited state molecular structures, the energies of the excited states and configurational mixing between MLCT excited states with other close in energy excited states.[6-8] Such information is particularly difficult to obtain for multi-metallic systems. Thus, the most reasonable approach in developing a multi-metallic system that may be useful for solar energy conversion is to study and define the properties of the individual mono-metallic complexes. This dissertation is focused on understanding the photosensitizer module.

Ruthenium-polypyridyl complexes are among the most attractive photosensitizer due to strong visible molar absorptivities in their ground state, relatively long-lived excited states at room temperature and relative ease of synthetic inclusion into multi-metallic systems. Electron transfer rates are functions of structural, molecular energy and solvational differences between reactants and products.[9-11] The parameters that govern electron transfer rates are often difficult to determine since the lifetime for some excited states of transition metal complexes are extremely short (ns to fs regime) and cannot be accurately determined by standard methodology used for molecular ground states. Due to such difficulty, it is generally assumed is that the reaction proceeds from the lowest energy excited state. Some indirect methods for characterizing excited state structures are vibronic sideband analysis based on low temperature emission spectra,[12] resonance Raman spectra,[13] density functional theory (DFT) modeling[14] and excited state x-ray structures.[15] The efficiency of transition metal complexes as photosensitizers depend on the lowest energy excited states and their corresponding lifetimes.[16] The excited state lifetime depends on the rate constants of the available relaxation channels and may be expressed as,

$$\tau_{obsd} = \left(\sum_{n} k_n \right)^{-1} = \left(k_{obsd} \right)^{-1} \qquad (1)$$

where τ_{obsd} is the observed lifetime of the excited state, k_n are the rate constants for n processes and k_{obsd} is the observed decay rate constant of the excited state. The general relaxation channels are: 1) intersystem crossing between excited states of different spin multiplicity, k_{ISC}, 2) internal conversion between excited states of the same spin multiplicity, k_{IC}, 3) non-radiative channels, k_{NRD} and 4) the radiative relaxation channel, k_{RAD}.[17] The excited state will usually decay through an emission that is characteristic of the chromophore when all other relaxation channels that are

not radiative are blocked. The rate of radiative relaxation dictates the maximum possible excited state lifetime.

It is conceptually convenient to view the properties of electronic excited states for ruthenium-polypyridyl systems as donor (D)-acceptor (A) systems, respectively. Initially the D and A are isolated in both the ground and charge transfer excited states,

$$\{DA\}^{6\text{-}8,\,12} + h\nu \rightarrow {}^{*}\{D^{+},A^{-}\} \qquad (2)$$

If the mixing between D and A is negligible and there are only two possible electronic configurations, then the properties of the excited state may be treated in terms of minor deviations from the properties of the isolated system.[18-20] Conversely, recent work from our group that combined spectroscopic determinations and DFT suggests several excited state properties of ruthenium-polypyridyl (donor-acceptor) systems that deviate from the electronically isolated models.[6-8, 14, 21] This deviation from simple limiting models arises due to the small energy differences between excited states in heavy metal complexes. This energy difference between excited states can arise from: 1) differences in molecular structures and electronic configurations, 2) various molecular excited state relaxation pathways and 3) internal conversion among the excited states.[16]

General Background

In the early 1950's, Mulliken[22-24] pioneered the elucidation of spectroscopic and thermodynamic characteristics of donor/acceptor interactions. In the mid-1950's Marcus[10, 25] began developing a theory for the rates of electron transfer reactions of donor/acceptor complexes. Originally the "Classical Marcus Theory" was describing outer-sphere electron

transfer (through-space) but was later extended to inner-sphere electron transfer (through-bond) by Hush[26].

The limits on the magnitudes of electronic coupling between donor and acceptor systems can be revealed by spectroscopic and electrochemical observations. The "simple" approach developed by Mulliken that deals with donor/acceptor pairs can be described by two states: Ψ_D and Ψ_A. The ground (Ψ_G) and excited (Ψ_E) state wave functions and mixing coefficient (α) can be represented as,[27]

$$\Psi_G = (\Psi_D + \alpha \Psi_A)N^2 \quad (3)$$

$$\Psi_E = (\alpha \Psi_D + \Psi_A)N^2 \quad (4)$$

where N is a normalizing factor for the each state.

Three limiting cases based on the Mulliken approach are:

a) Donor-Acceptor Coupling
b) Two-State Donor-Acceptor Charge Transfer (DACT)
c) Donor Acceptor Systems with Electronic Coupling between the DACT state and other CT state

The last limiting case described will be discussed more in detail in Part B of the discussion.

CHAPTER II: Experimental

A. Starting Materials

The following commercial chemicals were purchased from Sigma Aldrich and used without further purification: 1,4,7,10-tetrathiacyclododecane ([12]aneS_4), 1,4,8,11-tetrathiacyclotetradecane ([14]aneS_4); 1,4,7-trithiacyclononae ([9]aneS_3); 2,2'-bipyridine; 4,4'-dimethoxy-2,2'-bipyridine; 4,4'-dimethyl-2,2'-bipyridine; Ammonium hexafluorophosphate; Tetrakis(dimethylsulfoxide)dichlororuthenium(II) (or synthesized in the lab). Ruthenium (III) chloride hydrate was purchased from Oakwood Chemical. [Ru(bpy)(Cl_4)] and [Ru([9]aneS3)(DMSO)Cl_2] were synthesized from a literature procedures.[28-29] The cyclo-6,6'-[1,9-(2,5,8-trithianonane)]-2,2'-bipyridine ([15]deneS_3bpy) ligand was previously synthesized and supplied to us by Professor David B. Rorabacher. Butyronitrile (≥99%) was purchased from Sigma Aldrich, Ethanol (≥99%) was purchased from Decon, and Methanol (≥99%) was purchased from Fisher Scientific for spectroscopic experiments.

B. Syntheses

Syntheses were done under an Ar atmosphere using a schlenk line setup in the dark. Purification of the compounds was performed by recrystallization, vapor diffusion and/or column chromatography (Al_2O_3) techniques.

[Ru(DMSO)Cl(L)][PF_6][30]

A mixture of [Ru(DMSO)$_4Cl_2$] (.487g, 1.0 mmol) and 1,4,8,11- tetrathiacyclotetradecane (L) (.268g, 1.0 mmol) were dissolved in ethanol/water (1:1, 20mL). The solution was brought to reflux for 4 h. The mixture was cooled to room temperature and excess solid NH_4PF_6 was added.

The mixture was left overnight at 0-2°C. The precipitate was washed with water and then ethanol. It was dried in vacuo.

^{1}H NMR, ppm ([d^6] acetone, 400 MHz): 3.60–2.05 (m, 26H).

[Ru(L)(bpy)][PF_6]$_2$ [30]

A solution of Ru(DMSO)Cl(L)]PF_6 (0.3g, 0.4775 mmol) was prepared in ethanol/water (1:1, 20 mL). $AgNO_3$ (0.103mg, 1.3equiv) was added to the solution and the mixture was left at reflux for 4h. After removal of AgCl via gravity filtration, an ethanol solution of excess 2,2'-bipyridine (.118 g, 1.6 equiv) was slowly added to the mixture and was then brought to reflux for an additional 24 h. After cooling to room temperature, excess solid NH_4PF_6 was added to the mixture. The volume of the solution was reduced under vacuum and left overnight at 0-2°C. The precipitate was washed with ethanol, diethyl ether, and then dried in vacuo.

^{1}H NMR, ppm ([d^6] acetone, 400 MHz): bpy protons = 9.59 (s, H), 9.09 (s, 2H), 8.87 (ddd, 2H), 8.40 (s, 2H), 7.90 (s, 2H); [14]aneS_4 protons δ = 4.00 (s, CH_2), 3.87 (s, CH_2), 3.77 (s, CH_2), 3.61 (obscured, CH_2), 3.47 (obscured, CH_2), 3.30 (obscured, CH_2), 3.25 (obscured, CH_2), 2.51 (obscured, CH_2), 2.28 (obscured, CH_2), 2.21 (obscured, CH_2).

[Ru([14]aneS_4)(modified-bpy) or (phen)][PF_6]$_2$

The synthesis of the modified bipyridine or phenanthroline complexes follow the same procedures above with the inclusion of the modified bipyridine or phenanthroline instead of bipyridine.

$[Ru(S(CH_3)_2)_4(bpy)]^{2+}$

Multiple attempts were made to synthesize and purify $[Ru(S(CH_3)_2)_4(bpy)]^{2+}$. General procedures attempted were using $[Ru(bpy)Cl_4]^{m+}$ (in minimum water) and dimethyl sulfide (as the solvent) under both refluxing and non-refluxing conditions. Zinc granules were employed to reduce $[Ru(bpy)Cl_4]^{3 \text{ or } 4+}$ to $[Ru(bpy)Cl_4]^{2+}$. An alternative approach attempted used $RuCl_3$-trihydrate and dimethyl sulfide (as the solvent) under refluxing conditions to yield $[Ru(S(CH_3)_2)_4(Cl)_2]$. Bipyridine was added with $[Ru(S(CH_3)_2)_4(Cl)_2]$ under refluxing and non-refluxing conditions. All approaches for the synthetic preparation of $[Ru(S(CH_3)_2)_4(bpy)]^{2+}$ resulted in an impure compound. Recrystallization and/or basic Al_2O_3 column chromatography was performed with a toluene:acetonitrile mix. In all cases the efforts towards purifying the compound led to a more impure compound based on ^1H NMR and cyclic voltammetry. This compound proved to be unstable (denoted by a color change from red to green when left open to air).

$[Ru(MeCN)_4(bpy)][PF_6]_2$

A solution of $[Ru(bpy)(Cl_4)]$ (0.406 g, 1.02 mmol) was prepared in acetonitrile/water (1:2, 30 mL). Added to the solution was zinc granules (1g) for reduction and the mixture was left at reflux for 1h at 60ºC. The temperature was decreased to 40 ºC and stirred overnight. After removal of Zn(s) via gravity filtration and cooling to room temperature, excess solid NH_4PF_6 was added to the mixture. The volume of the solution was reduced under vacuum and left overnight at 0-2°C. The precipitate was washed acetonitrile/water then dried in vacuo.

^1H NMR: ppm ([d^6] DMSO, 400 MHz): 9.15 (d, 2H), 8.70 (d, 2H), 8.27 (t, 2H), 7.78 (t, 2H), 2.77 (s, 6H), 2.31 (s, 6H).

[Ru([9]aneS$_3$)(bpy)Cl][Cl] or [PF$_6$][29]

[Ru([9]aneS$_3$)(DMSO)Cl$_2$] (0.1684 g, 0.391 mmol) was added to a 3.5% excess of 2,2'-bipyridine (63.2 mg, .405 mmol) in 10mL of ethanol. The yellow mixture was refluxed for 20 min at 80ºC and an orange/red solution resulted. The solution was concentrated to dryness via rotovap and redissolved in ethanol/water. Upon standing, orange or red crystals were obtained.

^{1}H NMR, ppm (D$_2$O, 400 MHz): 8.97 (d, 2H), 8.33 (d, 2H), 8.02 (t, 2H), 7.51 (t, 2H)-(8H, bpy), 2.92 - 2.28m (12H, [9]aneS$_3$).

To obtain the same compound with PF$_6$ as the counterion, instead of letting the solution sit and precipitate out, 0.250 g of NH$_4$PF$_6$ in 5 mL water is dropwise added to the solution until saturation. Then the solution was rotovaped to ~ 2 mL and refrigerated overnight and recovered as orange-red precipitate.

^{1}H NMR, ppm ([d^6] DMSO, 400 MHz): 8.99 (d, 2H), 8.68 (d, 2H), 8.15 (t, 2H), 8.63 (t, 2H)-(8H, bpy), 2.87 - 2.63m (12H, [9]aneS$_3$).

[Ru([9]aneS$_3$)(bpy)MeCN][PF$_6$]$_2$[31]

[Ru([9]aneS$_3$)(bpy)Cl]Cl (79.2 mg, 0.156 mmol) and excess AgPF$_6$ (0.2764 g, 1.1 mmol) were mixed in acetonitrile and heated at reflux for 2 h. A color change from orange to yellow was noted. AgCl was filtered off via hot gravity filtration. The filtrate was concentrated by rotovap. The solid obtained was filtered and washed with cold distilled water.

^{1}H NMR, ppm ([d^6] DMSO, 400 MHz): 8.98 (d, 2H), 8.78 (d, 2H), 8.29t (2H), 7.74t (2H)-(8H, bpy), 2.97 - 2.55m (12H, [9]aneS$_3$), 2.26s (3H, acetonitrile)

[Ru([9]aneS$_3$)(bpy)CN][PF$_6$]^2

[Ru([9]aneS$_3$)(bpy)Cl]PF$_6$ (39.4 mg, 0.064 mmol) and excess KCN (5.0 mg, 0.768 mmol) were mixed in methanol and heated at reflux for 18h. The solution was cooled to room temperature and 0.250 g of NH_4PF_6 in 5 mL water is dropwise added to the solution until saturation. Then the solution was rotovaped to ~ 2 mL and the yellow precipitate was filtered off washed with diethyl ether. A basic Al_2O_3 column was performed with a toluene:acetonitrile mix.

^{1}H NMR, ppm ([d^6] DMSO, 400 MHz): 8.85,8.83 d (2H), 8.71, 8.69d (2H), 8.18t (2H), 7.64 (t, 2H)-(8H, bpy), 2.90 - 2.63m (12H, [9]aneS$_3$).

[Ru([15]dieneS$_3$bpy)Cl][Cl] or [PF$_6$]

[Ru(DMSO)$_4$Cl$_2$] (80.5 mg, 0.166 mmol) and [15]dieneS$_3$bpy (55.2 mg, 0.165 mmol) were mixed in 10 mL of ethanol. The yellow solution was heated at reflux for 20 mins at 80 and an orange/red solution resulted. The solution was concentrated to dryness via rotovap and redissolved in ethanol/water. Upon standing, orange or red crystals were obtained.

To obtain the same compound with PF_6 as the counterion, instead of letting the solution sit and precipitate out, 0.250 g of NH_4PF_6 in 5 mL water is dropwise added to the solution until saturation. Then the solution was rotovaped to ~ 2 mL and refrigerated overnight and recovered as orange-red precipitate.

^{1}H NMR, ppm ([d^6] DMSO, 400 MHz): 8.54 (d ,2H), 8.07 (d, 2H), 7.87 (d, 2H), 4.83 (q, 4H), 2.98 - 2.79 m (8H).

[Ru([15]dieneS$_3$bpy)MeCN][PF$_6$]$_2$

[Ru([15]dieneS$_3$bpy)Cl][PF$_6$] (0.1054 g, 0.171 mmol) and excess $AgNO_3$ (58 mg, 0.341 mmol) were mixed in acetonitrile and heated at reflux for 18 h. A color change from orange to yellow was noted. AgCl was filtered off via hot gravity filtration. 0.1075 g of NH_4PF_6 was added in 3 mL of distilled water to the filtrate which was concentrated by rotovap. The solid obtained was filtered and washed with cold distilled water.

^{1}H NMR, ppm ([d^6] DMSO, 400 MHz): 8.63 (d, 2H), 8.22 (d, 2H), 8.00 (d, 2H), 5.06 (q, 4H) 3.12 - 2.87 m (12H), 2.28 (s, 3H, acetonitrile)

[Ru([15]dieneS$_3$bpy)CN][PF$_6$]

[Ru([15]dieneS$_3$bpy)Cl]PF$_6$ (0.1305 g, 0.258 mmol) and excess KCN (21 mg, 0.309 mmol) were mixed in methanol and heated at reflux for 18h. The solution was cooled to room temperature and 0.250 g of NH_4PF_6 in 5 mL water is dropwise added to the solution until saturation. Then the solution was rotovaped to ~ 2 mL and the yellow precipitate was filtered off washed with diethyl ether.

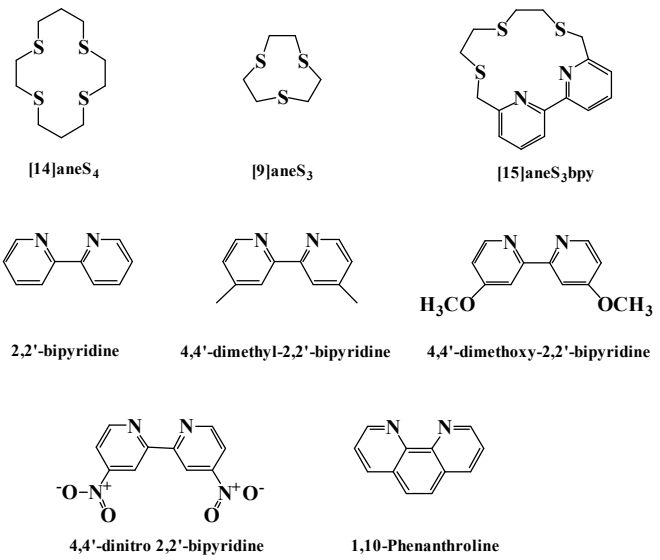

Figure 1: Macrocyclic and Polypyridyl Skeletal Structures

C. Proton Nuclear Magnetic Resonance Spectroscopy (^{1}H NMR)

^{1}H NMR spectra were collected for structural characterization using an Oxford 400 MHz magnet fitted with a default Varian 1H/19F/13C/31P PFG AutoSwitchable 5mm,VT (-20°C to +80°C) probe located in the Lumigen Instrumentation Center at Wayne State University. All spectra shown are from experiments performed at ambient temperature. Samples were dissolved in deuterated solvents (acetone (CD_6CO), acetonitrile (CD_3CN), dimethylsulfoxide (CD_6SO) and water (D_2O)). The peaks shaded yellow on the spectra is indicative of the deuterated solvent and/or water resonances present in the deuterated solvent. Most of the spectra can be separated by upfield (0.0 – 4.0 ppm) and downfield (7.0 – 10.0 ppm) chemical shifts. Typically the resonances found upfield are due to aliphatic protons of the macrocyclic rings and downfield are from the bipyridine (bpy) or phenanthroline (phen) ligands. Compounds were analyzed further if the integrated ratio between the bpy (or phen) and macrocyclic protons matched the expected ratio of a pure complex.

D. Electrochemistry

Electrochemical measurements were performed using dry acetonitrile and tetrabutylammonium hexaflurophosphate electrolyte and a BAS 100B electrochemical system. Cyclic voltammograms (CV) were obtained using a three-electrode system consisting of Ag/AgCl reference electrode, a Pt wire counter electrode, and a Pt disk working electrode. Solutions were purged with argon prior to each run and blanketed with argon during the experiment. The concentration of the supporting electrolyte was 0.1M Bu_4NPF_6. Typical sample concentrations range from 10^{-3} – 10^{-4} M. The working electrode was polished with 1μM diamond polish on a Buehler polishing cloth between series of scans. A scan rate of 150 mV/s was used unless otherwise noted. All measurements are started from zero and sweep in the

negative direction. Half-wave potentials were internally referenced to ferrocene (0.437 V). Replicate determinations average mean error was < 30 mV.

E. Absorption Spectroscopy

Routine 298 K absorption spectra in acetonitrile solutions were determined with a Shimadzu UV-2101PC spectrophotometer. Absorption spectra in 298 K and 90 K butyronitrile and alcohol (v/v' = 4/1 of ethanol/methanol) solution and glasses were also determined using a an Oriel Model 6045 calibrated Xe pen lamp emission lines for wavelength calibration and NIST traceable Oriel model 63966 Quartz Tungsten Halogen (QTH) lamp for intensity. The low temperature absorption spectra were collected using an Oxford Instruments OptistatCF Static Exchange Gas Continuous Flow Cryostat with liquid nitrogen as the cryogen was used at 90 K with NSG Precision Cells, Inc. cryogenic square 1 cm quartz cuvettes with an ANDOR Shamrock 500 spectrometer. The spectrometer was equipped with three gratings: 150 l/mm, 800 nm blaze; 300 l/mm, 500 nm blaze; and 300 l/mm, 1200 nm. ANDOR Newton DU920-BV CCD detector was employed for visible spectral detection with a useful range from 385 - 900 nm. Light was captured with 1” plano-convex optic and focused to an ANDOR SR500i F/# matcher by a Thorlabs 3 mm Core Liquid Light Guide LLG0338-4 (wavelength range 340 – 800 nm). The F/# matcher was constructed to match the optics of the ANDOR SR500i and has a F/# of 6.5, numerical aperture (NA) of 0.077, acceptance angle of 8.8º and 2.9 magnification. Using the liquid light guide and detector together resulted in a limit of 395 nm for the shortest wavelength spectral detection. The temperature was controlled by an Oxford Instruments Intelligent Temperature Controller (ITC) 503S. Temperature was gradually decreased from ambient temperature to 90 K to prevent the quartz cuvette from fracturing and solvent-glass cracking. The

cryostat requires two pumps: 1) Roughing pump (1 x 10^{-4} torr) for the inner vacuum chamber (IVC) and 2) Turbo-pump (10^{-3} – 10^{-5} mbar) for the outer vacuum chamber. The outer vacuum chamber is continuously pumped during the experiments for temperature stability. Sample concentrations were in the 10^{-4} - 10^{-5} M range.

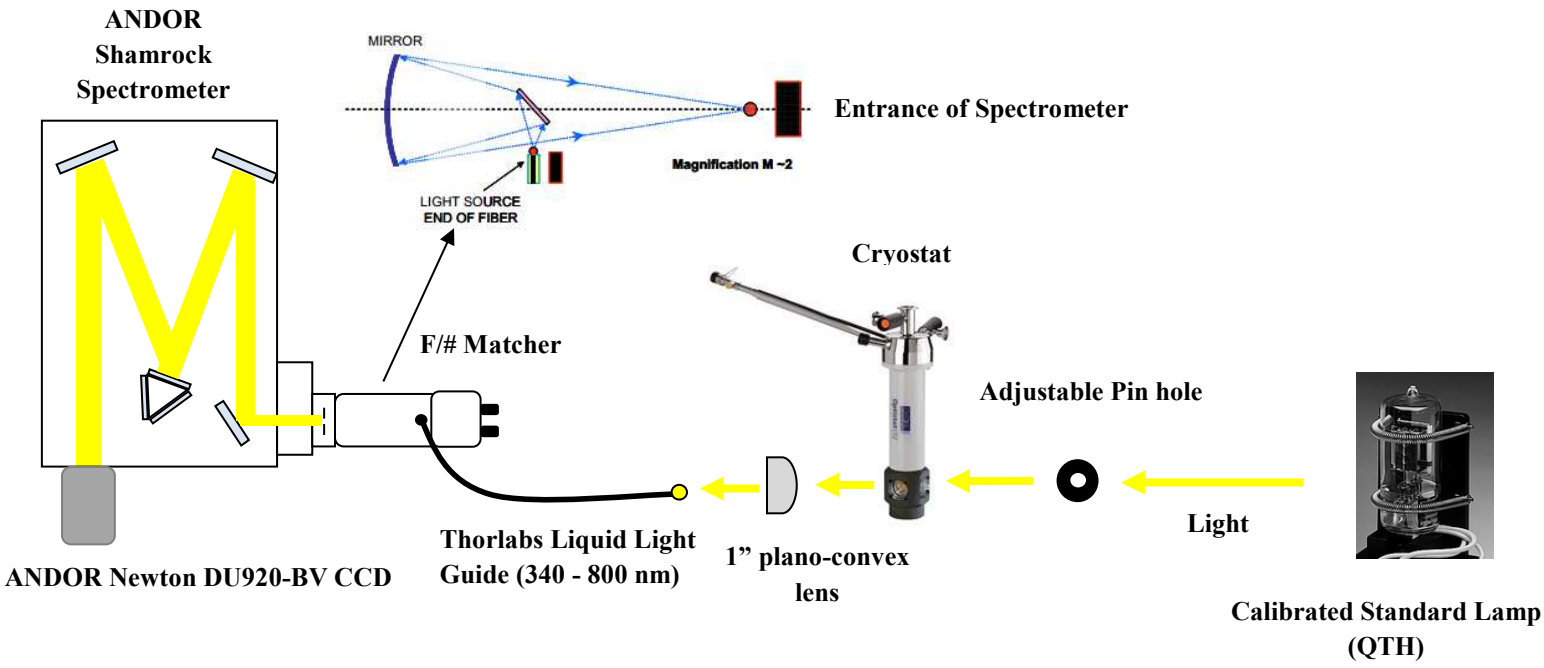

Figure 2: 90 K Absorption Spectroscopy Setup

F. Emission Spectroscopy and Lifetime Measurements

The 77 K emission spectra were determined using the same spectrometer, F/# matcher, detector and wavelength calibration as described in the "Absorption Spectroscopy" section. Light was captured with an optic and transmitted by means of an Oriel 3 mm Core Liquid Light Guide 77634 (wavelength range 420 – 2000 nm). Samples were irradiated in their MLCT absorption bands using 405 nm (50 mW, Power Technologies, Inc), 470 nm (5 mW, Changchun Industries Optoelectronics Tech Co. Ltd.) and 532 nm (50 mW, Changchun Industries Optoelectronics Tech Co. Ltd.) continuous wave diode laser modules. The 77 K emission samples were prepared in 2 mm i.d. cylindrical quartz cells in the dark with butyronitrile or alcohol (v/v' = 4/1 of ethanol/methanol) solvent and then immersed in a quartz dewar filled with liquid nitrogen. The sample cell and Dewar were optimized for each experiment to optimize the emissive signal. Excitation cut-off filters were used to minimize scattered light from the laser. Spectra was collected using Andor Solis software operated in step-and-glue mode. The calibrated spectral emission amplitudes were obtained in units of photons/second in order to properly assess emission bandshapes. The Oriel QTH lamps are in units of irradiance or (mW/m^2 nm). Power (W) is energy per unit time: W = E/s. Energy = (number of photons, N_p)(energy per photon). Energy per photon is equal to hν. Therefore, spectral irradiance (SI) is equal to $(N_p \times h\nu/s) \cdot m^{-2} \cdot nm^{-1}$; $nm^{-1} \propto h\nu$. The area of the detector is constant (m^2). To finally obtain the intensity in photons/second the calibration formula was mulitplied by the square of the emission wavelength $(\lambda em)^2$.

Emission lifetimes were determined using Spectra Physics 337205-00 nitrogen laser-pumped dye laser system for excitation and a Jobin-Yvon H-10 spectrometer for detection with PMT output digitized using a PC with a National Instruments NI PCI-5154, 2 GS/s, 1 GHz

digitizer with 8 MB/ch onboard memory PC card. Sample concentrations were in the 10^{-4} - 10^{-5} M range.

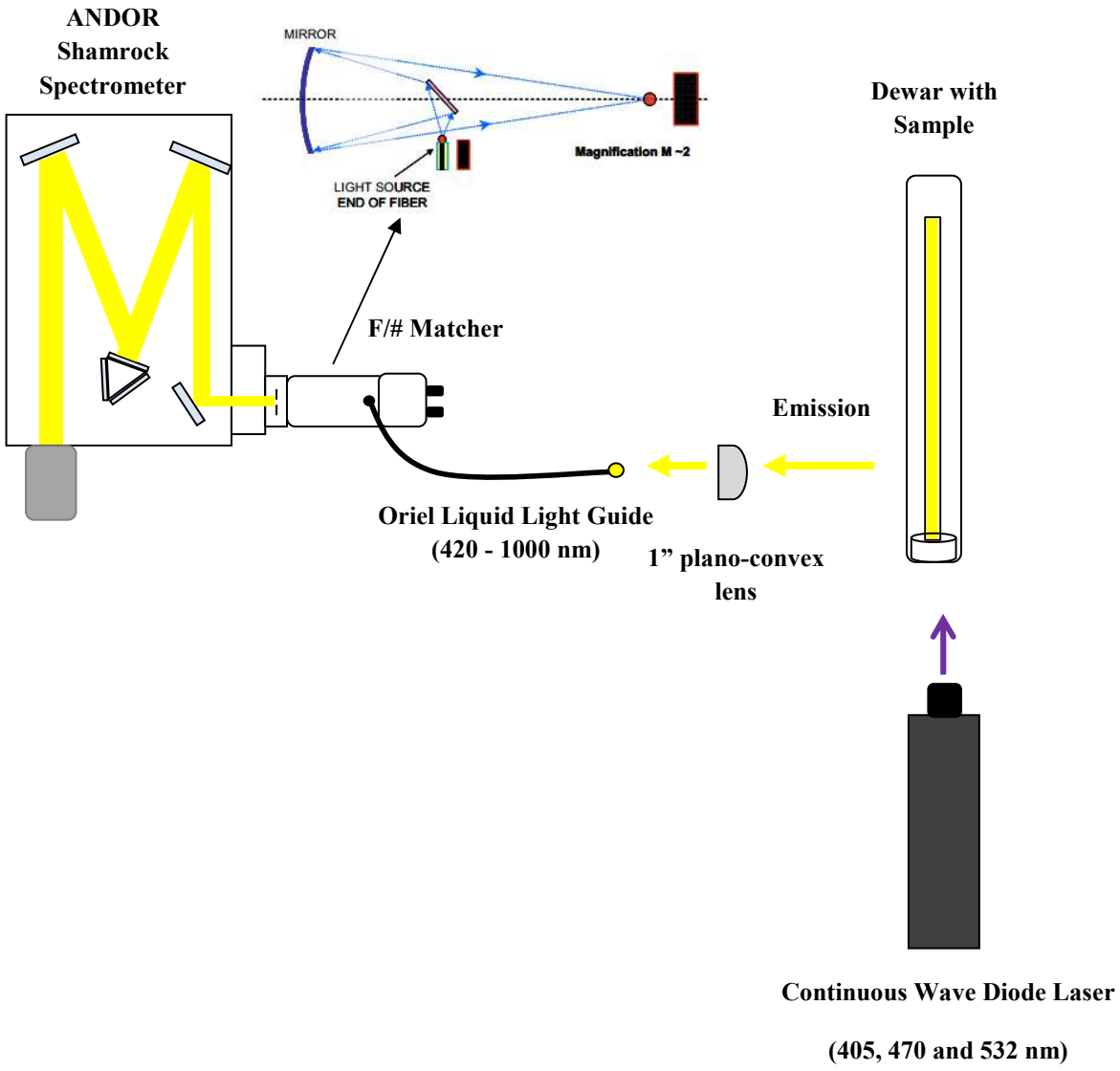

Figure 3: 77 K Emission Spectroscopy Setup

G. Quantum Yield and Radiative Rate Constant Procedures

Low-temperature relative emission quantum yields were determined using $[Ru(bpy)_3]^{2+}$ in 77 K with butyronitrile or alcohol (v/v' = 4/1 of ethanol/methanol) with an emission quantum yield of $\Phi_r = 0.45$ and 0.376 (±0.036)[32], respectively as the reference in this study. Equation 3 was used to calculate the relative quantum yield of the target sample complexes (Φ_s)[32]

$$\frac{\Phi_S}{\Phi_R} = \frac{I_S}{I_R}\frac{1-10^{-A_R}}{1-10^{-A_S}}\frac{\eta_S^2}{\eta_R^2} \qquad (3)$$

where I_S and I_R are the integrated areas of the emission spectral curves of the sample complex and the reference, respectively, A_S and A_R are the absorbances at the excitation wavelength, and η is the refractive index of the solvent system. When the solvent is the same for the reference and the target sample then $\eta_s^2/\ \eta_r^2 = 1$. Mean experimental error of replicate measurements for quantum yield was found to be ~ 15 – 25 %.

Equations (3) and (4) were used to obtain radiative (k_{RAD}) and non-radiative (k_{NRD}) rate constants, respectively.

$$k_{rad} = \Phi k_{obsd} \qquad (4)$$

$$k_{nrd} = k_{obsd} - k_{rad} \qquad (5)$$

CHAPTER III: Computational Procedures

Electronic structure calculations were determined with DFT [33] using Gaussian 09.[34] In a previous report on some related Ru-bpy complexes,[35] it was found that the B3PW91 functional [36-39] in combination with the SDDall basis set[39-42] correlated well with the experimental absorption spectra. In this report SDD basis set was used which employed the more flexible D95V basis set for main group atoms for a better description of the molecular geometries. [41] Additionally the B3PW91 functional was used to model the electronic structures to compare experimental bandshapes and wavelengths of the complexes. Wave functions were tested for SCF stability [43-44] and all optimized structures were confirmed as minima by analyzing the harmonic vibrational frequencies.[45] Solvation effects (in acetonitrile) were accounted for using recent implementation of the implicit IEF-PCM solvation model.[46-49] Vertical electronic excitation energies and intensities were evaluated with TD-DFT using 50 states.[50-52]

CHAPTER IV: Results

A. Proton Nuclear Magnetic Resonance Spectroscopy (^{1}H NMR)

The ^{1}H NMR spectra of the ruthenium complexes investigated in these projects are found in the following pages. Most of the spectra can separated by upfield (0.0 – 4.0 ppm) and downfield (7.0 – 10.0 ppm) chemical resonances. Typically the protons found upfield are due to aliphatic protons of the macrocyclic rings and downfield are from the bipyridine (bpy) ligand.

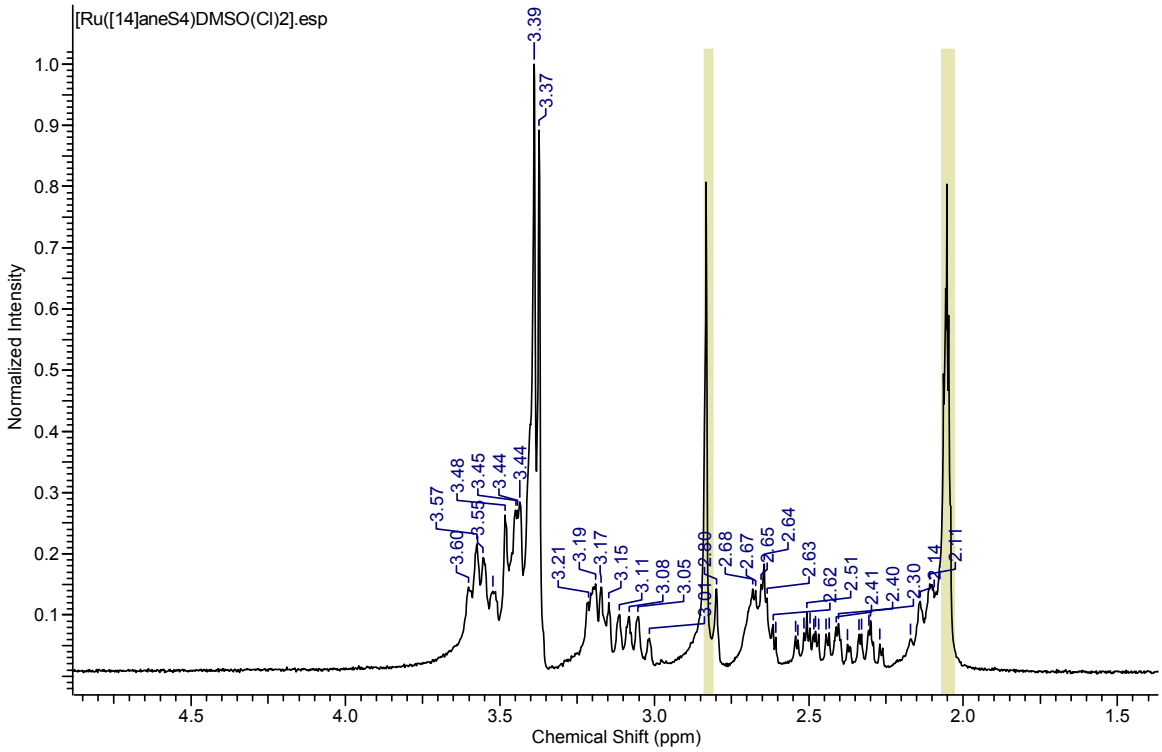

Figure 4: [Ru([14]aneS4)(DMSO)(Cl)]$^{+}$

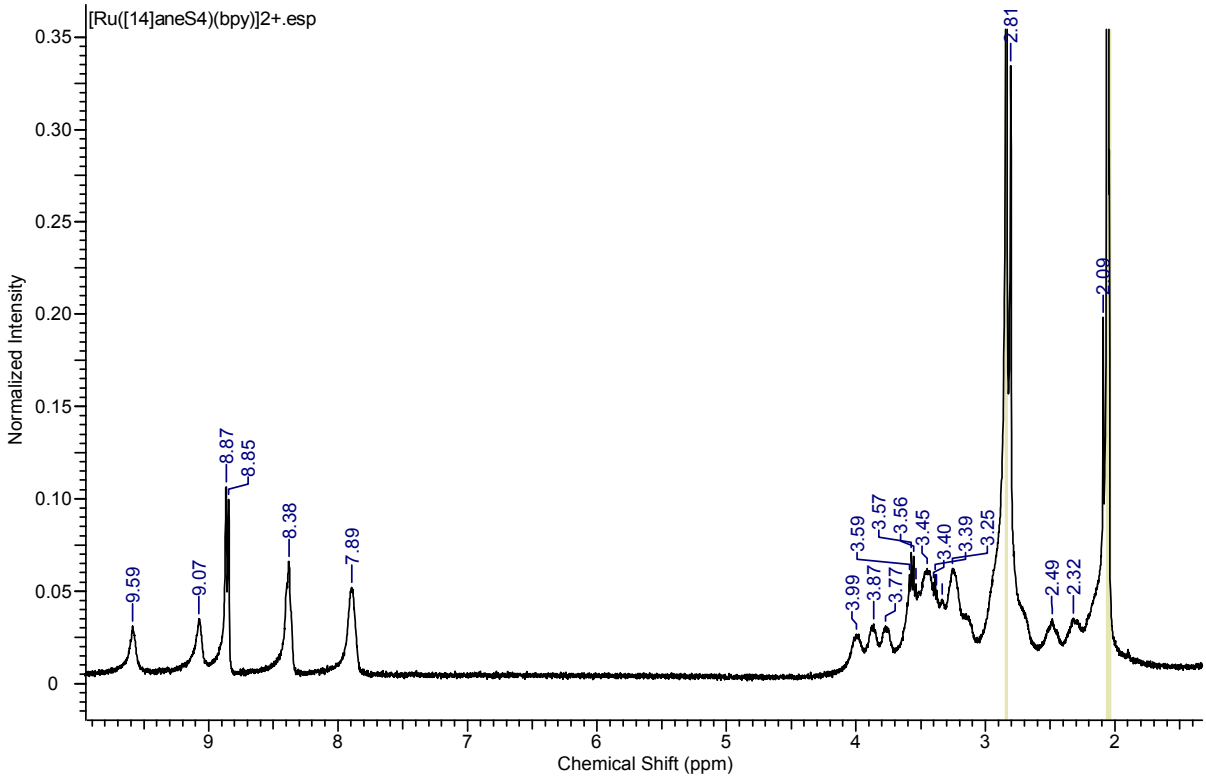

Figure 5: [Ru([14]aneS4)(bpy)]$^{2+}$

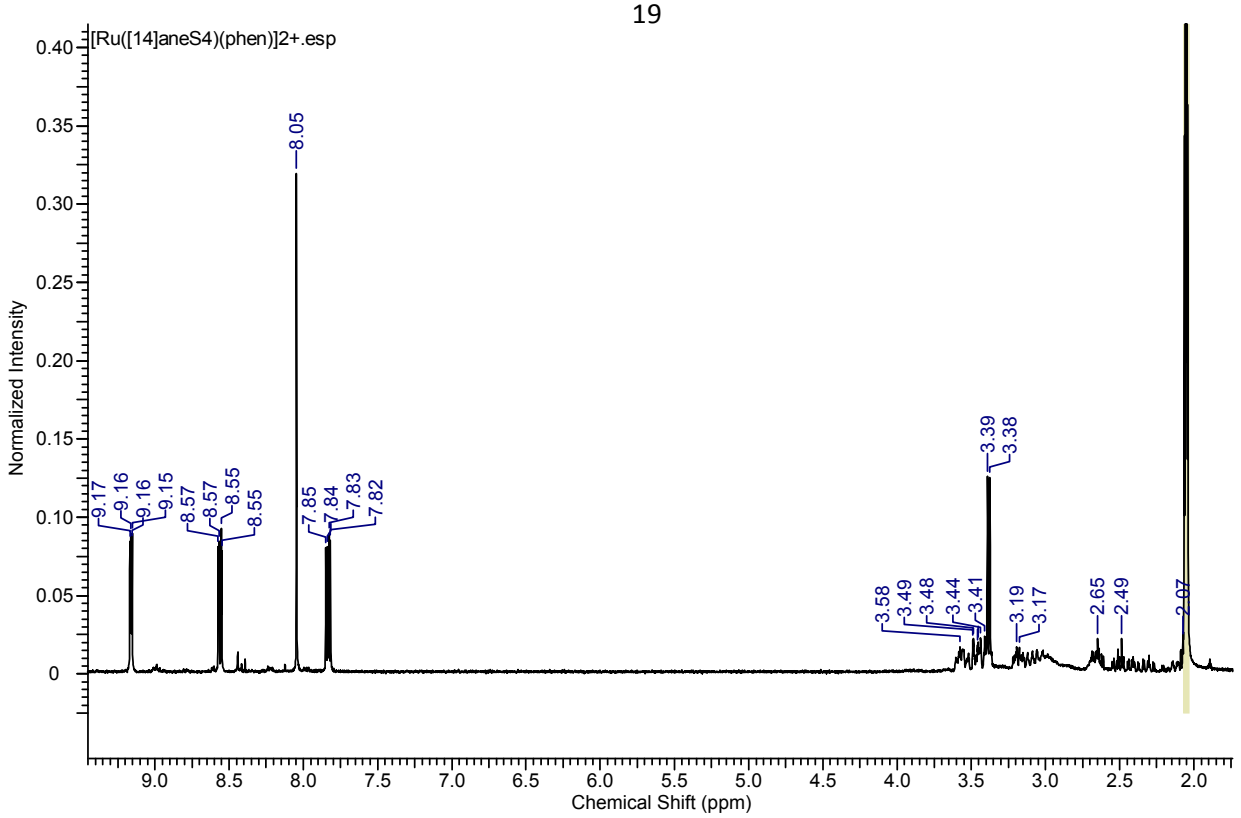

Figure 6: [Ru([14]aneS4)(phen)]$^{2+}$

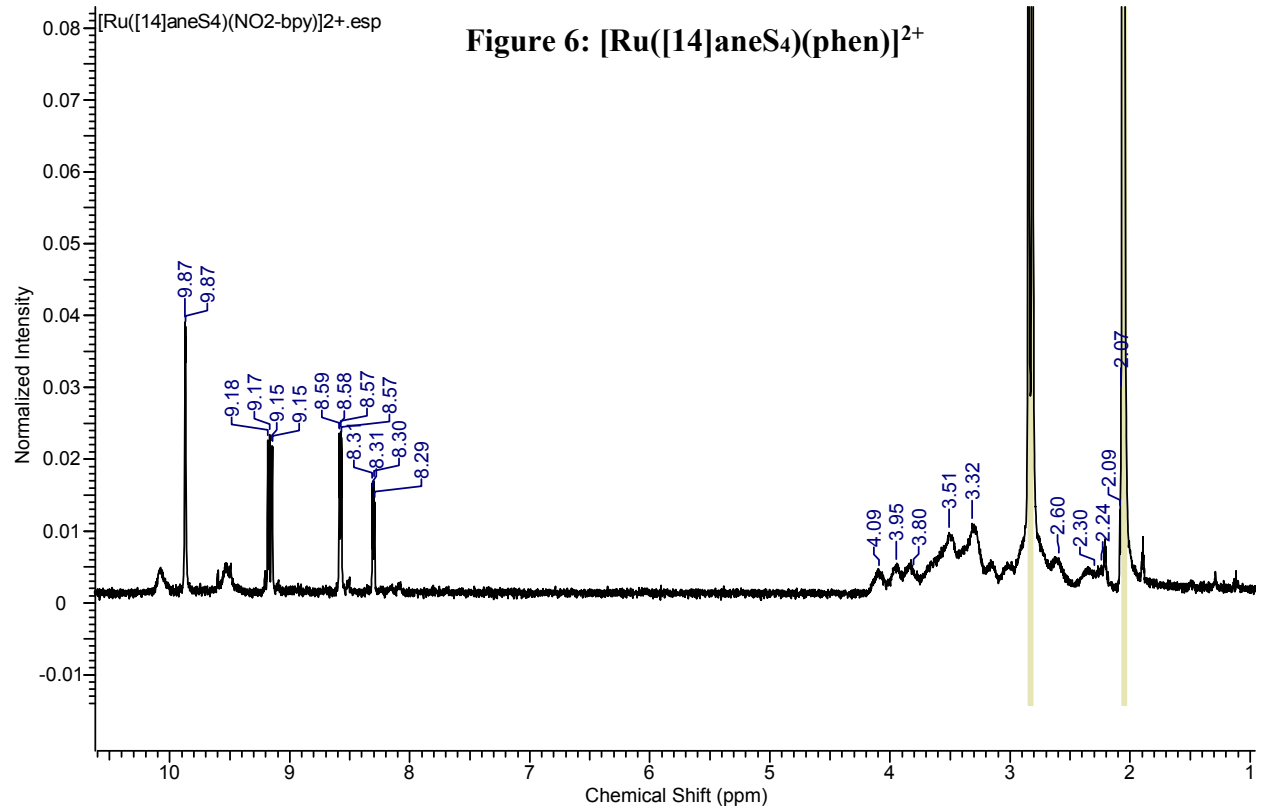

Figure 7: [Ru([14]aneS4)(4,4'-dinitro-2,2'-bpy)]$^{2+}$

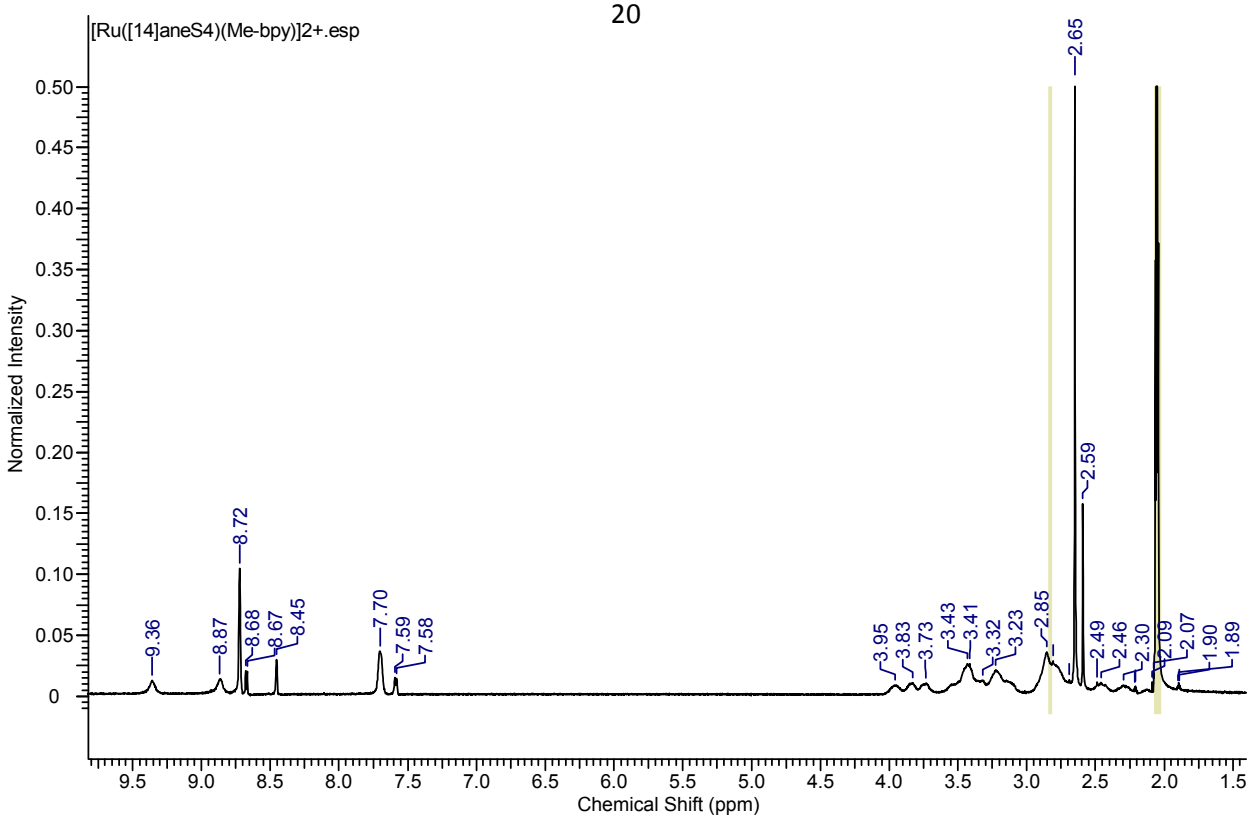

Figure 8: [Ru([14]aneS$_4$)(4,4'-dimethyl-2,2'-bpy)]$^{2+}$

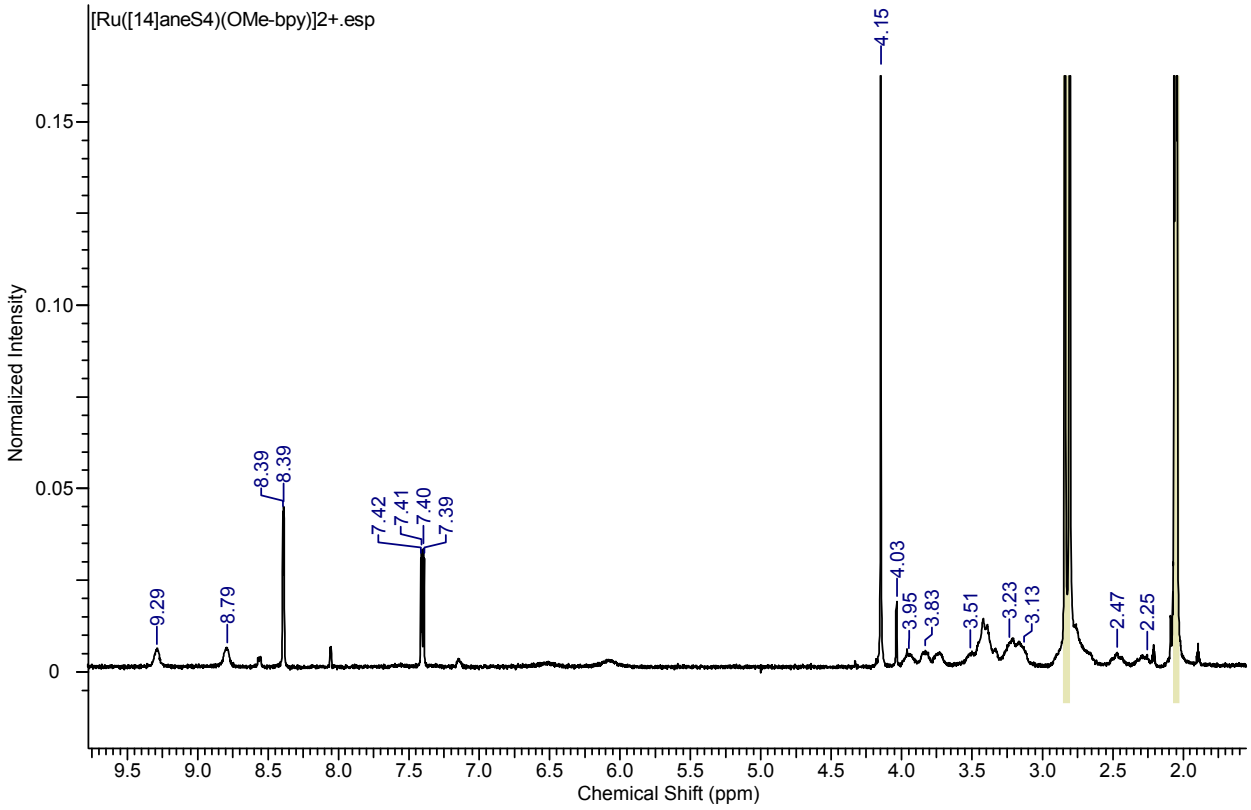

Figure 9: [Ru([14]aneS$_4$)(4,4'-dimethoxy-2,2'-bpy)]$^{2+}$

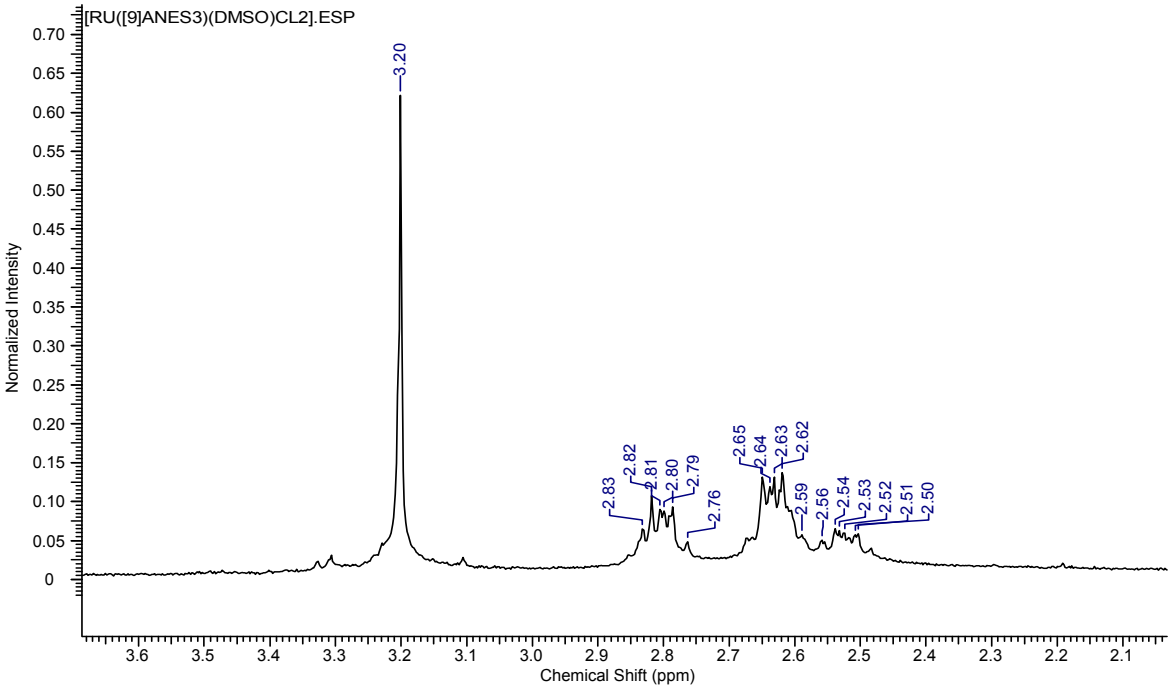

Figure 10: [Ru([9]aneS$_3$)(DMSO)Cl$_2$]

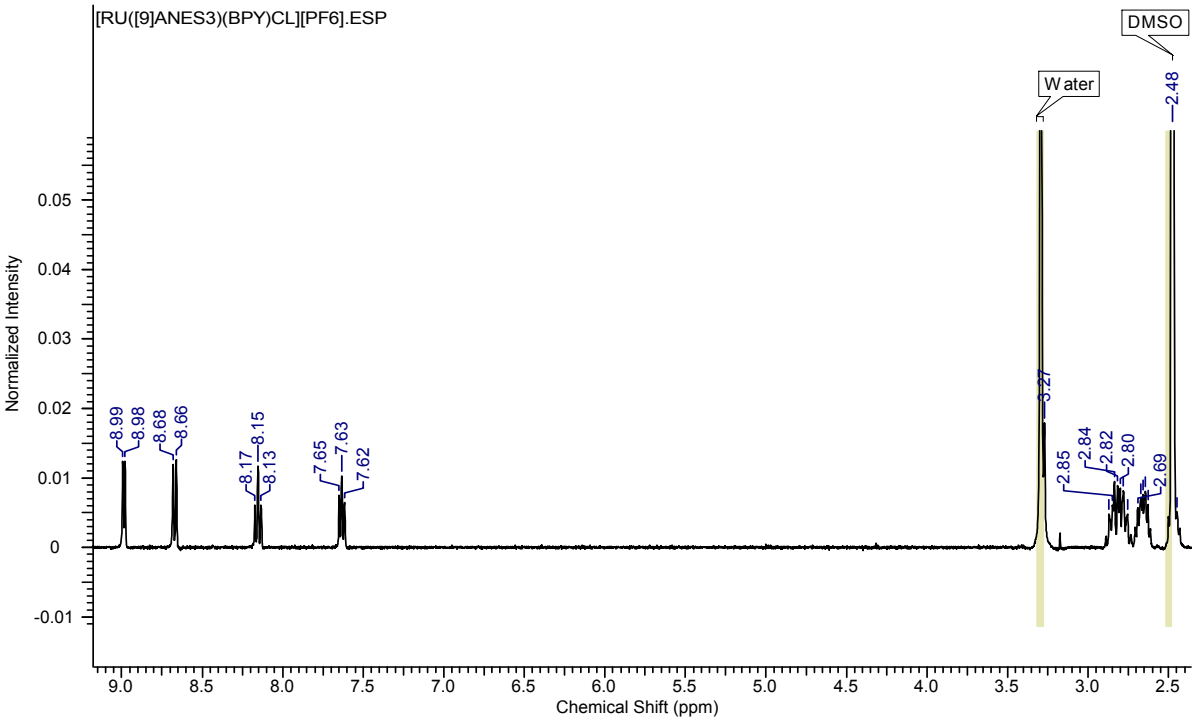

Figure 11: [Ru([9]aneS$_3$)(bpy)Cl]$^+$

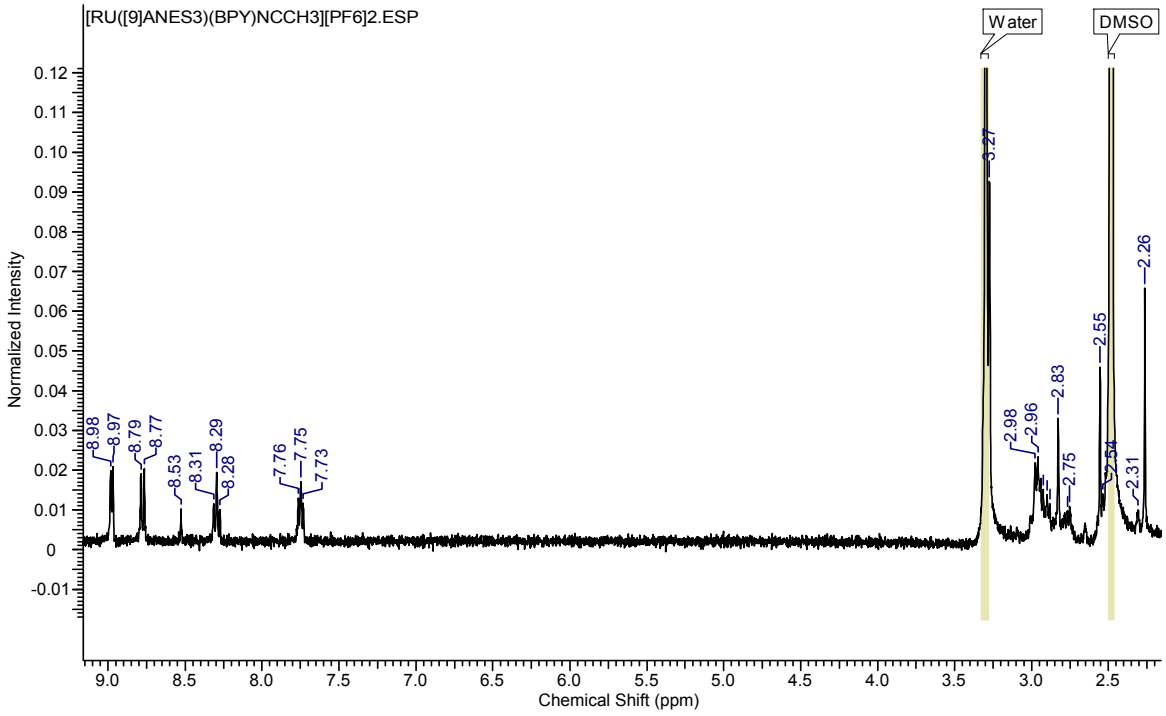

Figure 12: [Ru([9]aneS$_3$)(bpy)MeCN]$^{2+}$

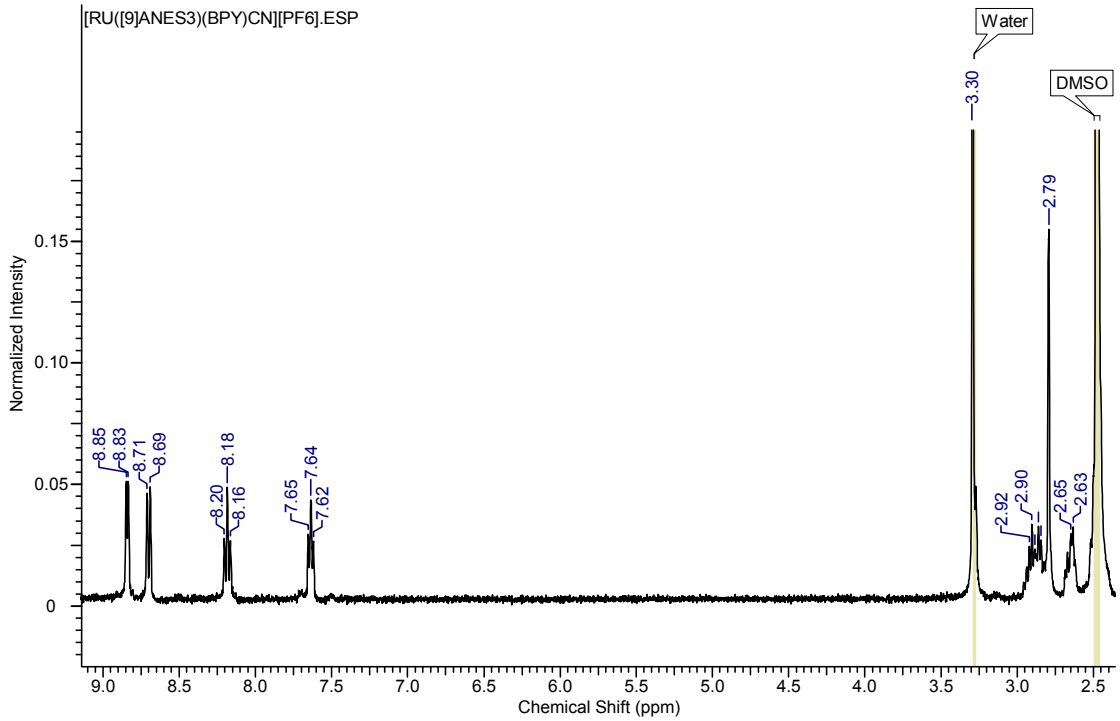

Figure 13: [Ru([9]aneS$_3$)(bpy)CN]$^{+}$

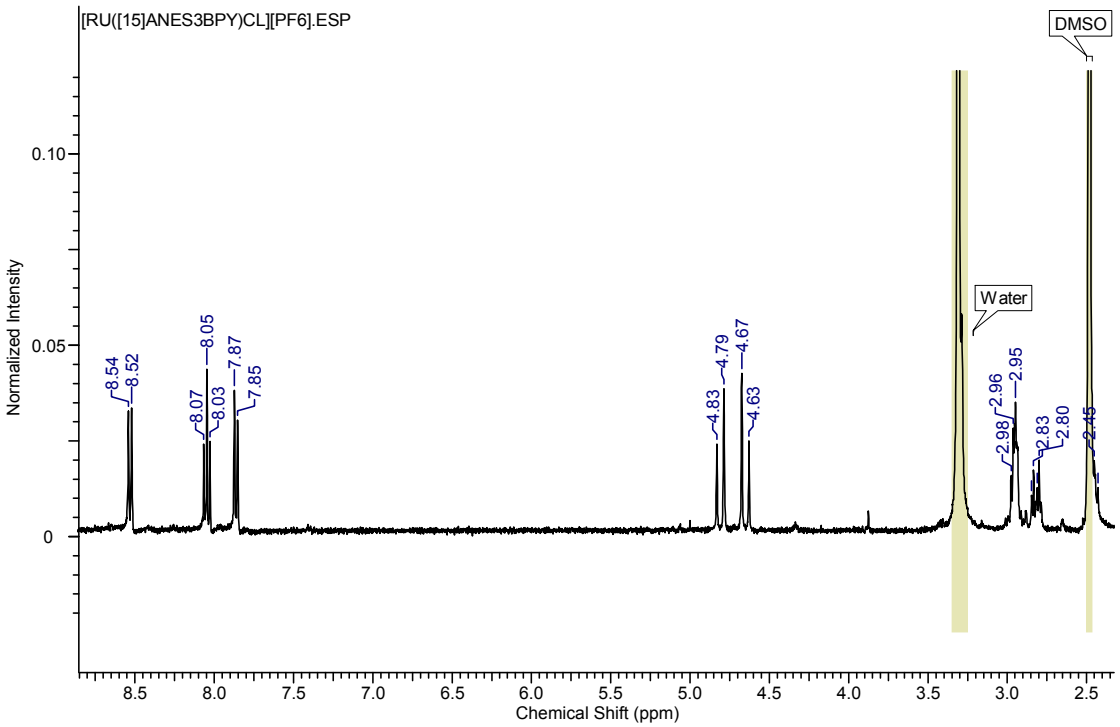

Figure 14: [Ru([15]dieneS$_3$bpy)Cl]$^+$

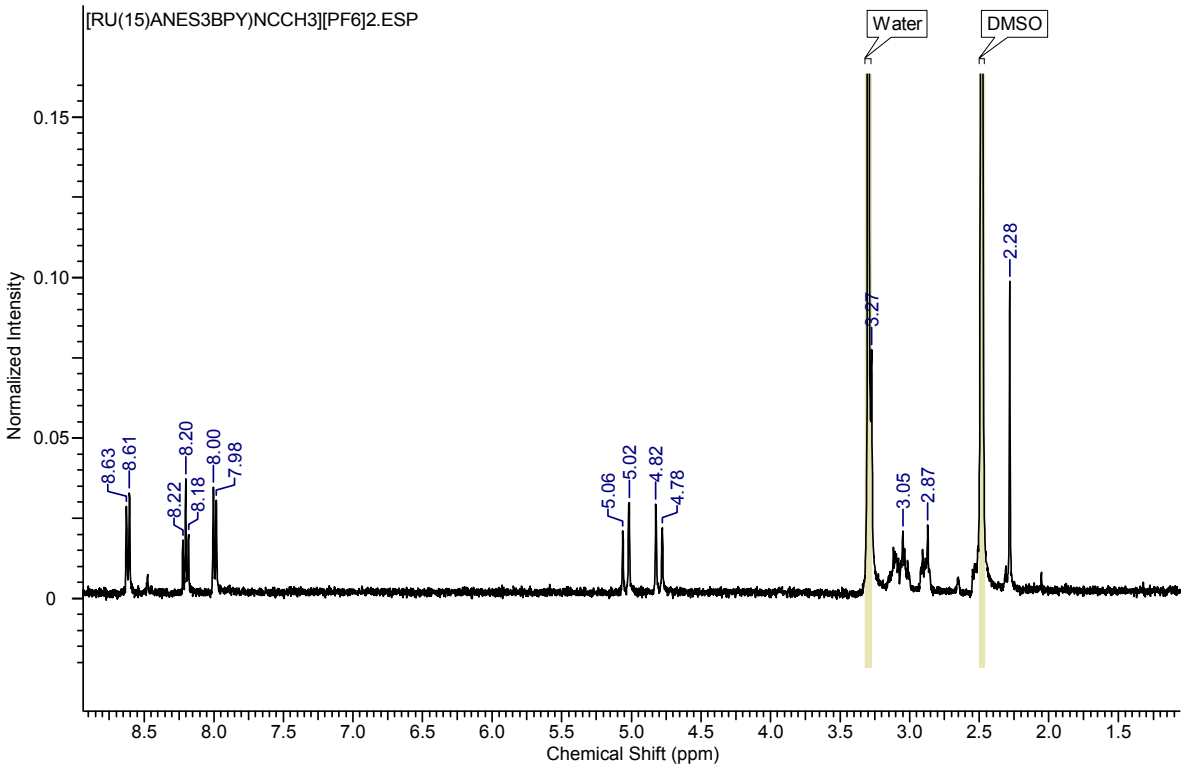

Figure 15: [Ru([15]dieneS$_3$bpy)MeCN]$^{2+}$

B. Electrochemistry

Figure 16 and Table 1 represents the electrochemistry for the [14]aneS$_4$ ligand based complexes. The black traces in the figure represents the blank scan which consists of 0.1M Bu_4NPF_6 in acetonitrile, the red traces represents the full cyclic voltammograms with both the oxidation and reduction processes, the blue traces represents the oxidation (positive potential) and reduction (negative potential) separately and the green traces are indicative of the differential pulse voltammetry potentials. For these experiments, the solvent was purged for 10 min with dry argon in an effort to get rid oxygen in the sample vessel. The typical scan sequence for the cyclic voltammograms was started at 0 V and scanned in the negative potential direction to -1800 V and the scan direction was swept back to the positive direction to 2000 V and finally swept again in the negative direction to -1800 V. This sequence represents one full cyclic voltammogram scan.

The potential range for the $Ru^{2+/3+}$ oxidation process is 1.3 to 1.8 V while the range for the bipyridine reduction is -1.3 to -1.6 V for this series of complexes. The peak separation between the cathodic and anodic waves are about 70 mV (except for [Ru([14]aneS$_4$)(d^8-bpy)]$^{2+}$) which is suggestive of one-electron processes and also compound purity.

Table 1: Redox Potentials of [Ru([14]aneS$_4$)(L)]$^{2+}$ Complexes[a]

[Ru([14]aneS$_4$)(L)]$^{2+}$	$E_{1/2}(Ru^{III/II})$ (V)	$\Delta E_p(Ru^{III/II})$ (mV)	$E_{1/2}$(L) (V)	ΔE_p(L) (mV)	$F\Delta E_{1/2}$, eV
[Ru([14]aneS$_4$)(bpy)]$^{2+}$	1.55	68	-1.29	72	2.84
[Ru([14]aneS$_4$)(d_8-bpy)]$^{2+}$	1.52	121	-1.36	114	2.88
[Ru([14]aneS$_4$)(4,4'-dimethyl 2,2'-bpy)]$^{2+}$	1.55	63	-1.33	64	2.88
[Ru([14]aneS$_4$)(4,4'-dimethoxy 2,2'-bpy)]$^{2+}$	1.29	64	-1.55	68	2.84
[Ru([14]aneS$_4$)(4,4'-dinitro 2,2'-bpy)]$^{2+}$	1.76	68	---	irr	---

[a]$E_{1/2}$ values in Acetonitrile/0.1M Bu_4NPF_6 at room temperature at 150 mV/s; referenced internally to $E_{1/2}$ ($Fc^{+/0}$) = 0.437 V. irr = irreversible.

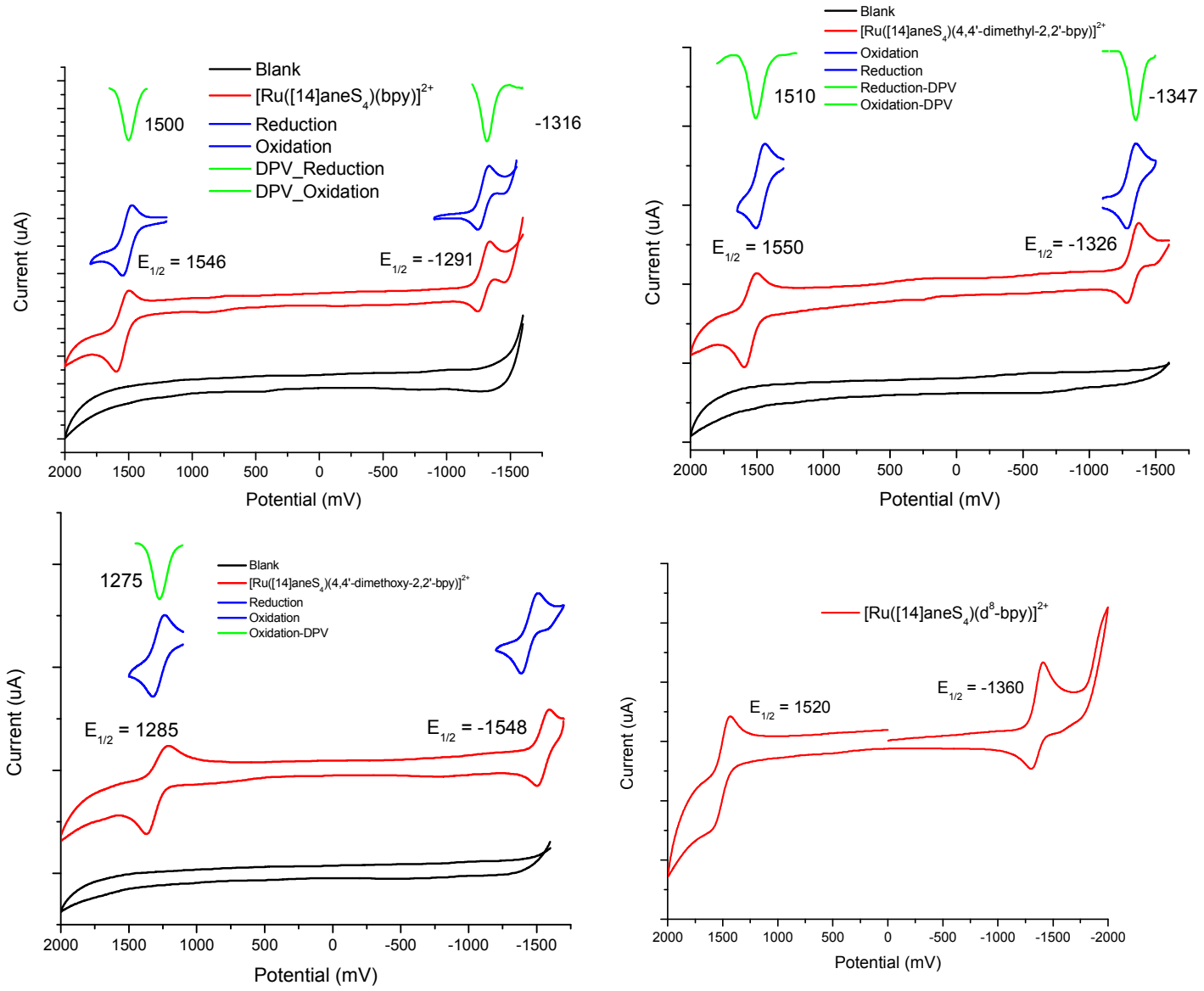

Figure 16: Cyclic Voltammograms of $[Ru([14]aneS_4)(bpy)]^{2+}$ (upper left), $[Ru([14]aneS_4)($ 4,4'-dimethyl 2,2'-bpy$)]^{2+}$ (upper right), $[Ru([14]aneS_4)($ 4,4'-dimethoxy 2,2'-bpy$)]^{2+}$ (lower left), and $[Ru([14]aneS_4)(d^8\text{-bpy})]^{2+}$ (lower right)

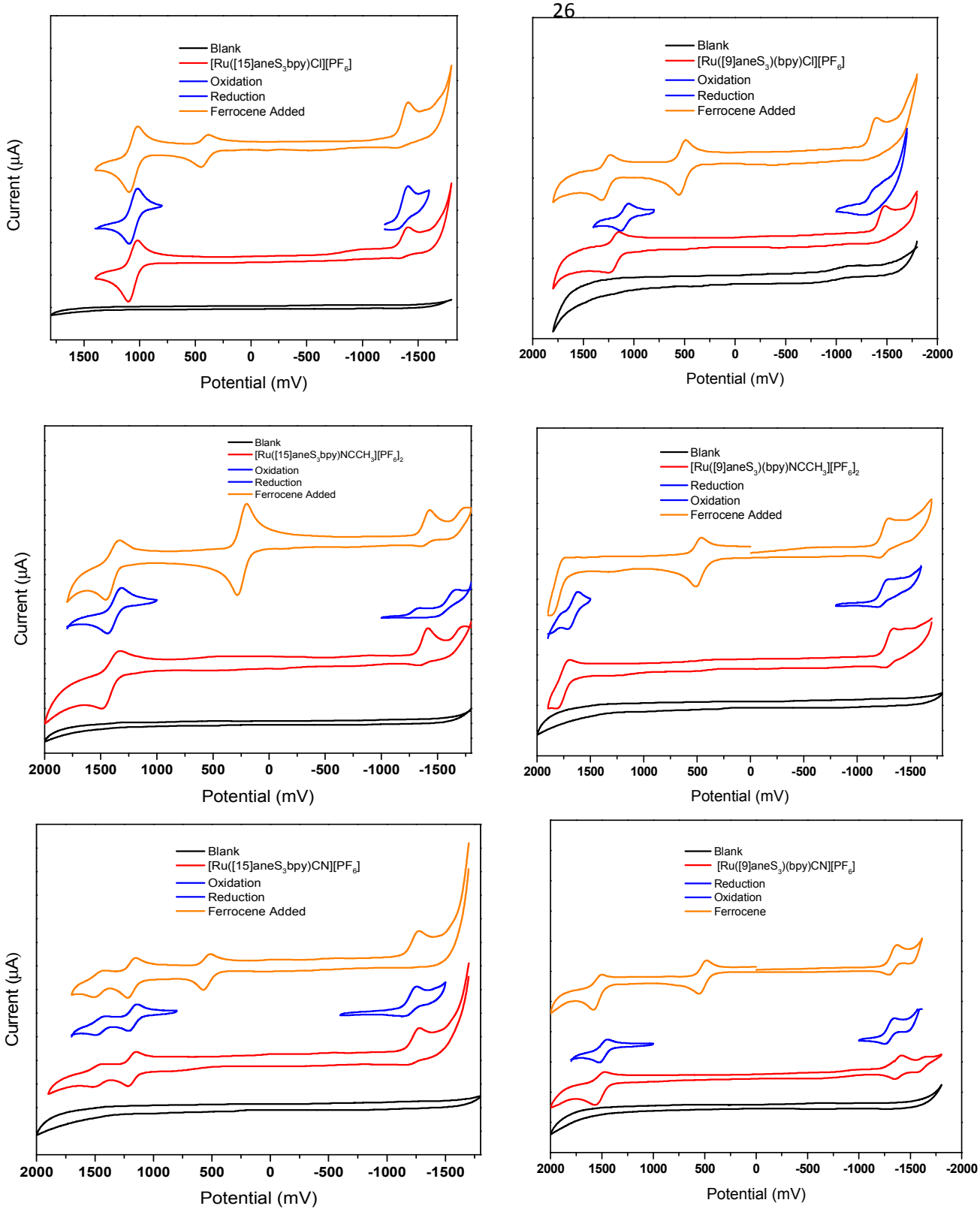

Figure 17: Cyclic Voltammograms of $[Ru([15]dieneS_3bpy)Cl]^+$ (upper left), $[Ru([9]aneS_3)(bpy)Cl]^+$ (upper right), $[Ru([15]dieneS_3bpy)MeCN]^{2+}$ (middle left), $[Ru([9]aneS_3)(bpy)MeCN]^+$ (middle right), $[Ru([15]dieneS_3bpy)CN]^+$(bottom left) and $[Ru([9]aneS_3)(bpy)CN]^+$ (bottom right)

Table 2 : Redox Potentials of $[Ru([15]dieneS_3bpy)X]^{m+}$ and $[Ru([9]aneS_3)(bpy)X]^{m+}$ Complexes[a]

Code	$[Ru([15]dieneS_3bpy)(X)]^{m+}$ or $[Ru([9]aneS_3)(X)]^{m+}$	$E_{1/2}(Ru^{III/II})$ (V)	$\Delta E_p(Ru^{III/II})$ (mV)	$E_{1/2}(L)$ (V)	$\Delta E_p(L)$ (mV)	$\Delta E_{1/2}$, V
1	$[Ru([15]dieneS_3bpy)(Cl)][PF_6]$	1.08	62	(irr)	--	--
2	$[Ru([9]aneS_3)(bpy)(Cl)][PF_6]$	1.34	65	(irr)	--	--
3	$[Ru([15]dieneS_3bpy)(CH_3CN)][PF_6]_2$	1.40	83	-1.40	65	2.8
4	$[Ru([9]aneS_3)(bpy)(CH_3CN)][PF_6]_2$	1.73	97	-1.32	67	3.05
5	$[Ru([15]dieneS_3bpy)(CN)][PF_6]$	1.36[b]	59[b]	-1.31	82	2.67
6	$[Ru([9]aneS_3)(bpy)(CN)][PF_6]$	1.54	66	-1.33	67	2.87

[a]$E_{1/2}$ values in Acetonitrile/0.1M Bu_4NPF_6 at room temperature at 150 mV/s; referenced internally to $E_{1/2}$ ($Fc^{+/0}$) = 0.437 V. irr = irreversible.

Figure 17 and Table 2 represents the electrochemistry for the $[9]aneS_3$ and $[15]dieneS_3bpy$ ligand based complexes. The black traces in the figure represents the blank scan which consists of 0.1M Bu_4NPF_6 in acetonitrile, the red traces represents the full cyclic voltammograms with both the oxidation and reduction processes, the blue traces represents the oxidation (positive potential) and reduction (negative potential) separately and the orange traces are indicative of the full scans with the internal reference ferrocene added. For these experiments, the solvent was purged for 10 min with dry argon in an effort to get rid oxygen in the sample vessel. The typical scan sequence for the cyclic voltammograms was started at 0 V and scanned in the negative potential direction to -1800 V and the scan direction was swept back to the positive direction to 2000 V and finally swept again in the negative direction to -1800 V. This sequence represents one full cyclic voltammogram scan.

The potential range for the $Ru^{2+/3+}$ oxidation process is 1.1 to 1.7 V while the range for the bipyridine reduction is -1.3 to -1.4 V for this series of complexes. The peak separation between the cathodic and anodic waves are around 70 mV (except for the $[Ru([9]aneS_3)(bpy)(CH_3CN)]^{2+}$ complex) which is suggestive of one-electron processes and also compound purity.

The chloro based complexes proves to have irreversible bipyridine reductions. This behavior may be apparent due to the strong electron affinity of the chloro atom and is consistent with only observing the cathodic wave. The $[Ru([15]dieneS_3bpy)(CN)]^{+}$ complex seems to have two oxidations. One of the oxidations may be due to the $[15]dieneS_3bpy$ ligand or conversely due to another $Ru^{2+/3+}$ oxidation.

C. Absorption Spectra

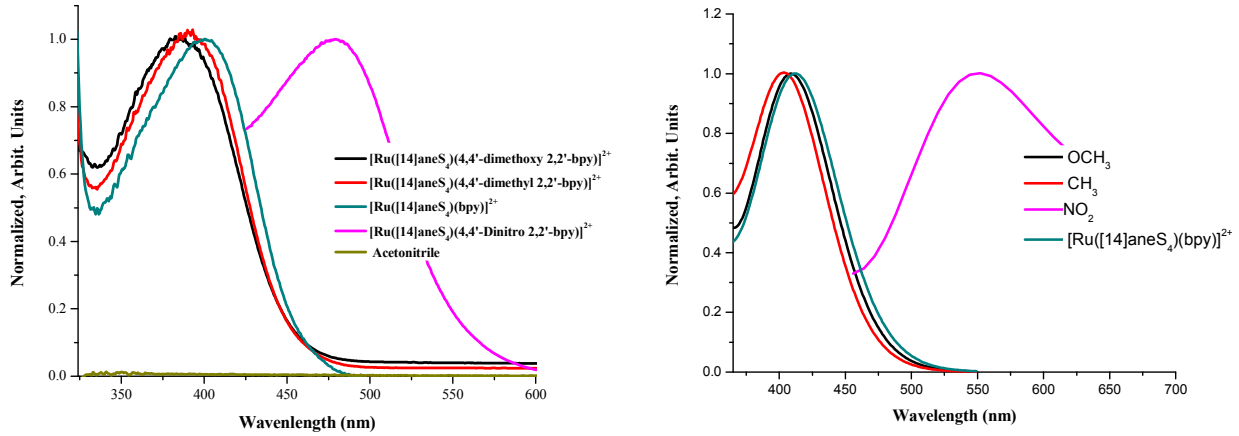

Figure 18: Ambient Absorption Spectra of $[Ru([14]aneS_4)(L)]^{2+}$ Complexes (experimental $[10^{-4} – 10^{-5}M]$on the left and calculated on the right) in acetonitrile

Figure 18 represents the ambient UV-vis absorption for the $[14]aneS_4$ based complexes both the experimental (left) and calculated (right). This figure is showing the normalized MLCT of the given complexes in acetonitrile solvent. The $[Ru([14]aneS_4)(bpy)]^{2+}$ (in green) complex

has a MLCT absorption band at 400nm, while the 4,4'-dimethyl 2,2'-bpy (in red) and 4,4'-dimethoxy 2,2'-bpy (in black) complexes exhibit MLCT absorption bands at 390nm and 382nm respectively. This indicates that there is a systematic hypsochromic shift (higher energy) from bpy < 4,4'-dimethyl 2,2'-bpy < 4,4'-dimethoxy 2,2'-bpy as the bpy is modified with the 4,4'-electron donating groups of CH_3 and OCH_3.

The computational work fit the experimental data reasonably well. The calculated oscillator energy strengths for the lowest energy transitions are within the range of $f = 0.0394 – 0.1002$.

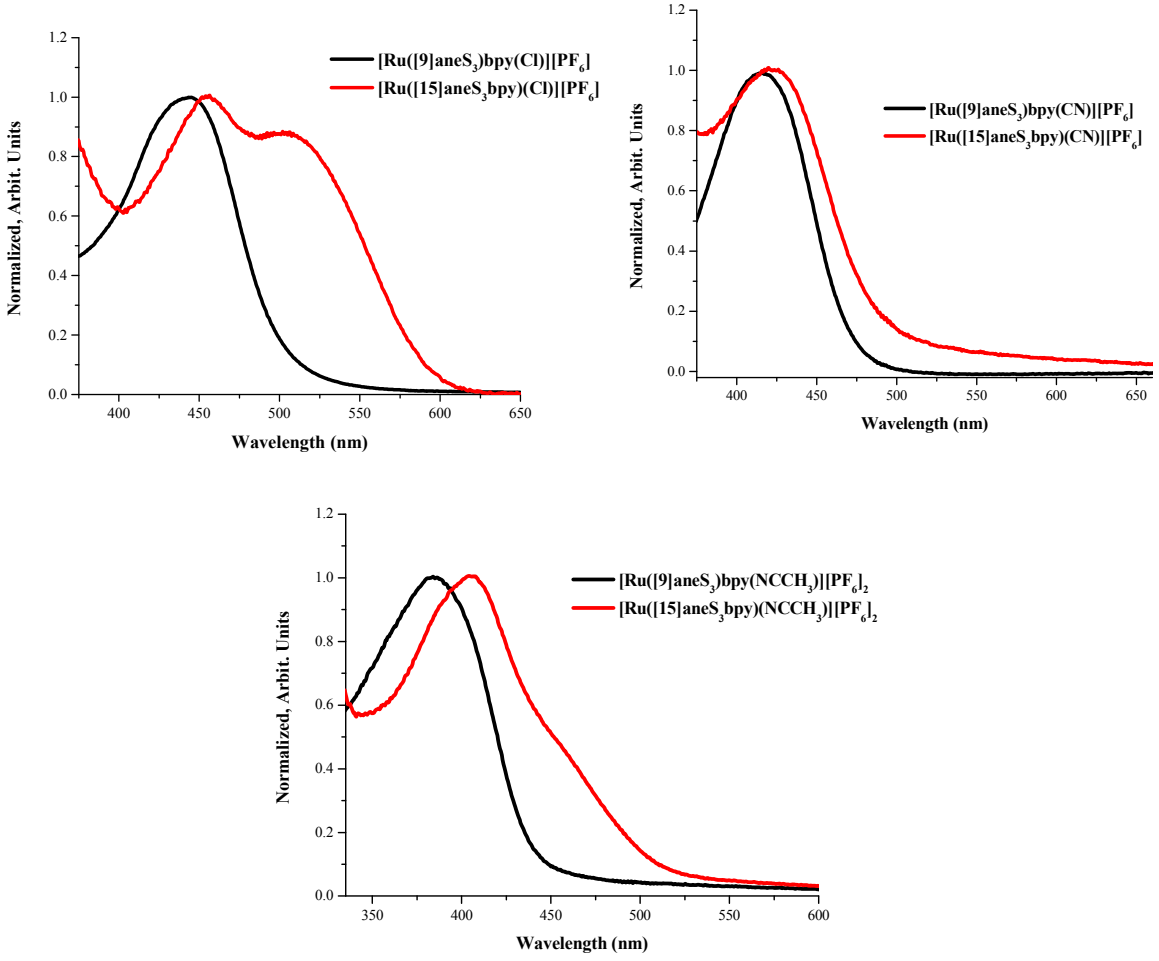

Figure 19: Ambient Absorption Spectra of $[Ru([9]aneS_3)(bpy)X]^{m+}$ and $[Ru([15]dieneS_3bpy)X]^{m+}$ Complexes in acetonitrile at ambient conditions ($10^{-4} – 10^{-5}$M)

Figure 19 illustrates the differences in absorption spectra for the [9]aneS_3 complexes versus the [15]dieneS_3bpy complexes with the same coordinated ligand (Cl, CN and MeCN). The spectra are quite similar in relative energies and bandshape except for the [Ru([15]dieneS_3bpy)Cl]$^+$ complex. The additional feature appearing at longer wavelengths may be due to differences in the Ru-Cl elongation being affected by the more constrained [15]dieneS_3bpy ligand. This observation is a bit pecuilar since the other [15]dieneS_3bpy based complexes are similar to their direct [9]aneS_3 analogs.

Figures 20 – 32 represent the low temperature (90 K) absorption spectra for the compounds investigated in these projects. The 90 K absorption is needed for low temperature relative quantum yield measurements. The trace in black represents the ambient spectra for the specific complexes while the red trace is the 90 K spectra. Both the ambient and low temperature absorptions were obtained using NSG Precision Cells, Inc. cryogenic square 1 cm quartz cuvettes with an ANDOR Shamrock 500 spectrometer in an Oxford Instruments OptistatCF Static Exchange Gas Continuous Flow Cryostat. Using the liquid light guide and detector together resulted in the shortest wavelength spectral detection at 395 nm.

In most cases the observed 90 K absorption reveals more resolved processes that are convoluted in the broad ambient absorption spectrums. This is more obvious when comparing the ambient absorption to the low temperature profile of [Ru(TQA)$(NCS)_2$] found in figure 32.

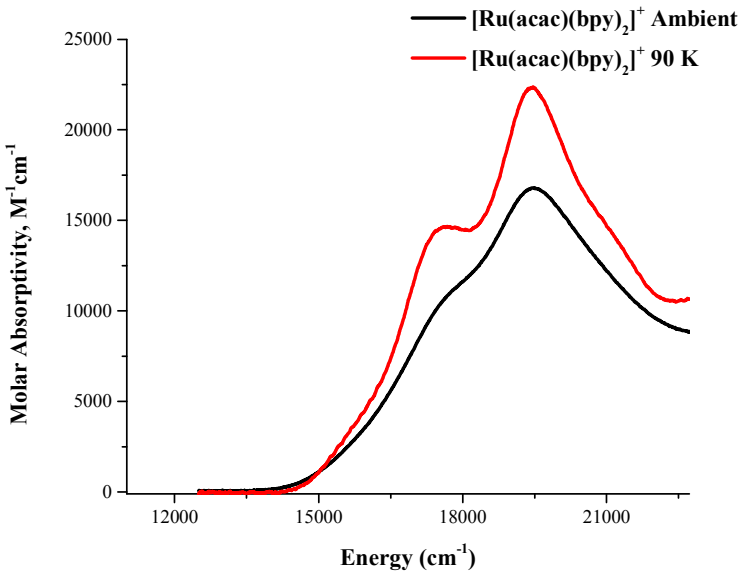

Figure 20: 90 K (red) Absorption Spectrum of $[Ru(acac)(bpy)_2]^+$ (4.6×10^{-5} M) in Alcohol[7]

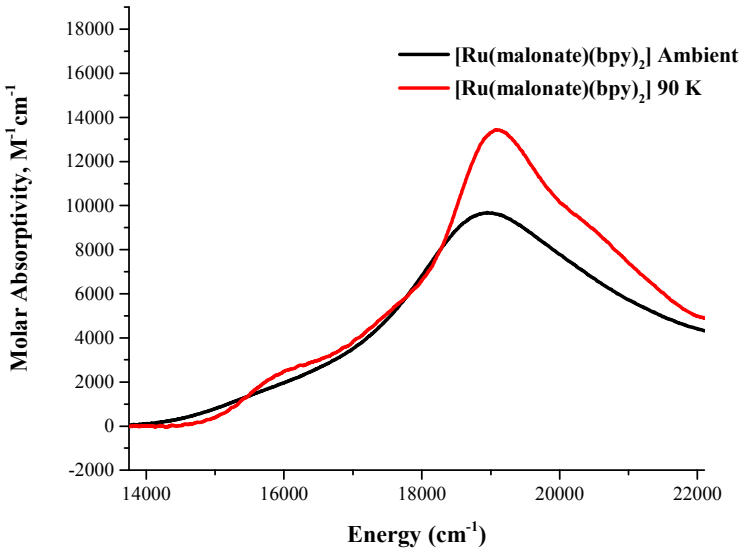

Figure 21: 90 K (red) Absorption Spectrum of $[Ru(malonate)(bpy)_2]$ (6.1×10^{-5} M) in Alcohol[7]

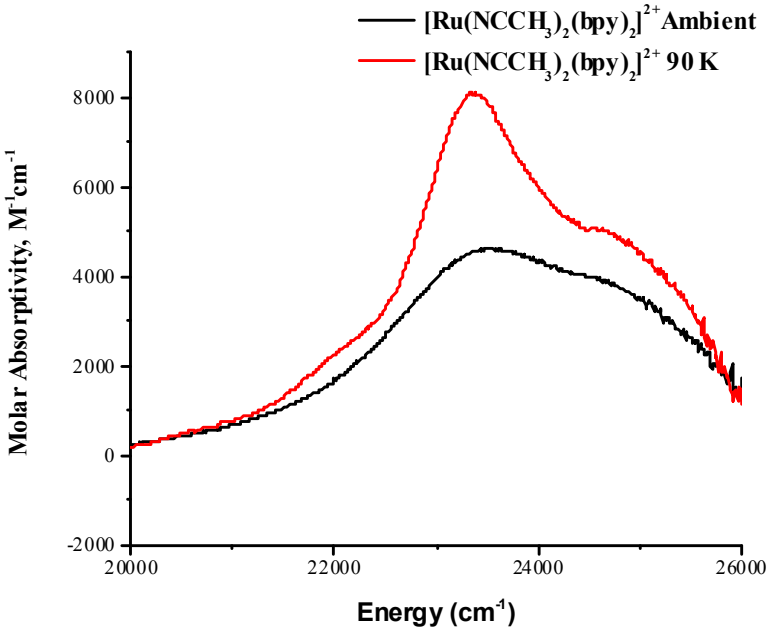

Figure 22: 90 K (red) Absorption Spectrum of $[Ru(MeCN)_2(bpy)_2]^{2+}$ (6.2×10^{-5} M) in Alcohol[7]

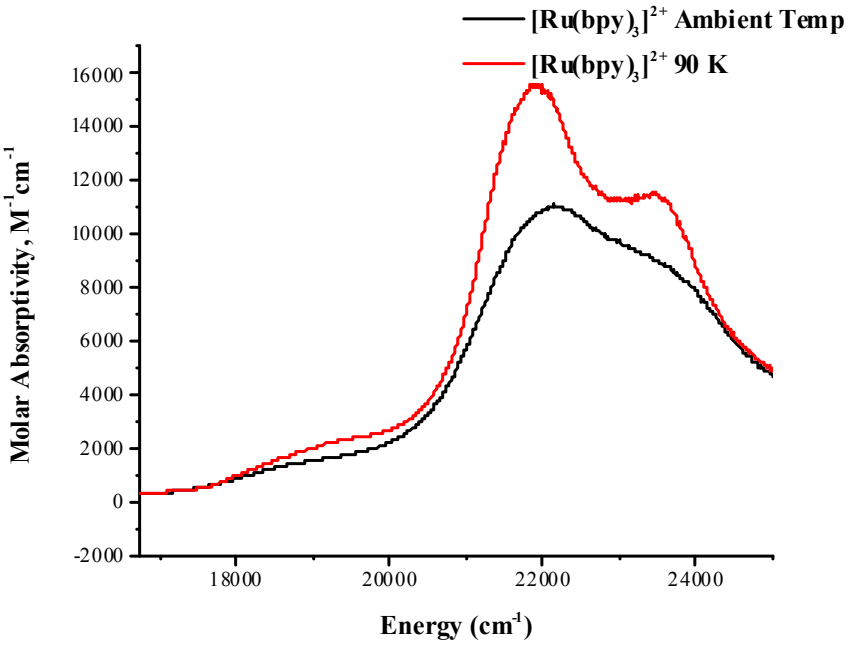

Figure 23: 90 K (red) Absorption Spectrum of $[Ru(bpy)_3]^{2+}$ (1.1×10^{-4} M) in Alcohol[7]

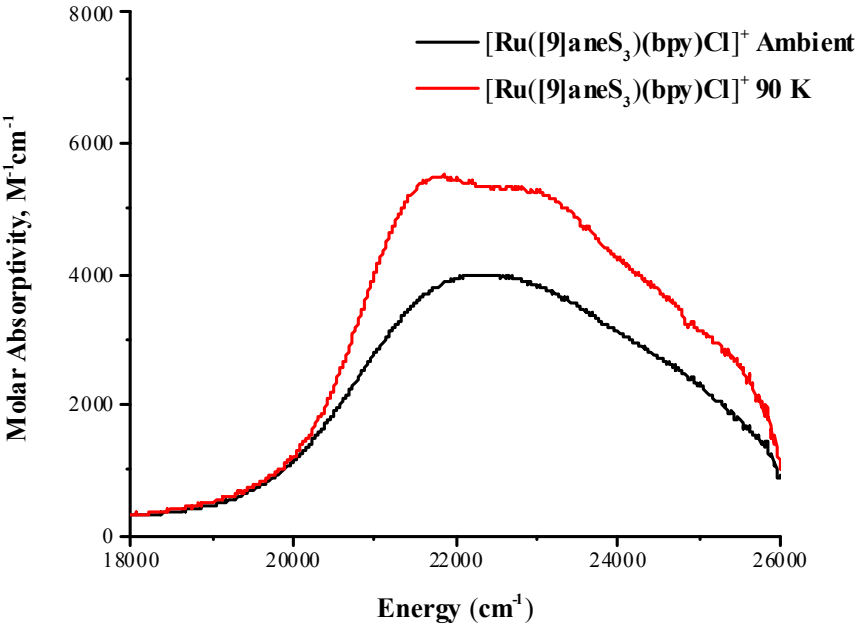

Figure 24: 90 K (red) Absorption Spectrum of [Ru([9]aneS$_3$)(bpy)Cl]$^+$ (1.2 x 10^{-4} M) in Butyronitrile

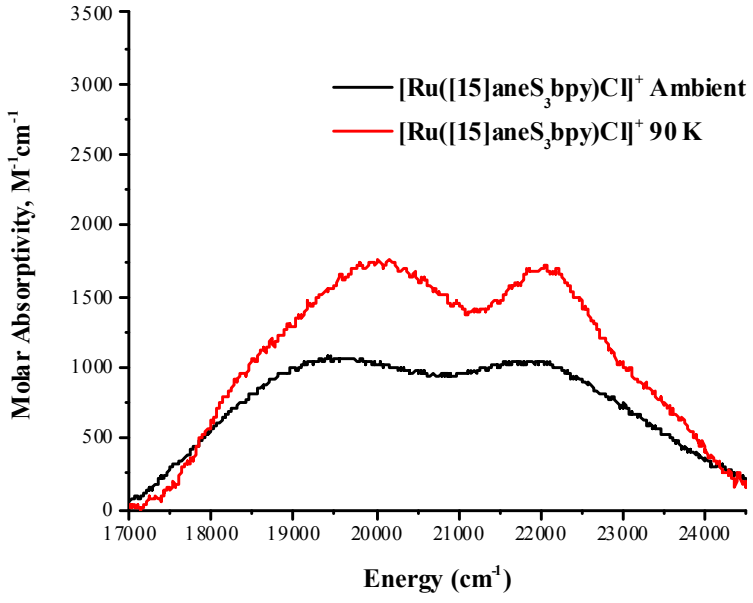

Figure 25: 90 K (red) Absorption Spectrum of [Ru([15]dieneS$_3$bpy)Cl]$^+$ (7.8 x 10^{-5} M)in Butyronitrile

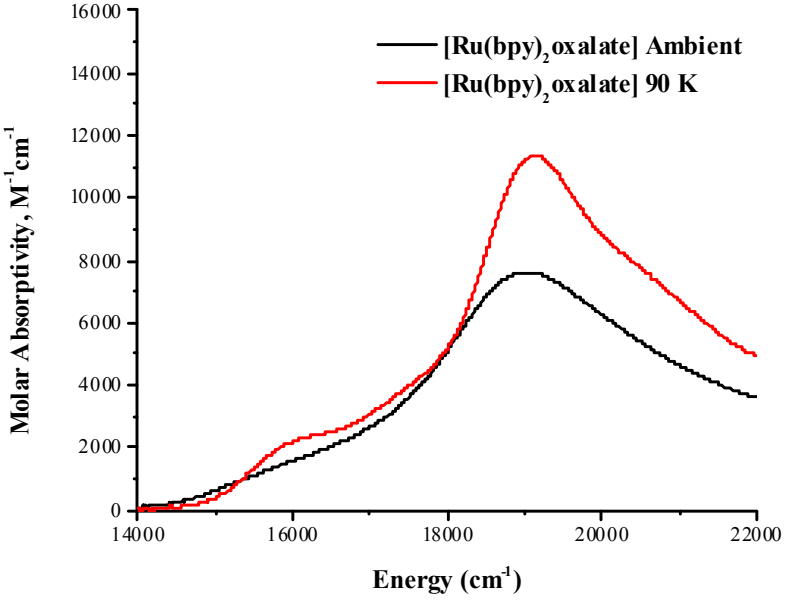

Figure 26: 90 K (red) Absorption Spectrum of [Ru(bpy)$_2$oxalate] (9.6 x 10^{-5} M) in Alcohol[7]

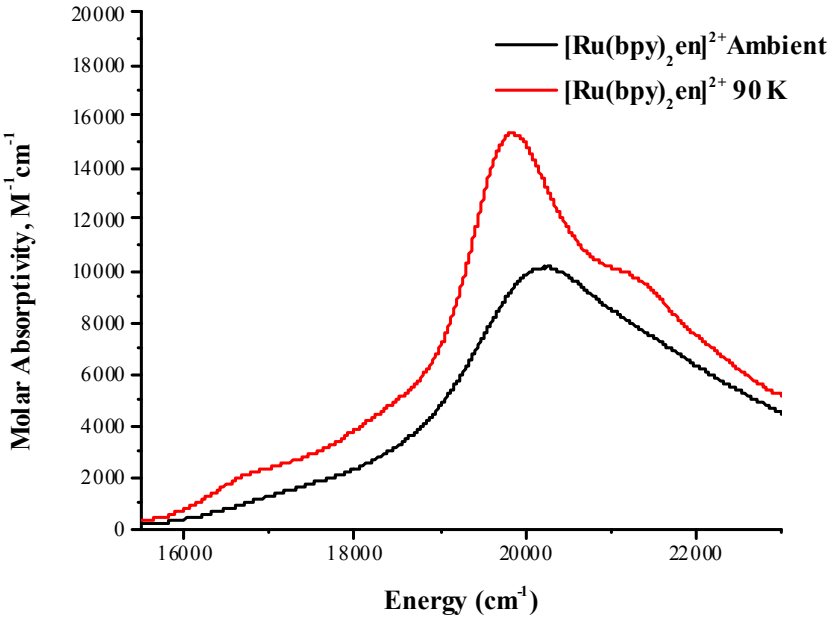

Figure 27: 90 K (red) Absorption Spectrum of [Ru(bpy)$_2$en]$^{2+}$ (1.0 x 10^{-4} M) in Alcohol[7]

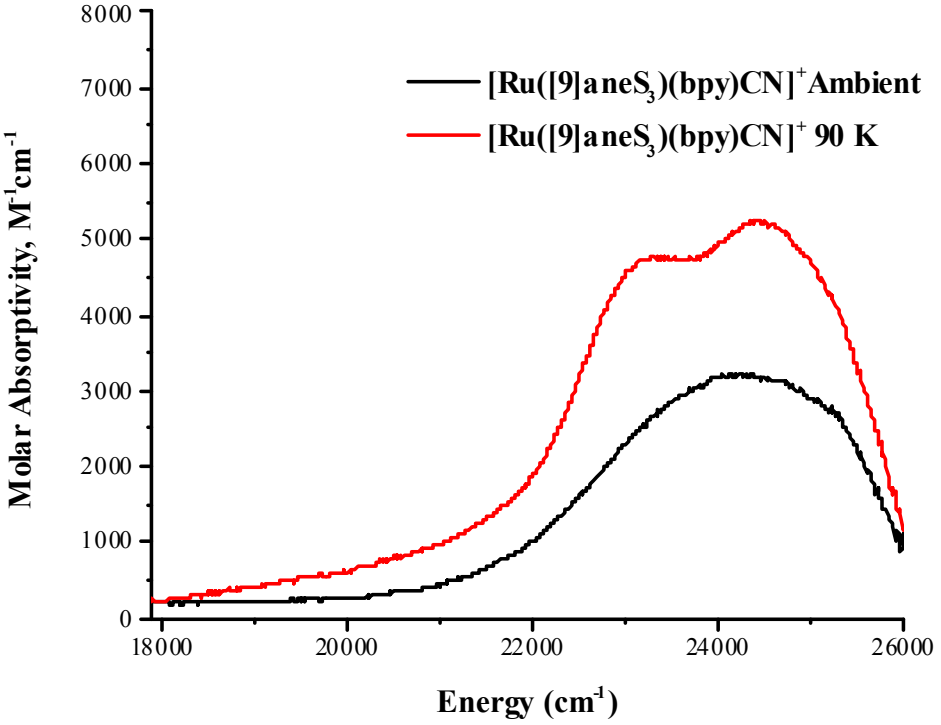

Figure 28: 90 K (red) Absorption Spectrum of $[Ru([9]aneS_3)(bpy)CN]^+$ (5.3×10^{-5} M) in Alcohol[7]

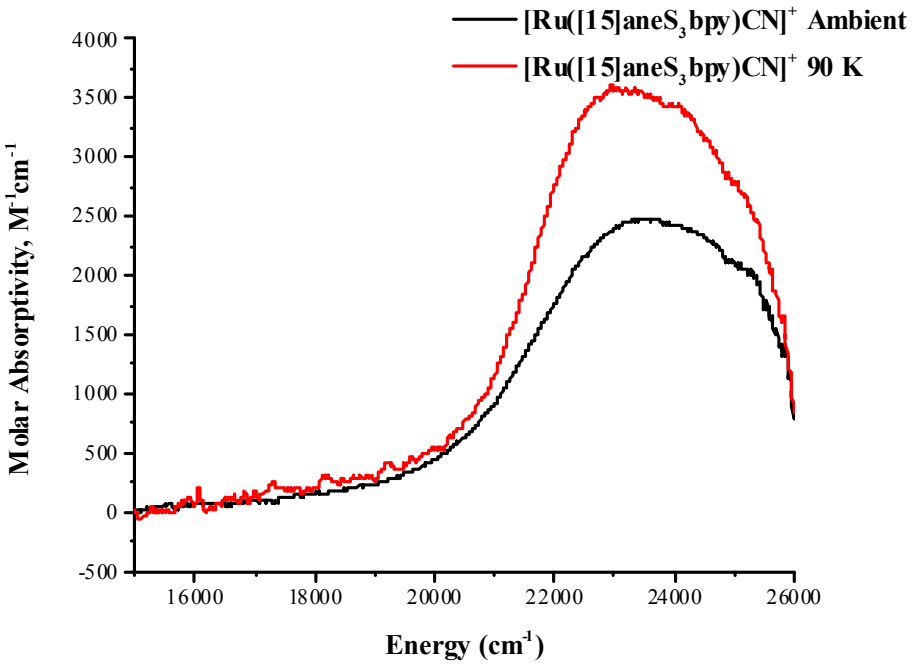

Figure 29: 90 K (red) Absorption Spectrum of $[Ru([15]dieneS_3bpy)CN]^+$ (1.6×10^{-4} M)in Butyronitrile

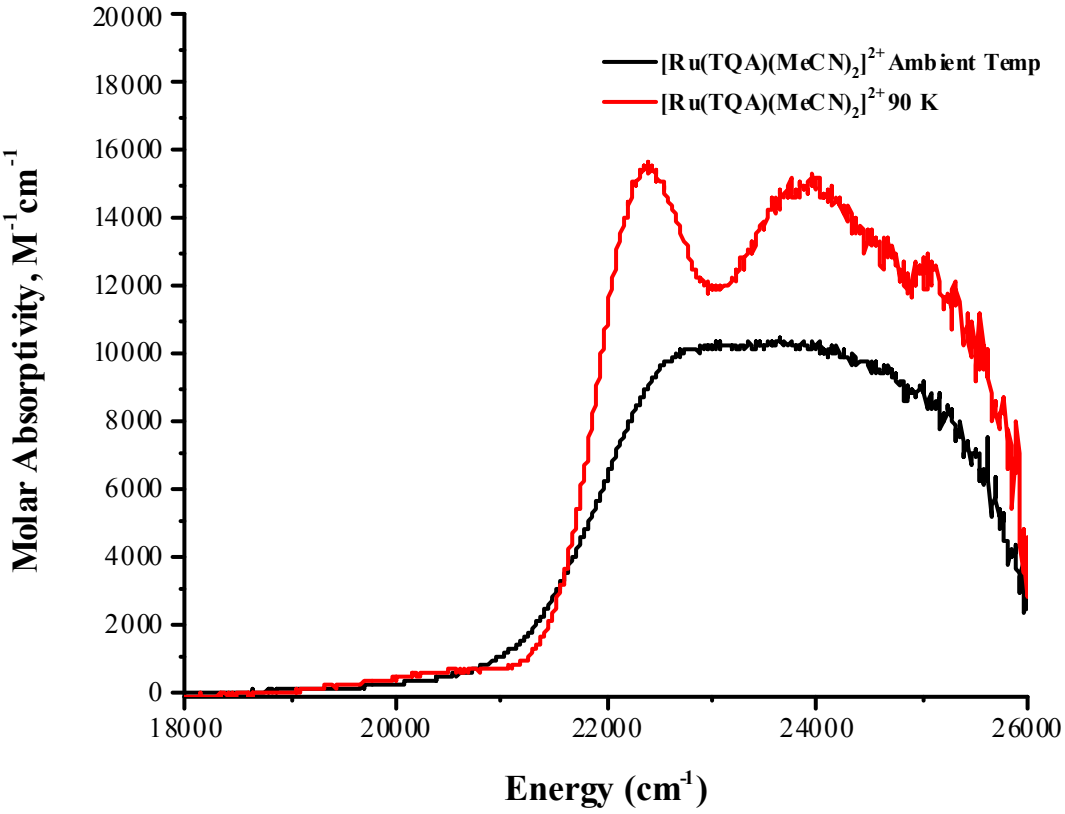

Figure 30: 90 K (red) Absorption Spectrum of $[Ru(TQA)(MeCN)_2]^{2+}$ (6.2×10^{-5} M) in Alcohol[8]

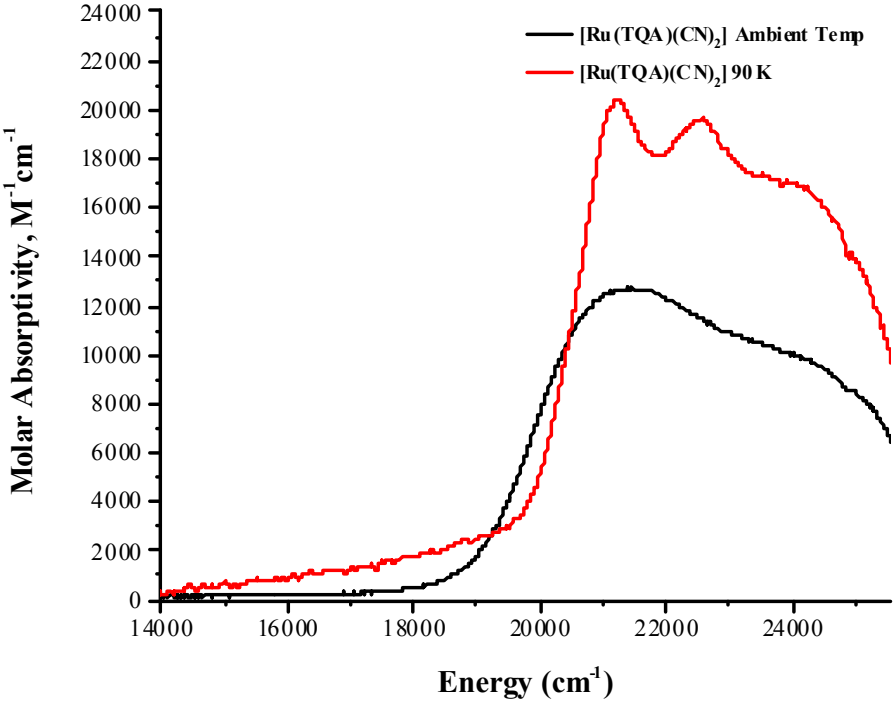

Figure 31: 90 K (red) Absorption Spectrum of $[Ru(TQA)(CN)_2]$ (5.1×10^{-5} M) in Alcohol[8]

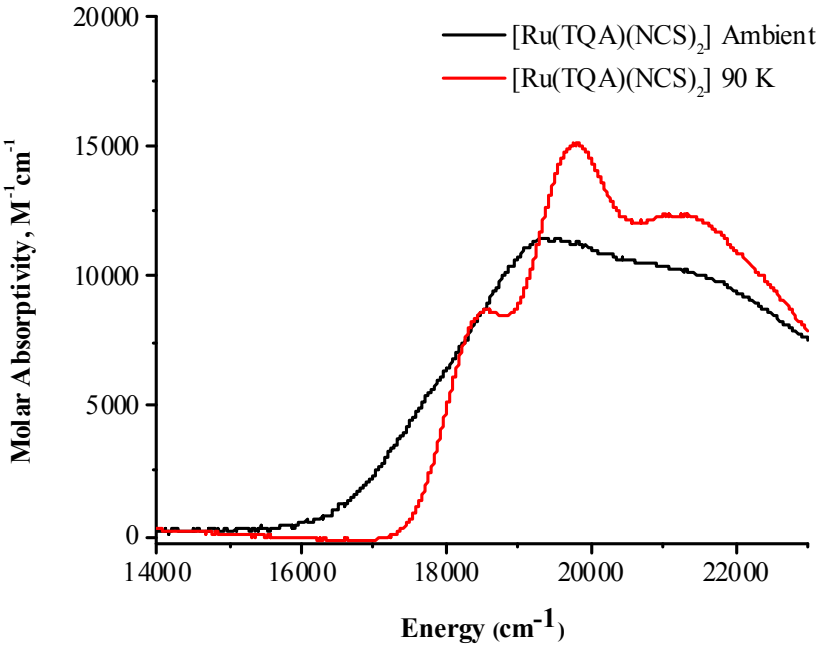

Figure 32: 90 K (red) Absorption Spectrum of [Ru(TQA)(NCS)$_2$] (7.3 x 10^{-5} M) in Butyronitrile[8]

D. Emission Spectra, Lifetime Measurements and Quantum Yield Data

This section is reserved for the photophysical measurements of all complexes investigated the individual projects. Figure 33 compares the energy and bandshapes of the emission spectra for [Ru([14]aneS$_4$)(bpy)]$^{2+}$ (black) and [Ru(MeCN)$_4$(bpy)]$^{2+}$ (red). These two complexes have very similar emission envelopes but quite different emission decays with [Ru(MeCN)$_4$(bpy)]$^{2+}$ (6000 ns) complex being orders of magnitude larger than that of [Ru([14]aneS$_4$)(bpy)]$^{2+}$ (20 ns) complex.

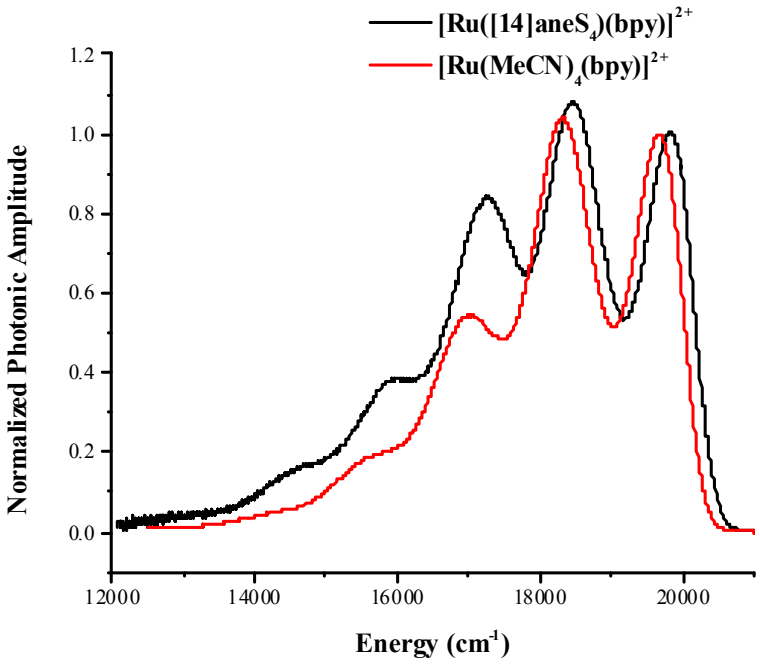

Figure 33: 77 K Emission Spectra of $[Ru([14]aneS_4)(bpy)]^{2+}$ (black, 10^{-4} M) and $[Ru(MeCN)_4(bpy)]^{2+}$ (red, 10^{-4} M) in Butyronitrile using 405 nm excitation[21]

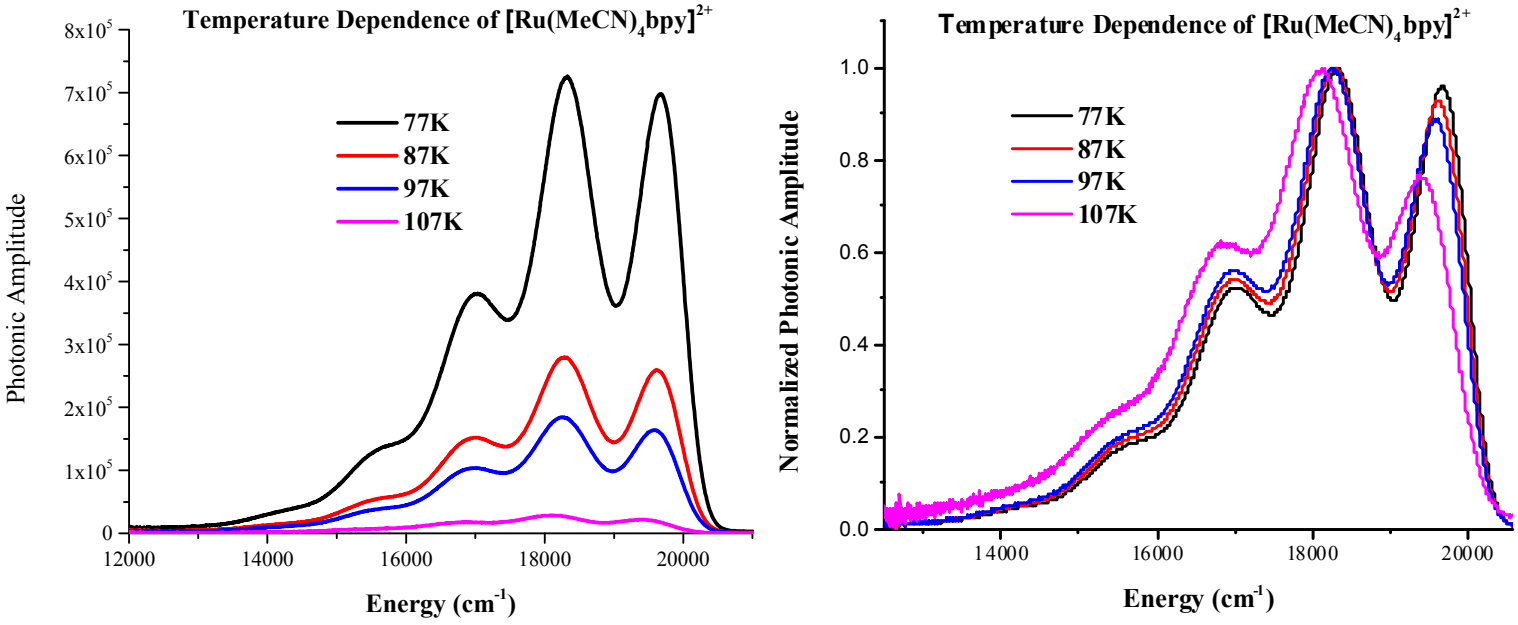

Figure 34: Deareated 77 - 107 K Emission Spectra of $[Ru(MeCN)_4(bpy)]^{2+}$ (2.4 x 10^{-4} M) in Butyronitrile using 405 nm continuous wave excitation for Unnormalized (left) and Normalized (right)[6]

Results from the temperature-dependent emission studies for the $[Ru(MeCN)_4(bpy)]^{2+}$ complex are found in figure 34. The main difference between the left panel and right panel in figure 34 is normalization. The spectra in the left panel was not normalized to emphasize the effect that temperature has on the emission intensity. When the spectra is normalized on the highest relative amplitude peak, it is most noticeable that the highest energy component is decreasing dramatically with the increase in temperature. An additional feature as the temperatue is raised may be an overall band broadening which is may be observed in the energy range of 14,000 – 19,000 cm^{-1}.

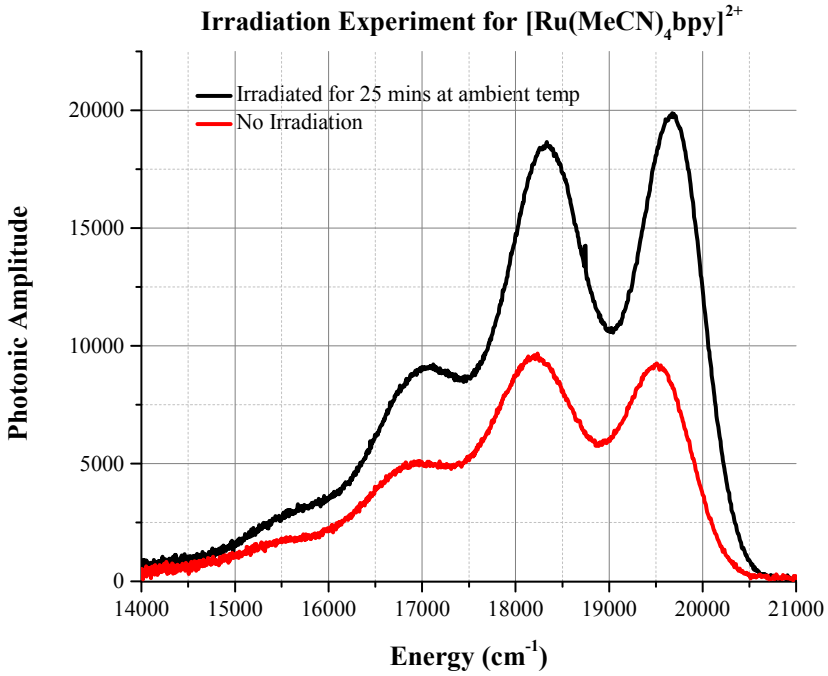

Figure 35: Irradiated at ambient temperature (black) vs. Non-Irradiated (red) Deareated 77 K emission spectra for $[Ru(MeCN)_4(bpy)]^{2+}$ (10^{-4} M) using 405 nm excitation in Butyronitrile

Figure 35 reveals the emission spectra of $[Ru(MeCN)_4(bpy)]^{2+}$ in butyronitrile when the sample is irradiated with a 405 nm (50 mW) continuous wave laser at room temperature for 20 mins prior to a 77 K emission spectrum measurement (black). The trace in red represents the 77 K emission spectrum measurement without prior irradiation. For these emission experiments, the settings for the spectrometer and detector were configured such that it takes 1 min to capture an emission spectrum. The observation from the $[Ru(MeCN)_4(bpy)]^{2+}$ in butyronitrile emission spectra is that there are significant changes in the spectral profile when the sample is subjected to prior irradiation before a low temperature emission spectrum is acquired. These results are consistent with an acetonitrile ligand being replaced by the butyronitrile solvent and contributing to energy shifts and increased spectral amplitude due to a new compound be formed that has a different emission profile than the parent $[Ru(MeCN)_4(bpy)]^{2+}$ complex.

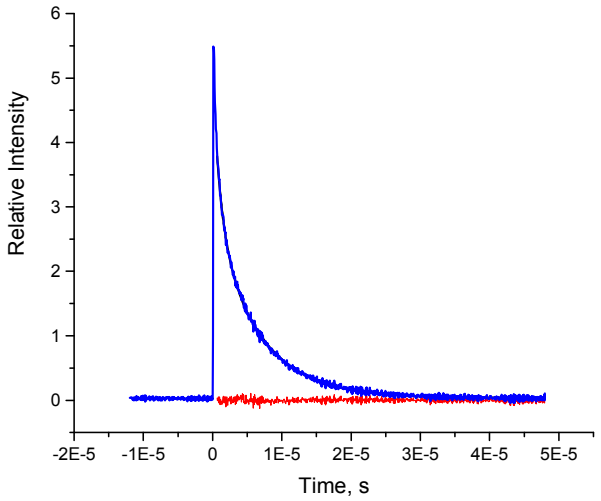

Figure 36: 77 K Emission decay of $[Ru(MeCN)_4bpy]^{2+}$ (2.0×10^{-4} M) in Alcohol using 405 nm pulsed excitation monitored at 510 nm. The two exponential fit (black) and original signal (blue) are indistinguishable; residuals are in red.[6]

The 77 K emission decay for $[Ru(MeCN)_4bpy]^{2+}$ in alcohol is found in figure 36. The decay measurement was done with two exponentials which resulted in random residuals (shown in red). Often times when a decay measurement is found to not have a reasonable monoexponential fit (which is determined by non-random residuals), the concern becomes one of compound purity and/or generated photochemical species. A relatively simple approach is to change the excitation wavelength while monitoring the emission decay at a constant wavelength and also change the emission monitoring wavelength while keeping the excitation wavelength constant. Table 3 examines the 77 K emission lifetime of $[Ru(MeCN)_4bpy]^{2+}$ in alcohol with varying excitation wavelengths between 375 – 415 nm and monitoring the decay at 510 nm. Table 4 represents the 77 K emission lifetime of $[Ru(MeCN)_4bpy]^{2+}$ in butyronitrile with constant 405 nm excitation while varying the monitoring wavelengths between 510 – 600 nm. The lifetime of the longer lived component was found to be about 87% of the overall emission spectrum when varying the excitation wavelength, monitoring wavelength and solvent conditions.

Table 3: 77 K Lifetime measurements of $[Ru(MeCN)_4bpy]^{2+}$ with different excitation wavelengths in Alcohol (Monitored at 510 nm)[6]

Excitation Wavelength (nm)	Single Exponential Fit		Double Exponential Fit[a]				% of 2 in Emission [b]
	Lifetime (μs)	Initial Amplitude	Lifetime 1 (μs)	Initial Amplitude 1	Lifetime 2 (μs)	Initial Amplitude 2	
375	4.7	3.3	1.06	2.2	6.2	2.4	87
380	4.9	3.9	1.00	2.7	6.5	3.0	88
385	5.1	4.1	1.12	2.7	6.7	3.0	87
390	5.2	4.3	1.06	2.9	6.8	3.2	88
395	5.1	3.9	1.12	2.4	6.6	2.9	89
400	5.3	4.0	1.06	2.4	6.6	3.1	89
405	5.1	3.7	1.06	2.2	6.4	2.9	89
410	4.6	2.3	1.17	1.4	6.2	1.6	86
415	4.5	1.9	1.17	1.2	6.1	1.3	85

[a] Fast decay labeled "1"; slow decay labeled "2"

[b] A = initial amplitude; Emission percentage = $100 \times [A(2)\tau(2)/(A(2)\tau(2) + A(1)\tau(1))]$

Table 4: 77 K Lifetime measurements of $[Ru(MeCN)_4bpy]^{2+}$ with different monitoring wavelengths in Butyronitrile (405 nm excitation)[6]

Wavelength Monitored nm	Single Exponential Fit		Double Exponential Fit[a]				% of 2 in Emission [a]
	Lifetime (μs)	Initial Amplitude	Lifetime 1 (μs)	Initial Amplitude 1	Lifetime 2 (μs)	Initial Amplitude 2	
510	5.0	3.9	1.02	3.2	7.0	2.8	86
520	5.3	4.3	0.98	3.9	7.5	3.1	86
530	5.2	4.0	1.03	3.2	7.2	2.9	86
540	5.3	3.9	1.04	2.9	7.1	2.9	87
550	5.2	3.7	1.08	2.7	7.0	2.6	86
560	5.1	3.5	1.11	2.3	6.9	2.6	87
570	5.0	2.9	1.23	1.9	6.8	2.1	86
580	4.8	2.2	1.20	1.5	6.7	1.5	85
590	4.9	2.1	1.35	1.3	6.7	1.5	85
600	4.7	1.8	1.22	1.1	6.4	1.3	86

[a] Fast decay labeled "1"; slow decay labeled "2"

[b] A = initial amplitude; Emission percentage = 100 × [A(2)τ(2)/(A(2)τ(2) + A(1)τ(1))]

Table 5: Temperature dependence of the emission decay lifetime for $[Ru(MeCN)_4bpy]^{2+}$ in Butyronitrile[6]

Temperature (K)	Double Exponential Fit [a]				Relative % Amplitude [b]	% of 2 in Emission [b]
	Lifetime 1 (μs)	Initial Amplitude 1	Lifetime 2 (μs)	Initial Amplitude 2	A1 , A2	
77 [c]	1.07	2.9	6.4	2.8	51 , 49	85
87 [c]	1.02	3.0	5.0	2.2	58 , 42	78
97 [c]	0.81	2.8	3.8	1.1	72 , 28	64
107 [c]	0.50	2.1	2.5	0.49	81 , 19	52
77 [d]	1.43	0.83	6.1	0.77	52 , 48	80
77 [e]	1.02	4.5	7.9	3.8	54 , 46	86
87 [e]	0.84	4.8	5.5	3.6	57 , 43	83
97 [e]	0.75	5.4	3.9	2.5	69 , 31	69
107 [e]	0.66	4.8	3.3	1.2	80 , 20	55

[a] Fast decay labelled "1"; slow decay labelled "2".

[b] A = initial amplitude; Emission percentage = $100 \times \left(\int (A2)e^{-\tau(2)t}dt\right) \div \left(\int (A2)e^{-\tau(2)t}dt + \int (A1)e^{-\tau(1)t}dt\right)$.

[c] Temperature ramped from 77 to 107 K; sample photolyzed for 3 min between lifetime measurements.

[d] Lifetime measurements using 10% T ND filter.

[e] Temperature ramped from 107 to 77 K; no intermediate photolysis.

To access how temperature correlates with the emission decay, temperature-dependent studies were performed on $[Ru(MeCN)_4bpy]^{2+}$ in butyronitrile and the results are summarized in table 5. The emission decay rates are somewhat temperature dependent in the range of 77 K to 107 K. The analysis is somewhat complicated by photochemical effects because the spectral bandshape changes as the temperature is increased. In an effort to determine how the photochemical effects alter the lifetime and amplitude determination, the temperature dependence of the emission decay was examined with and without irradiation periods in addition to varied cryostat cooling sequences.

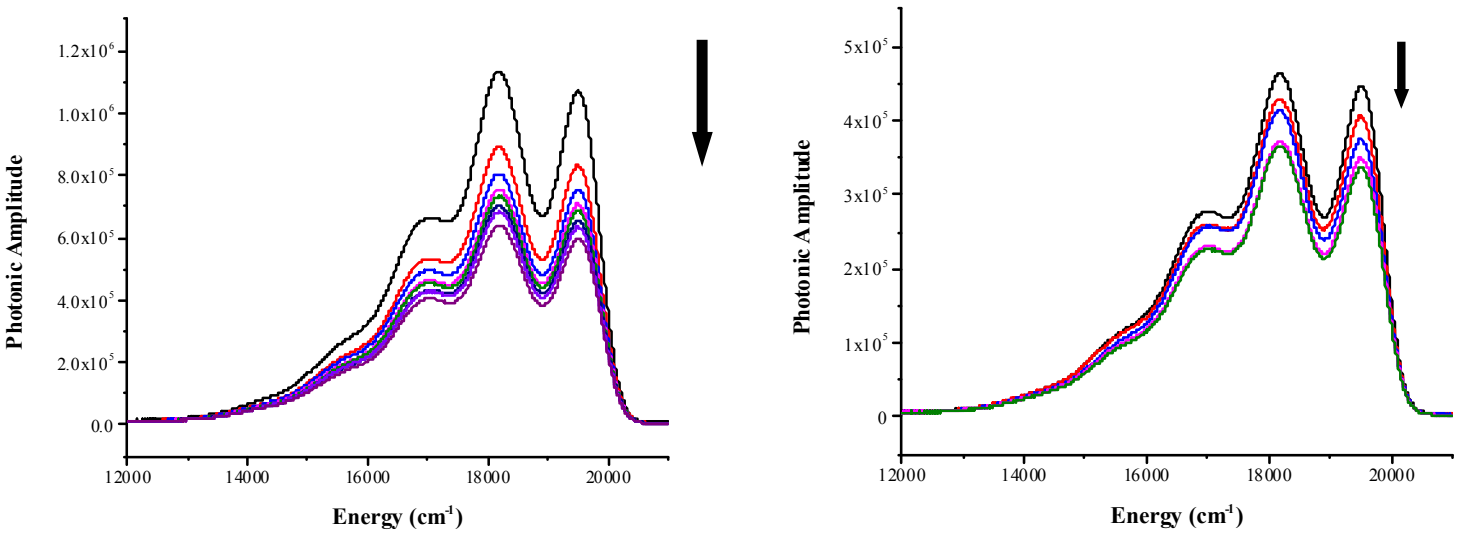

Figure 37: Continuous 405 nm irradiations of $[Ru(MeCN)_4bpy]^{2+}$ (8.4×10^{-4} M) in Alcohol without neutral density filter (left) and with 50% T neutral density filter (right)[6]

Figure 37 represents the continuous 405 nm irradiation experiment of $[Ru(MeCN)_4bpy]^{2+}$ in alcohol at 77 K. The spectral accumulations required 1 minute irradiation each. The arrows indicate increasing photolysis time and corresponding spectroscopic changes. The spectra in the left panel was irradiated with the unfiltered output of a 50 mW diode laser for 3 minutes between each spectral accumulation (seven irradiation periods) while the spectra was irradiated using a

50% T neutral density filter in the 50 mW diode laser excitation beam with irradiation periods of 360 s between the first four spectral accumulations and 180 s between the last two. The total irradiation time for both was 21 minutes. This experiment reveals that long periods of irradiation causes significant changes in the emission spectra when the laser beam is at 50 mW and ~ 25 mW respectively even at 77 K. These changes are linked to a new photochemical species being formed at 77 K that correlate an acetonitrile ligand being replaced by alcohol solvent and contributing to decreased spectral amplitude due to a new compound be formed that has a lower energy emission profile than the parent $[Ru(MeCN)_4(bpy)]^{2+}$ complex.

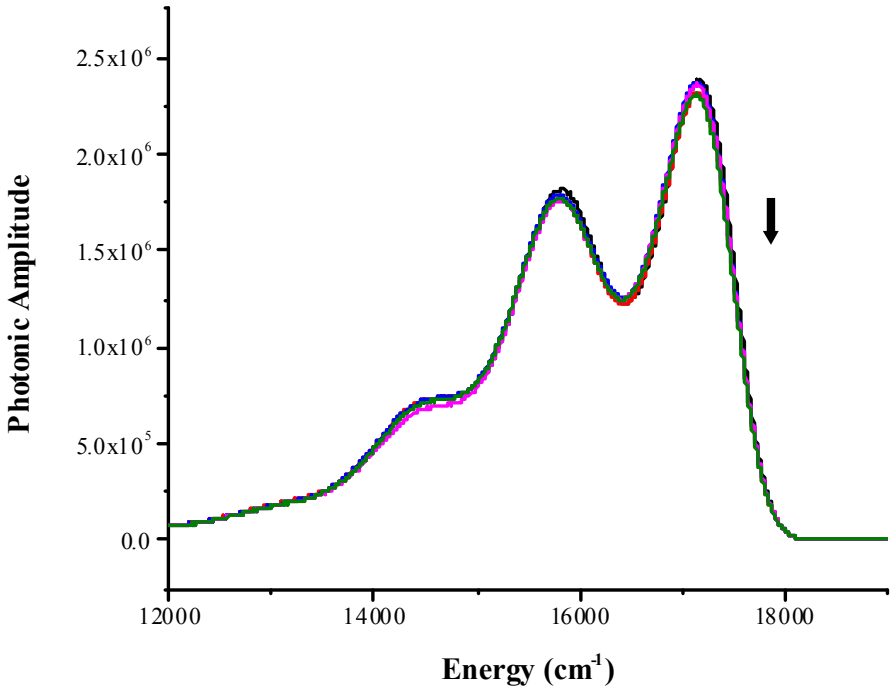

Figure 38: Continuous 405 nm irradiations of $[Ru(bpy)_3]^{2+}$ (10^{-4} M) in Alcohol[6]

Figure 38 is the collection of emission spectra for $[Ru(bpy)_3]^{2+}$ that was acquired using spectral accumulations of 1 minute irradiation for each spectrum. The arrow indicates increasing photolysis time and corresponding spectroscopic changes. The sample was irradiated using a 50% T neutral density filter in the 50 mW diode laser excitation beam with irradiation periods of

360 s between the first four spectral accumulations and 180 s between the last two. The total time of irradiation was 21 minutes. $[Ru(bpy)_3]^{2+}$ is used for many spectroscopic baseline experiments to assure that the experimental conditions are reasonably optimal prior to acquiring results for less "robust" compounds. The extent of spectral changes for $[Ru(bpy)_3]^{2+}$ is much less than $[Ru(MeCN)_4bpy]^{2+}$ under the same conditions.

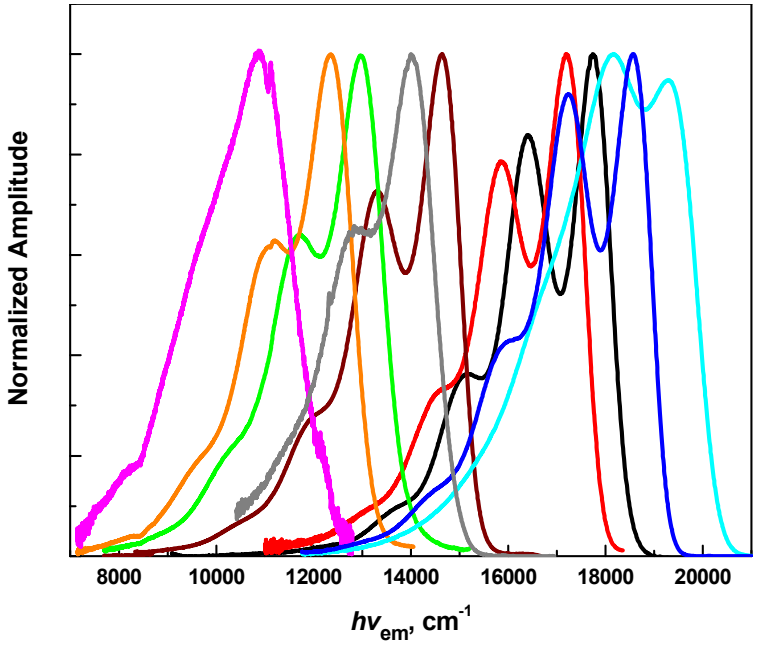

Figure 39: 77 K emission spectra of the complexes. From right to left, $[Ru(bpy)([9]aneS_3)(CN)]^+$ (cyan); $[Ru(bpy)_2(NCCH_3)_2]^{2+}$ (blue); $[Ru(tpm)(bpy)(CH_3CN)]^{2+}$ (black); $[Ru(bpy)_3]^{3+}$ (red); $[Ru(bpy)_2(NH_3)_2]^{2+}$ (wine); $[Ru(bpy)_2(acac)]^+$ (gray); $[Ru(bpy)(en)_2]^{2+}$ (green); $[Ru(bpy)(NH_3)_4]^{2+}$ (orange); $[Ru(bpy)(acac)_2]$ (magenta).[7]

Table 6: 77 K emission rate constants and quantum yields of some Ru-bpy complexes[a7]

Code	$(L)_4$ for $[Ru(L)_4bpy]^{m+}$ Complexes	$h\nu_{max}$(em), $cm^{-1}/10^3$ bun {alc}	$h\nu_{ave}$, $cm^{-1}/10^3$; bun {alc}	k_{obs}, μs^{-1} [b] bun {alc}	$\Phi \times 10^4$ [c] bun {alc}	k_{RAD}, μs^{-1} [d] bun {alc}	k_{NRD}, μs^{-1} [e] bun {alc}
1	**([9]aneS$_3$)(CN)**	{19.2}	{17.5}	{0.063}	{3600 ± 1100}	{0.023±0.007}	{0.040±0.007}
2	**(bpy)(CH$_3$CN)$_2$**	{18.5}	{16.8}	{0.120}	{6300 ± 1400}	{0.076±0.016}	{0.044±0.016}
3	**(tpm)(CH$_3$CN)**	17.74	16.50	**0.15**	5400 ± 800	0.081 ± 0.012	0.069± 0.012
4	**(bpy)$_2$**	17.25[f] {17.12} [g]	16.09 {16.04}	0.13 [f] {0.19} [g]	4500 ± 700 {3800}[g]	0.059 ± 0.009 {0.072}[g]	0.072 ± 0.009, {0.12}[g]
5	(bpy) $(CN)_2$	{17.12}[g]	{15.87}	{0.25} [g]	{2700}[g]	{0.068}[g]	{0.19}[g]
6	(bpy)(en)	15.11;[f] {14.78} [g]	14.21 {13.95}	0.69[f] {1.0 } [g]	570 ± 80; {0.022}[g]	0.039 ± 0.006; {0.023}[g]	0.65; {1.0}[g]
7	(bpy)$(NH_3)_2$	14.70;[f] {14.40}	13.73 {13.48}	1.7 [f] {2.9}	180 ± 40; {37 ± 7}	0.031 ± 0.006; {0.011 ± 0.002}	1.7; {2.9}
8	**(bpy)(ox)**	{14.2}[g]	{12.9}	{1.8}[g]	{130}[g]	{0.024}[g]	{1.8}[g]
9	**(bpy)(acac)**	{13.9}	{12.9}	{1.4}	{230±40}	{0.032±0.006}	{1.4}
10	$(NH_3)_3$(pz)	13.98[h] {13.78}	13.20 {12.91}	4.8[h] {8.7}	85 ± 17; {26 ± 6}	0.041 ± 0.008 {0.023 ± 0.005}	4.7 {8.7}
11	$(NH_3)_3(CH_3CN)$	13.81 {13.57}	12.92 {12.66}	4.6 ; {8.6}	55 ± 10; {29 ± 6}	0.025 ± 0.005 {0.025 ± 0.004}	4.5 ; {8.6}
12	$(NH_3)_3$(acpy)	13.78 {13.32}	12.93 {12.50}	5.9 ; {12}	56 ± 17; {25 ± 5}	0.033 ± 0.010 {0.029 ± 0.006}	5.9 ; {12}
13	$(NH_3)_3$(py)	13.48 [h] {13.11}	12.60 {12.21}	6.3;[h] {12}	36 ± 7; {13 ± 3}	0.023 ± 0.004 {0.016 ± 0.003}	6.2 {12}
14	([14]aneN_4)	13.99;[f] {13.84}	13.13 {13.04}	0.98;[f] {1.8}	86 ± 12 {26 ± 4}	0.0084 ± 0.0012 {0.0046 ± 0.0008}	0.97 {1.8}
15	$(en)_2$	13.01;[f] {12.70}	12.07 {11.82}	9.5[f] {19±1}	20 ± 4, {3.8 ± 0.8}	0.019 ± 0.004 {0.0070 ± 0.0017}	9.5 {19±1}
16	$(NH_3)_4$	12.4;[f] {11.89}	11.45 {11.07}	22;[f] {39}	5.5 ± 1.7; {1.2 ± 0.4}	0.012 ± 0.004 {0.0047 ± 0.0015}	22; {39}

[a] $h\nu_{max}$(em), determined in butyronitrile (bun) or ethanol/methanol (alc; v/v' = 4/1) solution. [b] Mean excited state decay rate constant, $k_{obs} = 1/\tau$. [c] emission quantum yield; error bars based on replicate determinations. [d] $k_{RAD} = \phi k_{obsd}$. [e] $k_{NRD} = k_{obsd} - k_{RAD}$. [f] Refs.[32, 53-54]. [g] Ref.[32, 55] [h] Ref. [56] . Compounds in **bold** where determined and/or redetermined by R. A. Thomas.

Figure 39 and table 6 summarizes the spectroscopic results observed for many Ru-bpy complexes examined in the radiative rate constant project. These particular complexes offer a useful emission energy range for comparison spanning from 10,000 – 20,000 cm^{-1}.

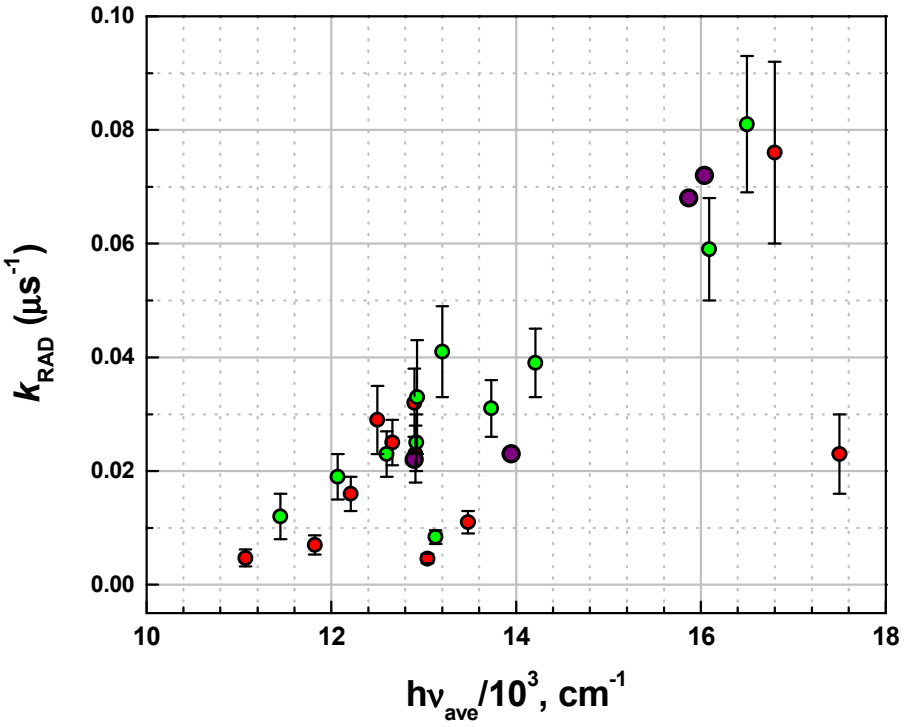

Figure 40: Comparison of the observed radiative rate constants (circles) with ($h\nu_{ave}$). Green circles, in butyronitrile; red circles, in alcohol; purple circles, Demas and Crosby data in alcohol.[7]

Figures 40 – 42 represents a detailed analysis of averaged emission energy and its correlation with radiative rate constants. Figure 40 contains all of the complexes that are investigated and revealed in table 6. Figure 41 is quite similar to figure 40 except that the complexes that are found to have ^{3}MC states lower in energy than the ^{3}MLCT states are removed from the analysis. Figure 42 compares the averaged emission energy to the observed radiative rate constant divided by the cubed averaged emission energy.

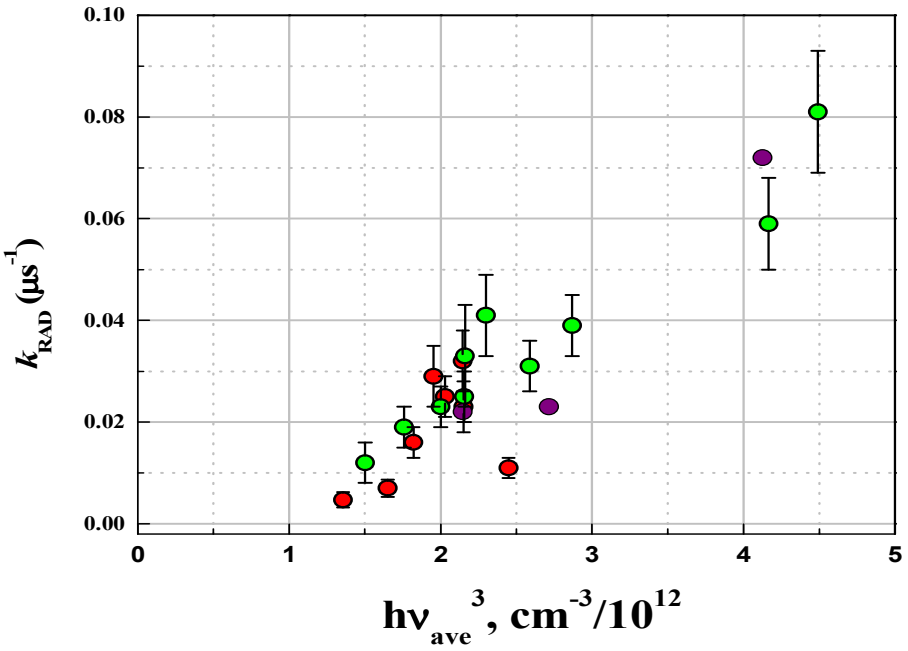

Figure 41: Comparison of the observed radiative rate constants (circles) with $(h\nu_{ave})^3$ for complexes with E(^{3}MC) > E(^{3}MLCT). Green circles, in butyronitrile; red circles, in alcohol; purple circles, Demas and Crosby data in alcohol. A least squares line through experimental data results in $R^2 = 0.82$.[7]

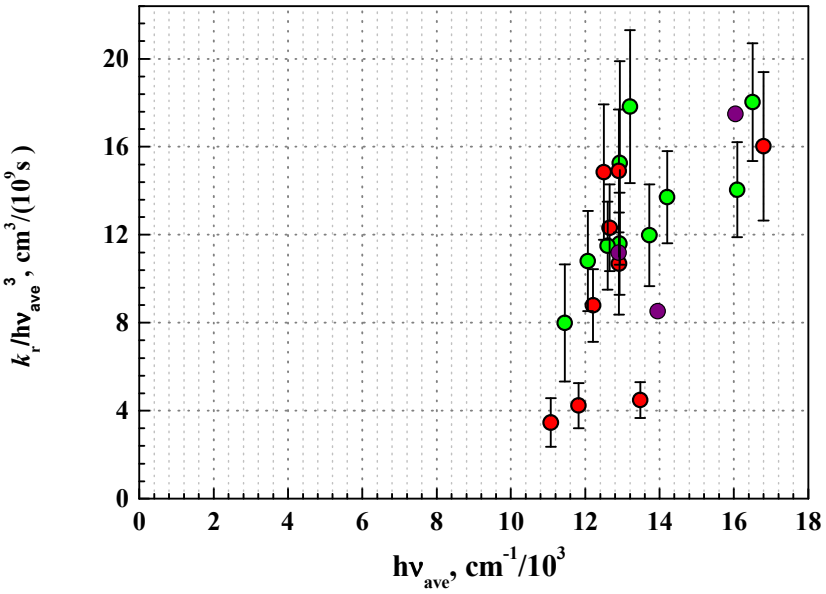

Figure 42: Comparison of the $k_{RAD}/(h\nu_{ave})^3$ with $h\nu_{ave}$ for complexes with E(^{3}MC) > E(^{3}MLCT). Green circles, in butyronitrile; red circles, in alcohol; purple circles, Demas and Crosby data in alcohol.[7]

Figure 43 and table 7 summarizes the spectroscopic measurements found for the [9]aneS_3 and [15]dieneS_3bpy complexes. These complexes span a fairly small emission energy range of 16,000 – 19,000 cm^{-1}. From this limited data set, the [9]aneS_3 based complexes seem to have higher emission energies than the [15]dieneS_3bpy. This effect may come from the extended conjugated macrocyclic network of the [15]dieneS_3bpy complexes. The $[Ru([9]aneS_3)(bpy)MeCN]^{2+}$ and $[Ru([15]dieneS_3bpy)MeCN]^{2+}$ complexes both proved to be troublesome with at least biexponential decays. Based on previous examinations of $[Ru(MeCN)_4bpy]^{2+}$ with acetonitrile ancillary ligands, the biexponential decay of the

$[Ru([9]aneS_3)(bpy)MeCN]^{2+}$ and $[Ru([15]dieneS_3bpy)MeCN]^{2+}$ complexes may be due to intrinsic behavior with Ru-bpy complexes with acetonitrile ligands.

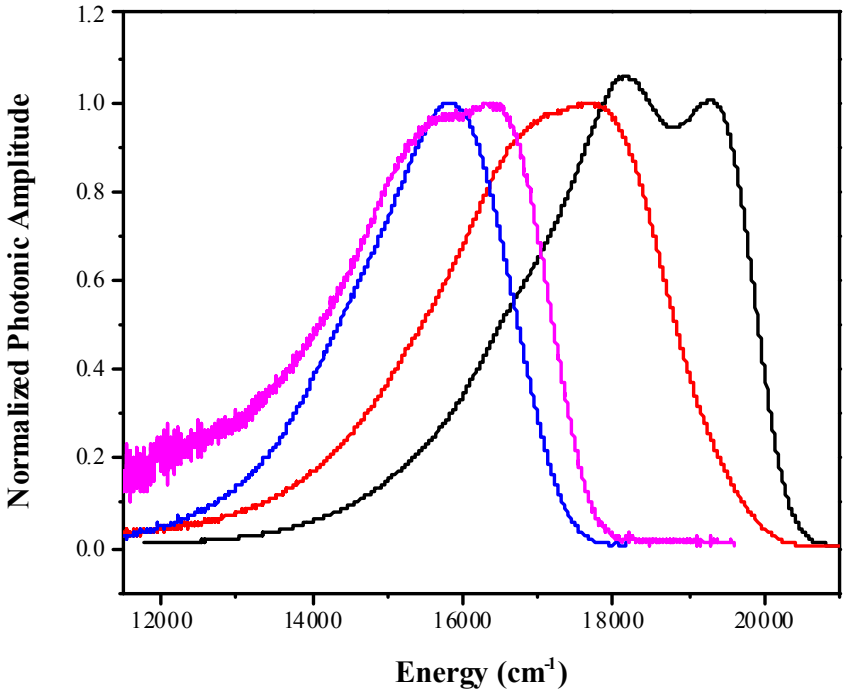

Figure 43: 77 K emission spectra of the complexes. From left to right, $[Ru([15]dieneS_3bpy)Cl]^+$ (blue), $[Ru([9]aneS_3)(bpy)Cl]^+$ (magenta), $[Ru([15]dieneS_3bpy)CN]^+$ (red) and $[Ru([9]aneS_3)(bpy)CN]^+$ (black) determined in Butyronitrile. The $[Ru([9]aneS_3)(bpy)CN]^+$ spectrum was determined in Alcohol.

Table 7: 77 K emission rate constants and quantum yields of the [9]aneS$_3$ and [15]dieneS$_3$bpy Complexes

[Ru([9]aneS$_3$)(bpy)(X)]$^{m+}$ or [Ru([15]dieneS$_3$bpy)(X)]$^{m+}$	hν_{max}(em), cm^{-1}/10^3 bun;{alc}	hν_{ave}, cm^{-1}/10^3 bun;{alc}	k_{obs}, μs^{-1} [b] bun;{alc}	Φ [c] bun; {alc}	k_r, μs^{-1} [d] bun; {alc}	k_{nr}, μs^{-1} [e] bun; {alc}
([9]aneS$_3$)(CN$^-$)	{19.2}	{17.5}	{0.063}	{0.361 ± 0.105}	{0.023±0.0067}	{0.040±0.0067}
([15]dieneS$_3$bpy)(CN$^-$)	17.7	16.3	0.065	0.124±0.002	0.0080±1E-4	0.057±1E-4
([9]aneS$_3$)(Cl$^-$)	16.7	14.7	50.0[f]	0.0623±0.0013	3.12±0.07	46.9±0.07
([15]dieneS$_3$bpy)(Cl$^-$)	15.9	14.9	55.9	0.132±0.003	7.38±0.17	48.52±0.17

[a] $h\nu_{max}$(em), determined in butyronitrile (bun) or ethanol/methanol (alc; v/v' = 4/1) solution. [b] Mean excited state decay rate constant, $k_{obs} = 1/\tau$. Reported values are the averaged result of at least 100 decay traces. [c] emission quantum yield; error bars based on replicate determinations. [d] $k_r = \phi k_{obsd}$. [e] $k_{nr} = k_{obsd} - k_r$. [f] *Organometallics*, **2010**, *29* (23), pp 6259–6266.

Figures 44 and 45 are representative of the 77 K emission and corresponding lifetime of the $[Ru(TQA)(L)_2]^{m+}$ complexes where L = MeCN, CN and NCS. These complexes have emission energies that are quite similar to the direct Ru-bpy analogs (summarized in Table 8), but much different radiative rate constants and lifetimes. For instance, $[Ru(TQA)(MeCN)_2]^{2+}$ has an emission lifetime of 145 μs while $[Ru(bpy)_2(MeCN)_2]^{2+}$ emission lifetime is 8 μs. The TQA complexes are interesting in that they represent a unique class of Ru-photosensitizers.

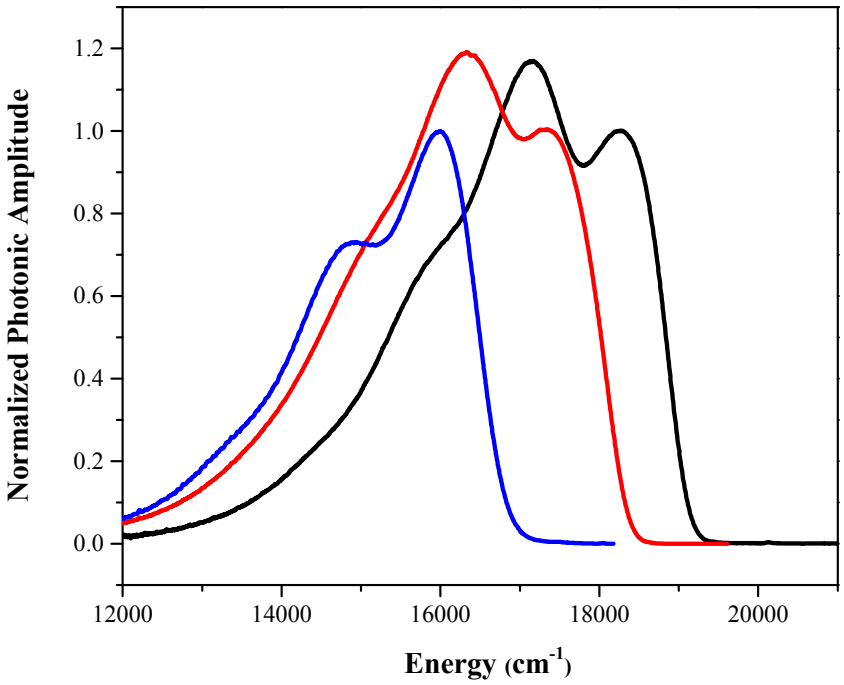

Figure 44: 77 K Emission Spectra of $[Ru(TQA)(L)_2]^{m+}$ complexes (L = MeCN (black) in Alcohol, CN (red) in Alcohol and NCS (blue) in Butyronitrile)

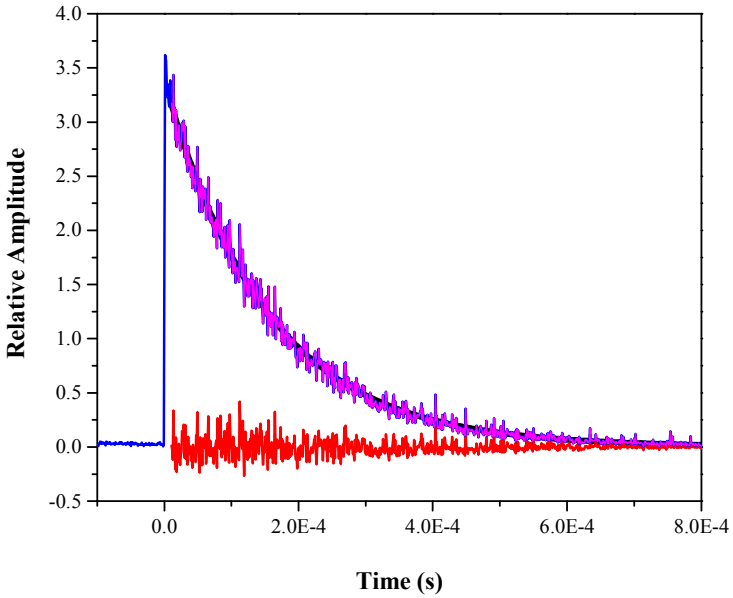

Figure 45: 77 K Emission decay of $[Ru(TQA)(MeCN)_2]^{2+}$ in Alcohol

Table 8: Emission Rate Constants and Quantum Yields for some-Ruthenium Complexes

Complex	$h\nu_{abs(max)}$[g] ($cm^{-1}/10^3$) 90 K; (298 K)	$h\nu_{em(max)}$[g] ($cm^1/10^3$) 77 K; (298 K)	k_{obs} (μs^{-1})[d] 77 K; (298 K)	Φ 77 K; (298 K)	k_r, (μs^{-1})[e] 77 K; (298 K)	k_{nr}, (μs^{-1})[f] 77 K; (298 K)
$[Ru(TQA)(MeCN)_2]^{2+}$[a]	22.4;(22.7)	18.3	0.0069	0.452±0.016	0.0031±1 x 10^{-4}	0.0036±1 x 10^{-4}
$[Ru(bpy)_2(MeCN)_2]^{2+}$[a]	23.3;(23.5)	18.5	0.120	0.63 ±0.14	0.076±0.016	0.044±0.016
$[Ru(TQA)(NCS)_2]$[h]	19.8;(19.3)	16.0	0.058	0.499±0.064	0.0290±0.004	0.0291±0.004
$[Ru(bpy)_2(NCS)_2]$[h]	19.8;(19.2)	14.9	1.74	0.0840	0.146	1.59
$[Ru(TQA)(CN)_2]$[a]	21.4;(21.3)	17.3	0.013	0.26±0.049	0.0034±6 x 10^{-4}	0.0097±6 x 10^{-4}
$[Ru(bpy)_2(CN)_2]$[a,56]	17.2;(21.6)	15.9	0.25	0.270	0.068	0.19
$[Ru(bpy)_3]^{2+}$[d]	(21.9)[b]	17.25[i] ;(16.1)[b]	0.13[h] ;(1.12)[b]	0.450[h] ;(0.059)[b]	0.059[h] ;(0.066)[b]	0.072[h] ;(1.05)[b]
mer-$[Ru((dqp)P)_2]^{2+}$[b 57]	(20.0)	(14.6)	(0.37)	(0.013)	(0.0048)	(0.36)
$[Ru(Ph\text{-}tpy)(L1)]^{2+}$[b,j 58]	(16.1)	(11.1)	(7.8)[i]	(0.001)	(0.0078)[i]	(7.7)[i]
$[Ru(p\text{-}Tolyl\text{-}tpy)(L1)]^{2+}$[b,j 58]	(16.1)	(11.1)	(11.2)[i]	(0.001)	(0.0112)[i]	(11.2)[i]
$[Ru(tpy)_2]^{2+}$[c]	(21.1)[b,c]	16.7[a,k] (15.9)[b,c]	0.091[a,k] (4000)[b,c]	0.48[a,k] (≤5 × 10^{-6})[b,c]	0.044[a,k](0.020)[b,c]	0.44[a,k](4000)[b,c]

[a] Determined in ethanol/methanol (v/v' = 4/1) solvent. [b] Acetonitrile. [c] From Maestri, M.; Armaroli, N.; Balzani, V.; Constable, E. C.; Thompson, A. M. W. C., *Inorg. Chem.* **1995,** *34*, 2759. [d] $k_{obs} = 1/\tau$. [e] $k_r = \Phi\ k_{obs}$ [f] $k_{nr} = k_{obs} - k_r$. [g] $h\nu_{abs(max)\ or}\ h\nu_{ems(max)}$ = highest energy component. [h] Butyronitrile. [i] Dominant lifetime component. [j] L1 = 2,6-diguanidylpyridine or dgpy. [k] From Sauvage, J-P.; Collin, J-P.; Chambron, J-C.; Guillerez, S.; Coudret, C.; Balzani, V.; Barigelletti, F.; De Cola, L.; Flamigni, L., Chem. Rev. **1994**, 94, 993.

E. Computational Results and Comparisons

Figure 46 and table 9 correspond to the computational results found for the electrochemistry for the [9]aneS$_3$ and [15]dieneS$_3$bpy complexes as compared to the experimental measurements. The figure illustrates a linear correlation (R^2 = 0.96) for the experimental to calculated results. Table 9 summarizes the computed values obtained for the electrochemical calculations determined at the B3PW91/SDD/6-311+G(d,p) level of theory.

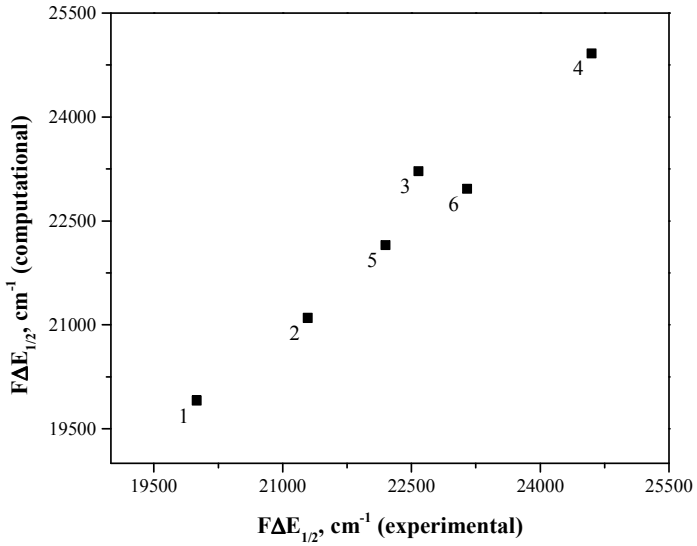

Figure 46: Experimental vs. Computational Electrochemical comparison for the [9]aneS$_3$ and [15]dieneS$_3$bpy complexes, 1 = [Ru([15]dieneS$_3$bpy)(Cl)][PF$_6$], 2 = [Ru([9]aneS$_3$)(bpy)(Cl)][PF$_6$], 3 = [Ru([15]dieneS$_3$bpy)(MeCN)$_2$][PF$_6$]$_2$, 4 = [Ru([9]aneS$_3$)(bpy)(MeCN)][PF$_6$]$_2$, 5 = [Ru([15]dieneS$_3$bpy)(CN)][PF$_6$] and 6 = [Ru([9]aneS$_3$)(bpy)(Cl)][PF$_6$]. R^2 = 0.96 (y = 1.09±0.095 - 2041)

Table 9: Calculated Redox potential differences for [9]aneS$_3$ and [15]dieneS$_3$bpy complexes

Ru([9]aneS3)(bpy)X	Redox St.	E(sol) Eh	G(corr) Eh	G(sol) Eh	ΔG (sol) eV	$E_{1/2}$(NHE) 4.43 ev	$F\Delta E_{1/2}$ (exp), cm^{-1}	$F\Delta E_{1/2}$ comp, cm^{-1}
Cl-	S=0 GS	-2480.338	0.292687	-2480.045	0			
	S=1/2 oxid	-2480.132	0.293567	-2479.838	-5.637025	1.207025		
	S=1/2 red	-2480.445	0.28891	-2480.156	-3.020823	-1.409176	21291.6	21099.6
CH_3CN	S=0 GS	-2152.715	0.337095	-2152.378	0			
	S=1/2 oxid	-2152.480	0.337755	-2152.142	-6.401719	1.971719		
	S=1/2 red	-2152.831	0.331331	-2152.499	-3.311818	-1.118181	24598.3	24920.0
CN-	S=0 GS	-2112.967	0.299867	-2112.667	0			
	S=1/2 oxid	-2112.749	0.300067	-2112.449	-5.916204	1.486204	23146.6	22966.3
	S=1/2 red	-2113.075	0.295698	-2112.779	-3.068550	-1.361449		

Ru([15]dieneS3bpy)X	Redox St.	E(sol) Eh	G(corr) Eh	G(sol) Eh	ΔG (sol) eV	$E_{1/2}$(NHE) 4.43 ev	$F\Delta E_{1/2}$ (exp), cm^{-1}	$F\Delta E_{1/2}$ (comp), cm^{-1}
Cl-	S=0 GS	-2479.141	0.271638	-2478.869	0			
	S=1/2 oxid	-2478.936	0.272583	-2478.664	-5.594819	1.164819	20001.2	19908.0
	S=1/2 red	-2479.250	0.266076	-2478.984	-3.126373	-1.303626		
CH_3CN	S=0 GS	-2151.517	0.315507	-2151.202	0			
	S=1/2 oxid	-2151.287	0.316423	-2150.971	-6.277103	1.847100	22582	23216.9
	S=1/2 red	-2151.635	0.30899	-2151.326	-3.398371	-1.031628		
CN-	S=0 GS	-2111.769	0.277212	-2111.492	0			
	S=1/2 oxid	-2111.554	0.277319	-2111.277	-5.851198	1.421198	22200	22150.6
	S=1/2 red	-2111.880	0.274174	-2111.606	-3.104686	-1.325313		

S = 0 implies $[Ru^{II}$(trithia ligand)(bpy)X$]^{m+}$ singlet ground state, S = 1/2 oxid implies $[Ru^{III}$(trithia ligand)(bpy)X$]^{(m+1)+}$ oxidized state, and S = 1/2 red implies $[Ru^{II}$(trithia ligand)(bpy^{-1})X$]^{(m-1)+}$ reduced state. E(sol) = E(SCF) + ΔG_{solv}, computed at the B3PW91/SDD/6-311+G(d,p) level of theory, where E(SCF) is the electronic energy and ΔGsolv is the continuum solvation energy stabilization for that ion. G_{corr} are the thermal corrections to go from E(sol) →G(sol), computed at the B3PW91/SDDall level of theory.

Figures 47 – 50 are the time-dependent density functional theory (TD-DFT) calculations (blue trace and black bars) determined for some Ru-bpy complexes as compared to their ambient (black trace) and low temperature (red trace) experimental absorptions. Overall there seems to be a systematic deviation from experimental results to the calculated determinations when comparing the dominant transitions but the general relative features of the experimental spectra are more apparent in the 90 K spectra. For instance, the calculated [Ru(bpy)$_2$malonate] (found in figure 47) , the dominant transitions at 16,293 cm^{-1} and 19,774 cm^{-1} differ from the experimental spectrum 440 cm^{-1} and 710 cm^{-1} respectively. The energy spacing between the dominant transitions for the calculated spectrum to the experimental spectrum are 3500 cm^{-1} to 3025 cm^{-1}, respectively.

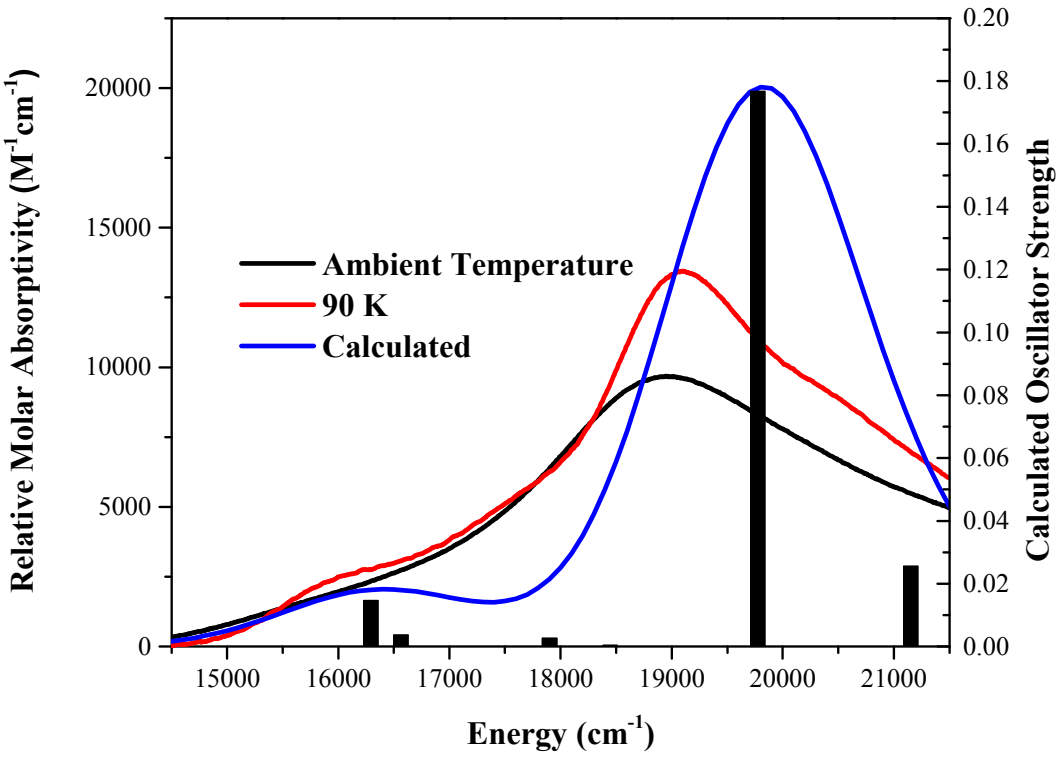

Figure 47: Theoretical (Blue line spectra and oscillator strengthbars) vs. Experimental (90 K in red and ambient in black) Absorption Spectra for [Ru(bpy)$_2$malonate] (Calculations from Inorg. Chem. **2010**, 49, 6840–6852.)

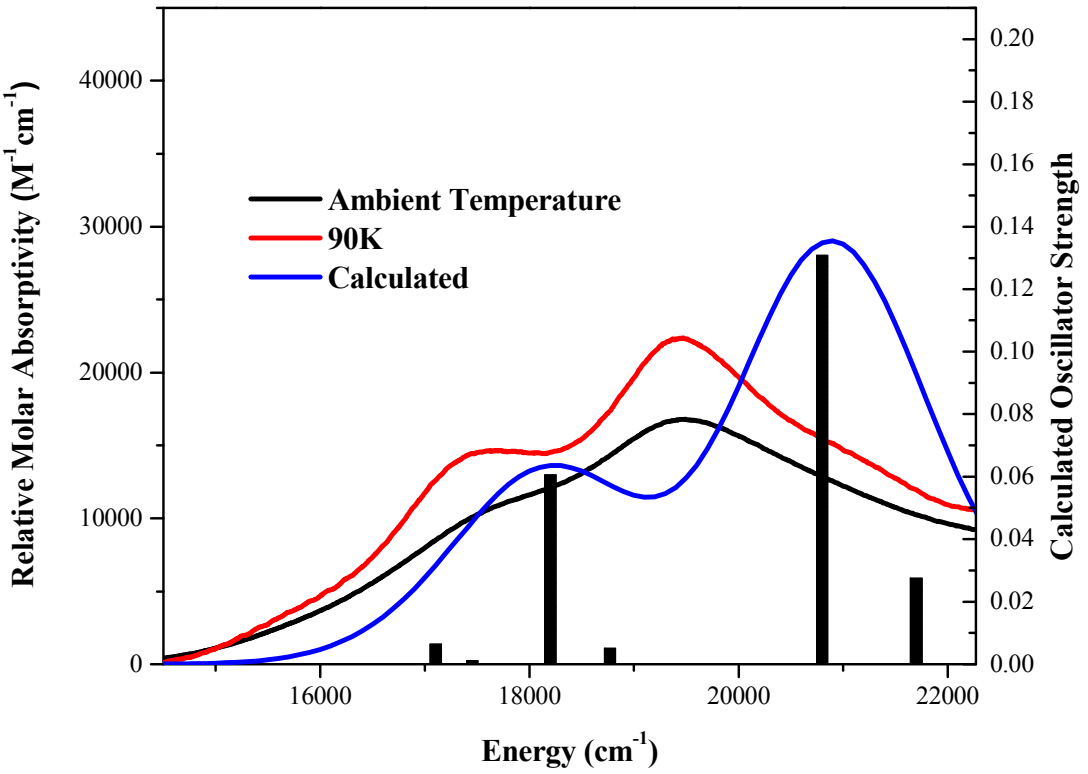

Figure 48: Theoretical (Blue line spectra and oscillator strengthbars) vs. Experimental (90 K in red and ambient in black) Absorption Spectra for $[Ru(bpy)_2acac]^+$ (Calculations from Inorg. Chem. **2010**, 49, 6840–6852.)

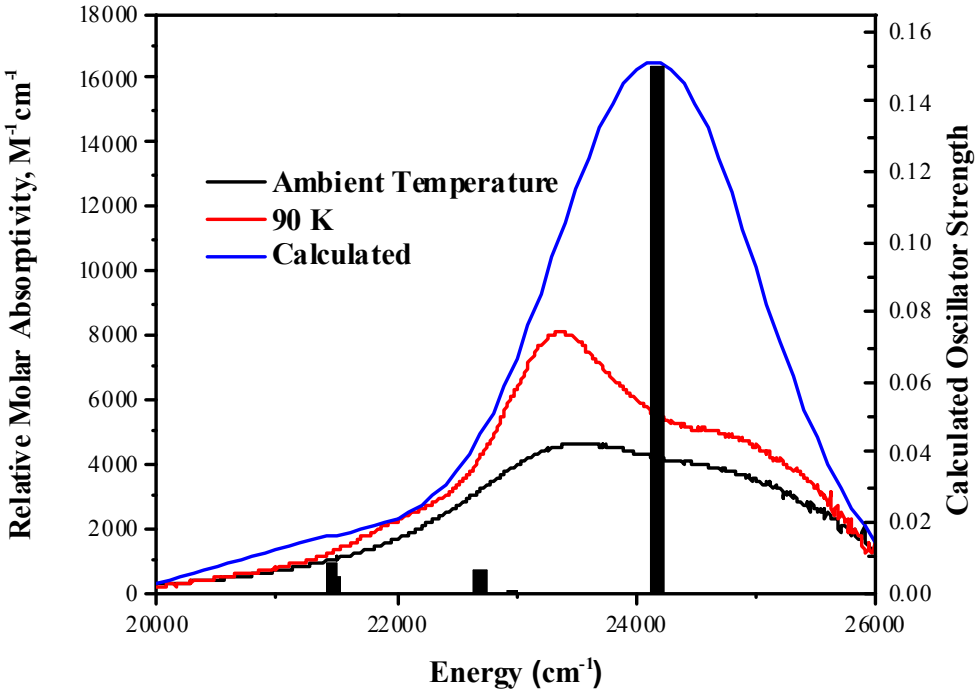

Figure 49: Theoretical (Blue line spectra and oscillator strengthbars) vs. Experimental (90 K in red and ambient in black) Absorption Spectra for $[Ru(bpy)_2(MeCN)_2]^{2+}$ (Calculations from Inorg. Chem. **2010**, 49, 6840–6852.)

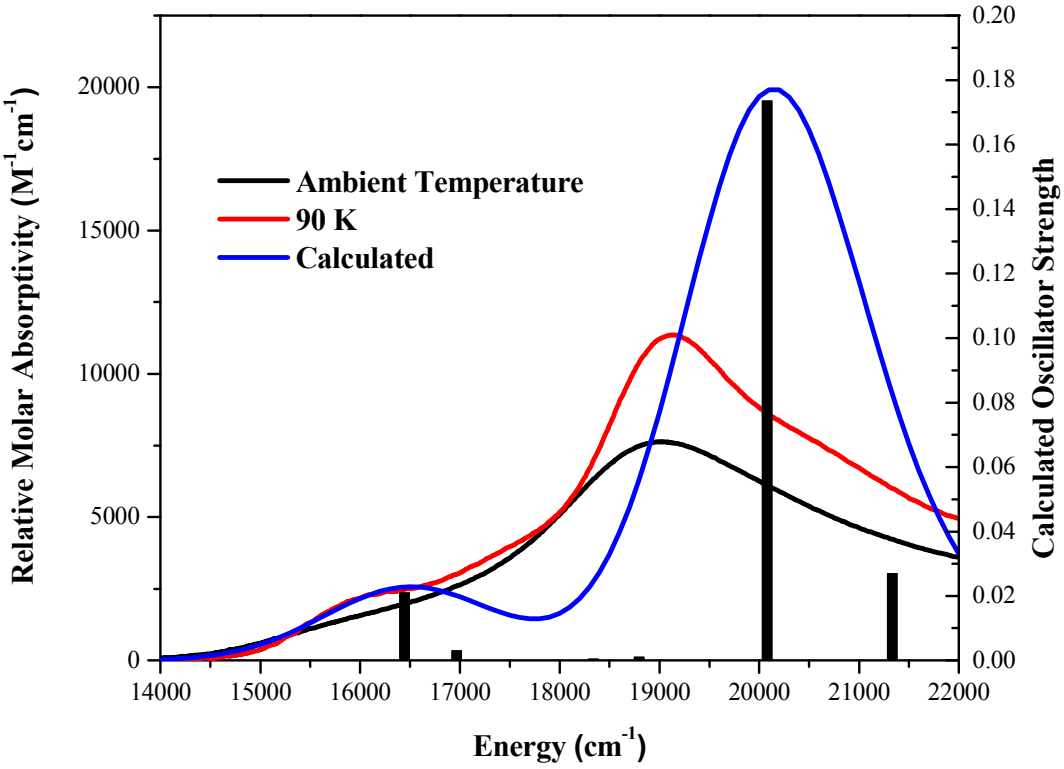

Figure 50: Theoretical (Blue line spectra and oscillator strengthbars) vs. Experimental (90 K in red and ambient in black) Absorption Spectra for [Ru(bpy)$_2$oxalate] (Calculations from Inorg. Chem. **2010**, 49, 6840–6852.)

CHAPTER V: Discussion and Conclusions for Individual Projects (A – D)

A. Triplet Metal-to-Ligand Charge Transfer (^{3}MLCT) Excited State Structures

The 77 K emission spectra of $[Ru(L)_4bpy]^{m+}$ complexes varies from 11,000 for $(L)_4$ = bis-acetonylacetonate (bis-acac) to about 20,000 cm^{-1} for (L) = 1,4,8,11-tetrathiacyclotetradecane ([14]aneS_4) and tetrakis-acetonitrile. The highest energy emitters are intriguing among all the complexes with Ru-bpy chromophore in that the first resolved vibronic component in their 77 K emission spectra has significantly greater amplitude than the highest energy components do, while the reverse is found for the lower energy emitters. This variation in bandshapes arises from much larger distortions of the bpy ligand in the higher energy ^{3}MLCT excited states and was reasonably well reproduced using computational modeling.[21]

$[Ru(MeCN)_4(bpy)]^{2+}$ and $[Ru([14]aneS_4)(bpy)]^{2+}$ complexes both emit in the 15,000 - 20,000 cm^{-1} region and their emission spectra have similar vibronic structures. The 77 K emission decay of $[Ru(MeCN)_4(bpy)]^{2+}$ (6000 ns) complex is orders of magnitude larger than that of $[Ru([14]aneS_4)(bpy)]^{2+}$ (20 ns) complex. These observations suggests that a lower energy ^{3}MC state is quenching the ^{3}MLCT state of $[Ru([14]aneS_4)(bpy)]^{2+}$ complex. The emission decay for the $[Ru(MeCN)_4(bpy)]^{2+}$ complex is similar to that of $[Ru(bpy)_3]^{2+}$, but the 300 K quantum yield for the photosubstitution of acetonitrile by water was reported to be 0.43.[59] This photosubstitution has been explained in terms of a highly distorted ^{3}MC state that has comparable energy with that of the lowest ^{3}MLCT state. When the ^{3}MC state is the lowest triplet excited state, the expectation is an extremely short lifetime such as what is found for $[Ru([14]aneS_4)(bpy)]^{2+}$.[21] In this work, $[Ru(MeCN)_4(bpy)]^{2+}$ and $[Ru([14]aneS_4)(bpy)]^{2+}$ complexes are interrogated to understand the photochemistry and photophysics of the unusual emission properties.

My role in this collaborative project was as the lead experimentalist. This involved synthesis and purity characterization by ^{1}H NMR, variable temperature emission and lifetime studies and 77 K emission and photodecomposition quantum yield determinations. Additionally, recently acquired new-to-the lab spectroscopic equipment (cryostat, liquid light guides and F/# matcher) was effectively implemented and utilized for the majority of this project. Triplet state modeling of the mentioned complexes was done with a collaboration with Professor Schlegel's group.

1. Photophysics and Photochemistry of $[Ru(MeCN)_4(bpy)]^{2+}$

The $[Ru(MeCN)_4(bpy)]^{2+}$ complex emits strongly in 77 K solvent glasses. The emission quantum yield in alcohol glasses was found to be 0.47 ±0.04 as compared to that of $[Ru(bpy)_3]^{2+}$ at 0.37. [32] The results of the spectroscopic and quantum yield determinations were plagued by: (i) substrate photodecomposition from extended time-periods of laser irradiation and/or the use of high-intensity diode laser excitation and (ii) unusual emission decay kinetics. Based on these complications, the excited state behavior of the $[Ru(MeCN)_4(bpy)]^{2+}$ complex is atypical for ruthenium-bipyridine complexes at 77 K.

2. 77 K Photodecomposition of $[Ru(MeCN)_4(bpy)]^{2+}$

Several minutes of irradiations using a diode laser at 405 nm and 50 mW resulted in significant changes in the emission spectra as shown in Fig. 37. These spectral changes may correspond to the substitution of an acetonitrile ligand by an alcohol solvent species. In butyronitrile solvent, there are shifts and changes in the relative intensities of the emission bands as shown in Fig. 35. These results are consistent with the substitution by an alcohol should result

in a lower energy ^{3}MLCT state, while substitution by butyronitrile would result in a similar complex with emission in the same region as the parent complex. It was found that the amount of photodecomposition decrease with the time period of the irradiation, which suggests second-order photolysis or photo-product filter effects. The emission spectral changes were used to gain an estimate of the photodecomposition quantum yields in 77 K alcohol solvent glasses.

One may define the quantum yield for photodecomposition, ϕ_{pd}, of a substrate S as:

$$\frac{d[S]}{dt} = -\phi_{pd} I_a \qquad (6)$$

where I_a = the intensity of light absorbed (s^{-1}) and may be defined by:

$$\Phi_{em} = \frac{N_{em}}{N_a} \qquad (7)$$

$$I_a = N_a \times \Delta t_a;\ I_{em} = N_{em} \times (\Delta t_a + t_{em}) \qquad (8)$$

where ϕ_{em} = the emission quantum yield, N_{em} = the number of photons of light emitted (s^{-1}), Na = the number of photons of light absorbed (s^{-1}), Δt_a = the time interval for spectral accumulation and t_{em} is the excited state lifetime. In these experiments Δt_a was on the order of minutes while t_{em} was on the order of microseconds. Thus,

$$I_a \approx \frac{I_{em}}{\Phi_{em}} \qquad (9)$$

$$\frac{d[S]}{dt} = -\phi_{pd} I_a/\Phi_{em} \qquad (10)$$

The total irradiation time is given by,

t_{rad} = [time for spectral accumulation, Δt_{sa}] + [irradiation interval, Δt_{ii}]

$$\approx 0.5\Delta t_{sa} + \sum_{j=0}\left(j\Delta t_{ii} + 0.5\, j\Delta t_{sa} \right) \qquad (11)$$

for j number of times the sample was irradiated. Thus,

$$\phi_{pd} \approx [\Delta I_{em}(j) \times \Delta t_{sa} \times \phi_{em}]/[I_{em}(av)_j \times t_{rad}(j)] \qquad (12)$$

where $I_{em}(av)_j = [I_{em}(j\text{-}1) + I_{em}(j)]/2$; $\Delta I_{em}(j) = [I_{em}(j\text{-}1) - I_{em}(j)]$. The relative substrate emission intensity is calculated from $I_{rel} = I_{em}(j)/[\ \phi_{em}\ I_{em}(j=0)]$; $\phi_{em} = 0.47$.

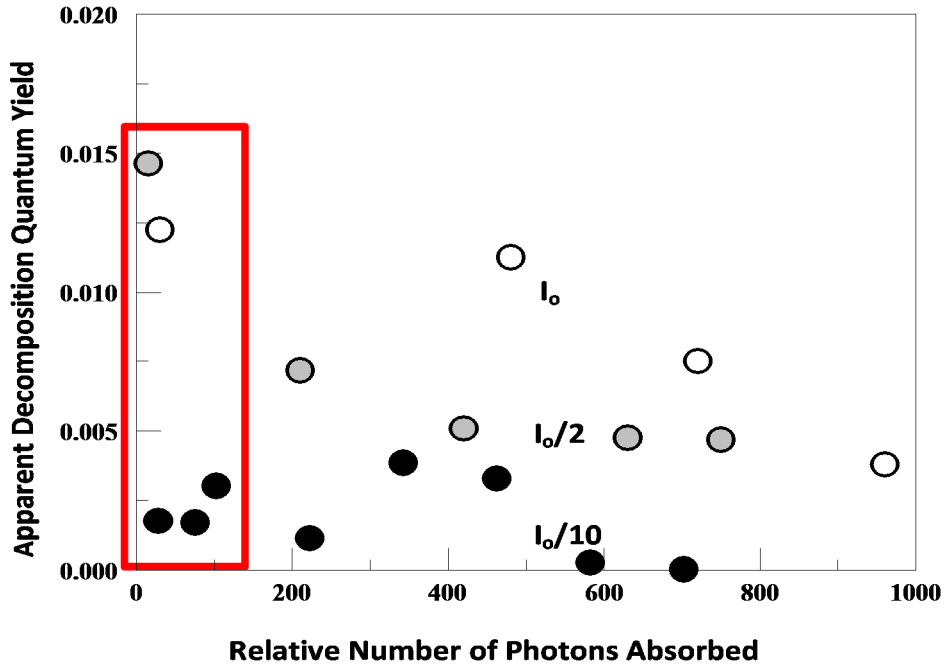

Figure 51: Variation of the quantum yield for the decrease of $[Ru(MeCN)_4(bpy)]^{2+}$ emission intensity with the extent of irradiation at different incident light intensities (I_o) in a ethanol:methanol glass. Irradiations at 50 mW 405 nm diode laser with 50% ($I_o/2$) and 90% ($I_o/10$) neutral density filters (I_o the diode laser output). The relative number of photons absorbed is calculated from $I_a(rel) \times t_{irrad} \times f$ (where f = 1 (for no ND filter), 0.5 or 0.10; t_{irrad} is the total time of irradiation; and $I_a(rel) = I_a(f\ )/\ I_a(f = 1\ )$.[6]

The photodecomposition quantum yields shown in Fig. 51 shows the apparent photodecomposition yield strongly decreases with radiation intensity (which is most obvious when comparing the data points squared in red) as one may expect for a two-photon process. Given the experimental uncertainties and the observation that a small enough value of I_o/n was not used to establish an irradiation intensity independent region for photodecomposition, the apparent photodecomposition is proportional to the intensity of radiation I_o - $0.1I_o$. These observations allow for an estimate of $\phi_{pd} < 0.0002$ for the quantum yield of the primary photoproducts at 77 K. The observation of photochemistry observed in the 77 K glasses is very rare.

The two-photon photochemistry is proposed to be a consequence of the irradiation of a transient ^{3}MLCT excited state that is derived from the bipyridine anion moiety which has an intense absorption around 390 nm.[60] The 405 nm excitation used for these experiments is at the low-energy tail of the intense absorption band. A proposed mechanism is illustrated in the following equations:

$$[(L)_4Ru^{II}(bpy)]^{2+} + h\nu_{405} \rightarrow {}^1\{\text{FC state}\} \rightarrow {}^3[(L)_4Ru^{III}(bpy^{-\bullet})]^{2+} \quad (11)$$

$${}^3[(L)_4Ru^{III}(bpy^{-\bullet})]^{2+} \rightarrow [(L)_4Ru^{II}(bpy)]^{2+}, (k_r + k_{nr}) \quad (12)$$

$${}^3[(L)_4Ru^{III}(bpy^{-\bullet})]^{2+} + h\nu_{405} \rightarrow [(L)_4Ru^{III}(bpy)]^{3+} + e^-(solv) \quad (13)$$

$${}^3[(L)_4Ru^{III}(bpy)]^{3+} + e^-(solv) \rightarrow {}^3[(L)_4Ru^{II}(bpy)]^{2+} [={}^3MC \text{ state}] \quad (13.1)$$

$${}^3[(L)_4Ru^{II}(bpy)]^{2+} + \text{solvent} \rightarrow [(L)_3(\text{solvent})Ru^{II}(bpy)]^{2+} + L \quad (13.2)$$

[where the ^{3}MC excited state is generated because the driving force for the ^{3}MC state is smaller than for the ground state; there was a study[61] on $[Ru(bpy)_3]^{2+}$ in which the solvated electron was detected and mostly recombined with the transient Ru^{III} complex]

3. Low-temperature decay measurements of $[Ru(MeCN)_4(bpy)]^{2+}$

The emission lifetime of this complex at 77 K is not monoexponential. The emission decay data was fitted with two exponentials with only random residuals as shown in Fig. 36. Although two components fit the data very well, one cannot rule out that more than two decays contribute to the total decay. At 77 K, the two emission components have very similar amplitudes within 5% of each other that are independent of the wavelength of excitation (375 – 415 nm), monitored wavelength (510 – 600 nm) or solvent glass (alcohol or butyronitrile) as presented in Tables 3 and 4. The slower decay of the two components makes a dominant contribution of ≥ 80% to the overall 77 K emission spectra. The relative contribution of the decay components are determined by:

$$\text{Fraction of contribution 2} = \frac{\int (A2)e^{-\tau(2)t}dt}{\int (A2)e^{-\tau(2)t}dt + \int (A1)e^{-\tau(1)t}dt} \qquad (14)$$

$$\approx \frac{(A2)(\tau 2)}{(A2)(\tau 2)+(A1)(\tau 1)}$$

It was found that $[Ru(MeCN)_4(bpy)]^{2+}$ emission decay rates are slightly temperature dependent between the ranges of 77 and 107 K as suggested in Table 5. The photochemical effects complicate the accurate measurement of this temperature dependence because the spectral bandshape changes seem to increase with the temperature. In an effort to verify how or if the photochemical effects described affect the accurate lifetime and amplitude determinations, the temperature dependence of the emission decay with and without intermediate laser irradiations

and varying the cooling sequence of the cryostat. The cryostat cooling sequence was varied as follows:

a) Table 4 data points were obtained under conditions that contributed to significant decomposition. The lifetimes were measured at the denoted temperature with the cryostat using 390 nm pulsed laser excitation and then emission spectra was captured using 1 minute laser irradiation periods using 405 nm 50 mW laser excitation. These experiments were performed with the cryostat from 77 to 107 K. Significant photodecomposition was observed even with the pulsed dye laser with a 4 ns pulse width. The decomposition was more dramatic when using the 405 nm 50 mW laser excitation.

b) An attempt to minimize photodecomposition was made by incorporating a 10% transmittance neutral density filter for the lifetime measurements. Moreover, the experiments were run with the cryostat from 107 to 77 K in the without intermediate periods of laser irradiations as illustrated at the bottom of Table 5. Additionally 410 nm pulsed excitation was used to try and get away from the low-energy tail of the intense absorption band at 390 nm as previously mentioned.

An attempt was made to characterize the minor 15% short-lived emission component. The same extent of this component was present even with two different solvent glasses and it seemed to be independent of the rate of sample cooling by varying the cryostat sequence. Tables 3 and 4 illustrates that this component's overall contribution to the emission is excitation wavelength independent. These observations suggest that the species that is responsible for the short-lived emission component has absorption and emission spectra that are similar to that of the dominant chromophore. A hypothesis that is consistent with the observations is that due to the acetonitrile ligand being a poor σ bond donor, any bond that it makes with Ru(III) will be weak. Thus, there may be an overall distribution of ^{3}MLCT species in the frozen solvent glass

that have slightly different Ru-Acetonitrile (ligand) bond lengths and decay lifetimes. The extent of photodecomposition in these experiments does not significantly alter our observations for the lifetimes of the $[Ru(MeCN)_4(bpy)]^{2+}$ complex. When internal conversion processes are absent, the observed (measured) lifetime, is inversely related to the radiative (RAD) and non-radiative (NRD) rate constants as follows,

$$1/\tau_{obs} \approx k_{RAD} + k_{NRD} \qquad (15)$$

The radiative rate constant is expected to be nearly temperature independent and at low temperature (77 K) the non-radiative rate constant should move toward a temperature-independent limit as described by Englman and Jortner.[62] Thus, the trapping of most of the excitation energy is in a local potential energy minimum (^{3}MLCT). The two components of the observed emission can be estimated from eq. 14 based on the individual fractional contributions. The majority of the change in emission intensity derives from the strong temperature dependent contributions of component 2, which decreases from about 85% at 77 K to 55% at 107 K. Because the observed behavior is nearly independent of the periods of irradiation or the sequence in which the temperature is changed, it cannot be attributed to contributions arising from the increase in photochemical products as temperature is increased. However, such an effect may arise from broadening of the distribution of ^{3}MLCT species with different bond lengths with increasing temperature.

4. 77 K Emission Quantum Yield of $[Ru(MeCN)_4(bpy)]^{2+}$

The spectrometer and detector/liquid light guide setup used for the spectroscopic determinations (as described in the experimental section) has limited response to wavelengths of light less than about 385 nm. As a result, partial 90 K absorption spectra were obtained for this complex. The ambient absorptivity at 405 nm agreed well with that obtained with a standard Shimadzu UV-2101PC spectrophotometer.

5. Conclusions

These studies were started because of the similar absorption and emission spectra of $[Ru(MeCN)_4(bpy)]^{2+}$ and $[Ru([14]aneS_4)(bpy)]^{2+}$ complexes, but remarkably different lifetimes. The shorter lifetime for $[Ru([14]aneS_4)(bpy)]^{2+}$ suggested a lower energy ^{3}MC than ^{3}MLCT excited state. Computational modeling revealed lower energy ^{3}MC excited states for both of the complexes. The observation that both complexes emit at 77 K and have lower energy ^{3}MC states is a direct violation of Kasha's Rule.[63] Much of the observed differences in the photochemistry and photophysics among the complexes appear to arise from the large differences in ^{3}MLCT/ ^{3}MC surfaces. The observed differences in the 77 K excited state lifetimes may be conceptualized in terms of electron transfer analogy in that the reorganizational energies are different for an intramolecular electron transfer of $bpy^{-\bullet}$ to Ru^{III} to form ^{3}MC excited states. This means that the excited state behavior of these two complexes is comparable to the classical patterns of the dependence of electron transfer rate constants on variations in metal-ligand bond lengths, with the rate constants for the transitions from the reactant (initial state) and product (final state) decreasing as the nuclear coordinates (bond lengths and bond angles) differences of these states increases. Calculations performed in Professor Schlegel's group indicate that the

^{3}MLCT and ^{3}MC potential energy minima differ by 3700 ± 100 cm^{-1} for both of these complexes.

Some observations from the current project suggest that: a) the ^{3}MLCT/^{3}MC configurational mixing is small, b) the emission of [Ru([14]aneS$_4$)(bpy)]$^{2+}$ has well-resolved vibronic components[21] despite a calculated ^{3}MLCT/^{3}MC crossing point that is near the energy to the ^{3}MLCT potential energy minimum and weak emission, c) the [Ru(MeCN)$_4$(bpy)]$^{2+}$ complex emission is very strong and d) the electronic configurations change suddenly in the calculated surface crossing regions. Additionally, these studies indicate that the excited state ^{3}MLCT/^{3}MC crossing energies may be altered using stereochemical constraints that restrict the extent of metal ligand distortions.

The low temperature emission properties of the [Ru(MeCN)$_4$(bpy)]$^{2+}$ complex lead to some unique features: a) the 77 K emission quantum yield is 0.47 (relatively large), b) the emission decay seems to be at least biphasic (but possible multiphasic), c) the two emission fractions have very small temperature dependencies and d) two-photon decomposition at 77 K is still a problem. The observation of a large quantum yield in view of the calculated lower energy ^{3}MC than ^{3}MLCT excited state is abnormal. Actually, most of the spectroscopic properties of this complex are normal for Ru-bpy chromophores. On the other hand, the arguments here suggest that its radiative rate constant is approximately 0.6 – 0.8 x 10^5 s^{-1}. This rate constant is comparable to a value of 0.7 x 10^5 s^{-1} for [Ru(bpy)$_3$]$^{2+}$. Given that the radiative rate constant is expected to increase strongly as the excited state energy increases[17], and that [Ru(MeCN)$_4$(bpy)]$^{2+}$ emits 2000 cm^{-1} higher energy than [Ru(bpy)$_3$]$^{2+}$, the comparable value of the former suggest an inefficient population of the emitting state.

While a strong emission from any state other than the lowest energy excited state is uncommon for ruthenium complexes, recent work from Sun and co-workers indicates that Ru-modified-bpy chromophores with lowest energy ^{3}MC states have a high percentage of higher energy ^{3}MLCT transiently populated at ambient temperature.[64] The authors calculates a ^{3}MC state 300 cm^{-1} lower in energy than the ^{3}MLCT state for $[Ru(6\text{-}Me\text{-}bpy)_3]^{2+}$ with transient lifetimes of 450 and 1.6 ps respectively in ambient solutions. This complex emits at 77 K with an emission max of 17,000 cm^{-1}, emission quantum yield = 0.097 and radiative rate constant = 2.4 x 10^4 s^{-1}.[65] These results are similar to the related compound $[Ru(MeCN)_4(bpy)]^{2+}$, but the interpretation is not clear since the chromophores are not the same (bpy vs. 6-me-bpy).

B. Energy Dependence of Metal-to-Ligand Charge Transfer Excited State Radiative Lifetimes

Excited state electron transfer processes are frequently primary factors for photocatalytic and solar energy conversion mechanisms.[1, 4-5, 9, 66-69] The efficiency of some transition metal complexes used in these mechanisms is prone to depend on the lowest energy excited states and their corresponding lifetimes, but such correlations have infrequently been identified. Excited state lifetimes depend on the rate constants for potential decay pathways and can be illustrated as shown in Eq. 1. The most pertinent decay pathways are commonly:[17] (1) intersystem crossing between excited states of the same spin multiplicity, k_{isc}; (2) internal conversion between excited states of the different spin multiplicity, k_{ic}; (3) non-radiative pathways, k_{NRD}, that depend on the rates of transfer of excited state energy to ground state vibrational modes;[17, 70] and (4) the radiative decay pathway, k_{RAD}. The rate of radiative relaxation determines the maximum possible excited state lifetime since if all other relaxation pathways are blocked ($k_n = 0$ for all $n \neq r$), the excited state will relax only by means of an emission characteristic of the chromophore. If the emitting state is not the lowest energy excited state or if it is close in energy to an excited state with a different electronic configuration (k_{isc} and k_{ic}, respectively, for crossings that do and do not involve a change in spin multiplicity), then (3) the crossing from the potential energy (PE) surface of the emitting state to the PE surface of a different electronic state (possibly metal-centered, ^{3}MC) can be an important relaxation pathway. The last relaxation pathway has not been much discussed, but it may account for the more than 500-fold shorter lifetime and much weaker emission intensity of the $[Ru([14]aneS_4)bpy]^{2+}$ complex than the $[Ru(MeCN)_4bpy]^{2+}$.[6] Additionally, the assumption that the emitting state is always the lowest in energy excited state (Kasha's Rule)[63] is not the case in some Ru-bpy complexes that exhibit strong phosphorescent emissions from MLCT excited states.[6] Such deviations from the rule complicates the

interpretation of the lifetime of the excited state. The value of the non-radiative decay (k_{NRD}) should decrease as the excited state energy increases while k_{rad} is expected to increase. Thus, the radiative rate constant can be an important factor in determining the lifetime of high energy photosensitizers.[17] Furthermore, the formalisms for the radiative rate constant are usually based on those from Einstein's theory of atomic fluorescence.[17] Phosphorescent molecules require other considerations. This work is a result of many attempts to understand implications of the excited state energy dependence of the vibronic sideband amplitudes that are found in emission spectra of Ru-bpy complexes. The radiative rate constants offer a straightforward probe of the variations in excited state structures.

Numerous compounds were prepared and characterized for their spectroscopic parameters as shown in Fig. 39 and Table 6 and most of these Ru-bpy complexes offer a range of useful model systems for this study. The emitting state of these complexes is from the triplet metal-to-ligand, ^{3}MLCT, excited state to the singlet ground state state, S_0 and necessarily involves a change of spin multiplicity. The general formalisms discussed for k_{RAD} are based on an "Einstenian" expression for atomic fluorescence spectra,[17]

$$k_{RAD} = C_r \nu^3 \eta^3 M^2 \qquad (16)$$

where $\left|\vec{M}\right|$ is the transition dipole moment, ν is the transition frequency (corresponding to an emission energy $h\nu$), η is the refractive index, $C_r = \frac{16\pi^3}{3\varepsilon_o c^3 h}$ and ε_o is the vacuum permittivity. The phosphoresecent emission nature of molecular excited states require a great deal more attention. One of the most important considerations is how to most accurately take care of $\left|\vec{M}\right|$. This transition dipole moment can be separated into two contributions, a) the electronic

contribution, $M_{el(DA)}$ and b) the Franck-Condon factor, (FC), which accounts for the emission contributions of the excited state vibronic transitions, $\vec{M} = \vec{M}_{el}(FC)$. In the limit of weak electronic coupling between the excited states and the ground state in a donor/acceptor complex (D/A), $\vec{M}_{el}$ can be represented by,[27, 71]

$$\vec{M}_{el(DA)} \approx \frac{H_{DA}}{\nu_{DA}} \overrightarrow{\Delta\mu_{DA}} \qquad (17)$$

where H_{DA} is the electronic matrix element for mixing the ground state (DA) and excited state (D^+A^-) electronic configurations, ν_{DA} is the (DA)$\rightarrow$ (D^+A^-) transition frequency and $\Delta\mu_{DA}$ is the difference in ground state and excited state molecular dipole moments.

Most of the formalisms of the transition moment described above do not consider that complications will arise due to mixing of different electronic excited states. An exception to this assumption was discussed by Mulliken and Person[27]. When a local transition is strongly allowed with respect to the spin multiplicity and near in proximity to the donor-acceptor charge transfer (DACT) excited state, then it can contribute to altered values of $\left|\vec{M}\right|$. Therefore, the configurational mixing of two excited states can be expressed as,[7, 27]

$$\vec{M} \approx \left(\overrightarrow{M_{D^+A^-}} + \alpha_{CT,IL}\overrightarrow{M_{IL}}\right)N \qquad (18)$$

where N is the normalizing constant, $\overrightarrow{M_{D^+A^-}}$ represents the transition dipole moment for a "pure" unmixed (diabatic) DACT transition, $\alpha_{CT,IL} \approx \frac{H_{CT,IL}}{\Delta E_{CT,IL}}$ where $H_{CT,IL}$ is the matrix element for the mixing of the excited states, $\Delta E_{CT,IL}$ is the vertical energy difference between the charge transfer (CT) and internal ligand (IL) excited states and $\overrightarrow{M_{IL}}$ is the transition dipole moment for a “pure” (diabatic) local transition.[27]

A few other factors should be considered when evaluation the transition dipole moments for phosphorescence in Ru-bpy chromophoric complexes: a) the overall difference in spin multiplicity of the (DA) and (D^+A^-) states requires a multiplicity factor which contributes to the forbidden nature of the transition and b) Molecular distortions are found in numerous vibrational modes which can couple to the electronic transition, as shown in Fig. 52 and is evident from the vibronic side bands found in the emission spectra.[53] Thus, the observed values of k_{RAD} correspond to the composite of the different vibrations that are contributed by the vibronic transitions. These considerations requires the use of spectrally-weighted average energy and can be approximated [17] and is discussed further in section 1 below.

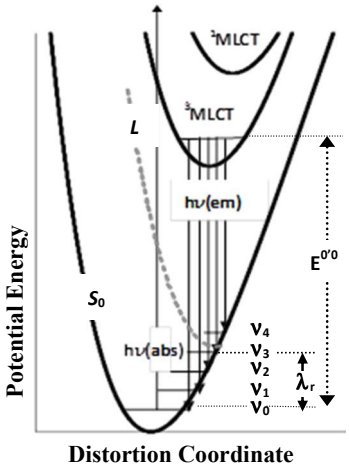

Figure 52. Qualitative PE curves illustrating features of the emission from a charge transfer excited state which is distorted in several vibrational modes, ν_n (n = 0, 1, 2, etc.). The dashed curve, *L*, illustrates the limit in which $E^{0'0} = \lambda_r$.[7]

The work in this project is a result of our group's attempts to understand excited state energy dependence of the vibronic sideband amplitudes that are commonly found in the emission spectra of Ru-bpy chromophores.[21] Computational modeling performed in Professor Schlegel's

group indicated that the wide range of excited state distortions found for the systems in this study are derived from the electronic mixing of the Ru-centered orbitals of the Ru/bpy ^{3}MLCT excited state with the bpy ligand π and π^* orbitals, or from the electronic mixing between the ^{3}MLCT ($\{D^+,A^-\}$) and $\pi\pi^*$ excited states.[21]

1. Some experimental and data analysis considerations

The observed emission intensity, I_{em}, is proportional to the emission quantum yield, Φ_{em}. The efficiency of forming the emitting state (γ) can be limited by alternative relaxation channels. There are reasons to suspect that $\gamma < 1$ for some Ru^{II} complexes which emit strongly even though they have lower ^{3}MC excited states.[6] For complexes that the DFT modeling indicates that a ^{3}MLCT excited state is the lowest energy triplet state, we have assumed that $\gamma = 1$ in the following equation,[7]

$$\phi_{em} = \gamma \frac{k_{RAD}}{k_{RAD} + k_{NRD}} \qquad (19)$$

The component band widths in the observed spectra are typically hundreds of wave numbers in 77 K solvent glasses and there is significant overlap of vibronic intensity contributions. Thus, the effective value of $k_{RAD(m)}$ at any observed emission energy, $h\nu_m$, is the sum over all the vibronic intensity contributions of each single vibrational mode, ν_i, weighted by its amplitude, A_i, at $h\nu_m$. However, the excited states of this class of complexes have distortions in more than 10 fundamental vibrational modes in the range of 100-1700 cm^{-1} [13, 21, 72] which leads to a large number of higher order contributions from harmonics and combination bands to the observed emission spectra.[21, 53-54, 73] Birks has suggested a more reasonable solution to treating molecular emission spectra for this limit,[17] by representing k_{RAD} as a function of $\nu_{(ave)}$, (the

subscript "m" designates the frequency (in wavenumbers when energy is involved) of the measurement) in the following equation,[17]

$$\nu_{ave} \approx \frac{\int \nu_m I_m d\nu_m}{\int I_m d\nu_m} \qquad (20)$$

Thus, values of $h\nu_{ave}$ were used to analyze the energy dependency of the Ru-bpy radiative lifetimes.

2. Excited state energy dependence of k_{RAD}

Fig. 41 compares the observed values of k_{RAD} on the same scale suggested by the "Einstenian" approach as found in eq. 16. These results strongly suggest that k_{RAD} is not only dependent on $(h\nu_{ave})^3$ as suggested by the equation. The energy dependence observed requires either an intercept on the x-axis or that the dependence for $h\nu_{ave} < 10{,}000\ cm^{-1}$ is much weaker than that for $h\nu_{ave} > 10{,}000\ cm^{-1}$. A linear fit of the data in Fig. 41 suggests an apparent intercept that can be best interpreted by $\left(\overrightarrow{M_{D^+A^-}}\right)^2 \approx \left(\alpha_{CT,IL}\overrightarrow{M_{IL}}\right)^2$ from eq. 18 where the additional energy dependence observed in Fig. 42 is derived from the mixing coefficient, $\alpha_{CT,IL} \approx (H_{CT,IL})/(E_{IL} - E_{CT})$. The possibility that the apparent intercept for a linear fit of $(\Phi_m/\gamma)k_{obsd}$ in Fig. 41 originates from values of populating the emitting excited state (γ) < 1 from eq. 19 also should be considered. Some first observations are : a) many of the emission quantum yields for the complexes in the high energy range are 0.5±0.2, so that for those complexes γ must be greater than or equal to 0.3 and if this were the case for all of the complexes used in this analysis, then the correction for the effect would alter the slope of any correlation fit, but not change the value

of the intercept, and b) $\gamma = 1.0$ has previously been deteremined for $[Ru(bpy)_3]^{2+}$[74] complex and this complex is included in the correlation for this project. The very weak energy dependence for $h\nu_{ave} < 10{,}000\ cm^{-1}$ is suggestive and consistent with eq. 18. Therefore, eq. 18 is the most appropriate available approach for describing the transition dipole and k_{RAD} in these complexes.

The observed deviations in the experimental data are significant. Much of this scatter results from errors in the determination of low temperature absorption spectra for the quantum yield measurments. Of course, there may also be systematic sources of other error that is being neglected.

There are many complexes that have calculated ^{3}MC states lower or equal to the calculated energy of the lowest ^{3}MLCT excited state. Experimentally these complexes tend to have values of k_{RAD} that are smaller than those expected based on the current correlations such as found in Fig. 40 and our previous report.[6] As a result, the systems that have calculated $E(^3MLCT) > E(^3MC)$ are excluded from comparisons as shown in Fig. 41 and Fig. 42. Furthermore, some of the complexes with $E(^3MC) \leq E(^3MLCT)$ emit very intensely (as shown in Table 6 and Fig. 39) which is a direct violation of Kasha's Rule.[63] This behavior may arise for these complexes because of the distortions in the ^{3}MC excited states are so much larger and in different vibrational modes than those of the ^{3}MLCT excited states that the nuclear reorganizational energy barriers to internal conversion can be very large compared to k_BT at 77 K.[6]

DFT modeling has found metal centered excited states with lower energies than the emitting ^{3}MLCT excited states. The extremely large metal-ligand distortions are characteristic to the ^{3}MC excited states of this class of complexes and primarily varies over a smaller energy range than does $E(^3MLCT)$. Experimentally, substrate photodecomposition at 77 K has made it

difficult to accurately determine k_{RAD} for some complexes with $h\nu_{max}$ > 17,000. This photodecomposition appears to originate from the near-ultraviolet irradiation of the ^{3}MLCT transient excited states.[6]

3. Experimental values of k_{RAD} at various energies

Values obtained for k_{RAD} suggest that the observed emission of Ru-bpy ^{3}MLCT excited states achieve much of their apparent intensities from mixing with "local" bpy-ligand-centered, $\pi\pi^*$(bpy), excited states which is most consistent with the intensity stealing model that has been discussed by Mulliken and Person[27] and applied towards linked organic D/A complexes by Bixon (et. al)[75].

Based on eq. 16, a plot of k_{RAD} vs. $(h\nu_{ave})^3$ should be linear and pass through the origin. However, in Fig. 41 the experimental data seems to require an intercept of 10,000 cm^{-1}. This observed behavior is more consistent with eq. 18 and implies that a "pure" diabatic MLCT transition would only be apparent at the lowest excited state energies (emission $h\nu_{ave}$ ~10,000 - 11,500 cm^{-1}). Additionally, the values of k_{RAD} seem to largely be the consequence of configurational mixing between the ^{3}MLCT and $\pi\pi^*$(bpy) excited states, or based on eq. 18 and setting IL = $\pi\pi^*$ for these complexes,[7]

$$k_{RAD} \approx C_r \nu^3 \eta^3 \left(M^2_{D^+A^-} + \alpha^2_{CT,\pi\pi^*} M^2_{\pi\pi^*} \right) N^2$$

$$\approx (h\nu_{ave})^3 \left[\left(M^{dia}_{MLCT(el)} \right)^2 \left(FC^{dia}_{MLCT} \right)^2 + \alpha^2_{CT\pi\pi^*} \left(M^{dia}_{\pi\pi^*(el)} \right)^2 \left(FC^{dia}_{\pi\pi^*} \right)^2 \right] A \qquad (21)$$

where the constants A and B are based on eqs. 16 and 18 and the transition moments and Franck-Condon factors in the braces are those that correspond to a "pure" diabatic (dia) MLCT transition and from MLCT/ππ* mixing, respectively. This analysis suggests “intensity stealing” by a very weak, “pure” MLCT transition from a strongly allowed transition localized on the acceptor ligand (note that ππ*(bpy) absorption bands are typically far more intense than MLCT absorptions).

Equation 16, 18 and 21 suggests that dividing the experimental data (k_{RAD}) found in Fig. 41 should result in a quantity proportional to M^2. In eq. 16, the result should be independent of $h\nu_{ave}$, but for eq. 18 there should be two clearly separated regions: a) A regime that is energy independent and b) A regime that is energy dependent. As shown in Fig. 42, there are two different energy regimes that are consistent with eqs. 18 and 21. The values of $k_{RAD}/(h\nu_{ave})^3$ increase as excited state energy increases over a small range of ~ 7,000 cm^{-1} of $h\nu_{ave}$.

Equations 18 and 21 are considerably consistent with the extreme rise in the values of k_{RAD} with $h\nu_{ave}$ since $E_{CT,\pi\pi^*} = E_v(\pi\pi^*) - E_0(MLCT)$, where the energies are in the nuclear coordinates of the PE minimum (E_0) of the ^{3}MLCT excited state. Based on spin density calculations, complexes with the highest energy ^{3}MLCT excited states examined ($h\nu_{0'0}$ ~ 19,000 cm^{-1}) places the ππ* states higher than the ^{3}MLCT which is consistent with the studies of Nozaki (et. al)[76] for $[Zn(bpy)_3]^{2+}$ that place the ππ* states ≥ 21,000 cm^{-1}. As $E_{0'}(^3MLCT)$ or the observed $h\nu_{ave}$ decreases, the $\Delta E_{CT,\pi\pi^*} = E_v(\pi\pi^*) - E_0(MLCT)$ increases and $\alpha^2_{CT,\pi\pi^*} = \left(\frac{H_{CT,\pi\pi^*}}{E_{CT,\pi\pi^*}}\right)^2$ rapidly becomes small. Thus, for complexes with small excited state energies, $E(^3MLCT) < 10{,}000$ cm^{-1} $\alpha_{CT,\pi\pi^*}$ is expected to be insignificant and eq. 18 implies that the apparent values of k_{RAD} will

approach those of "pure" diabatic or unmixed ^{3}MLCT excited states with the values of M^2 virtually constant.

4. Contributions of bipyridine ligand to the "metal-centered" singly occupied molecular orbital (SOMO) of the ^{3}MLCT excited states

Computational modeling performed in Professor Schlegel's group reveals the singly occupied molecular orbitals (SOMOs), illustrated in Fig. 53, of the triplet MLCT excited states for some of the Ru-complexes mentioned in this project.

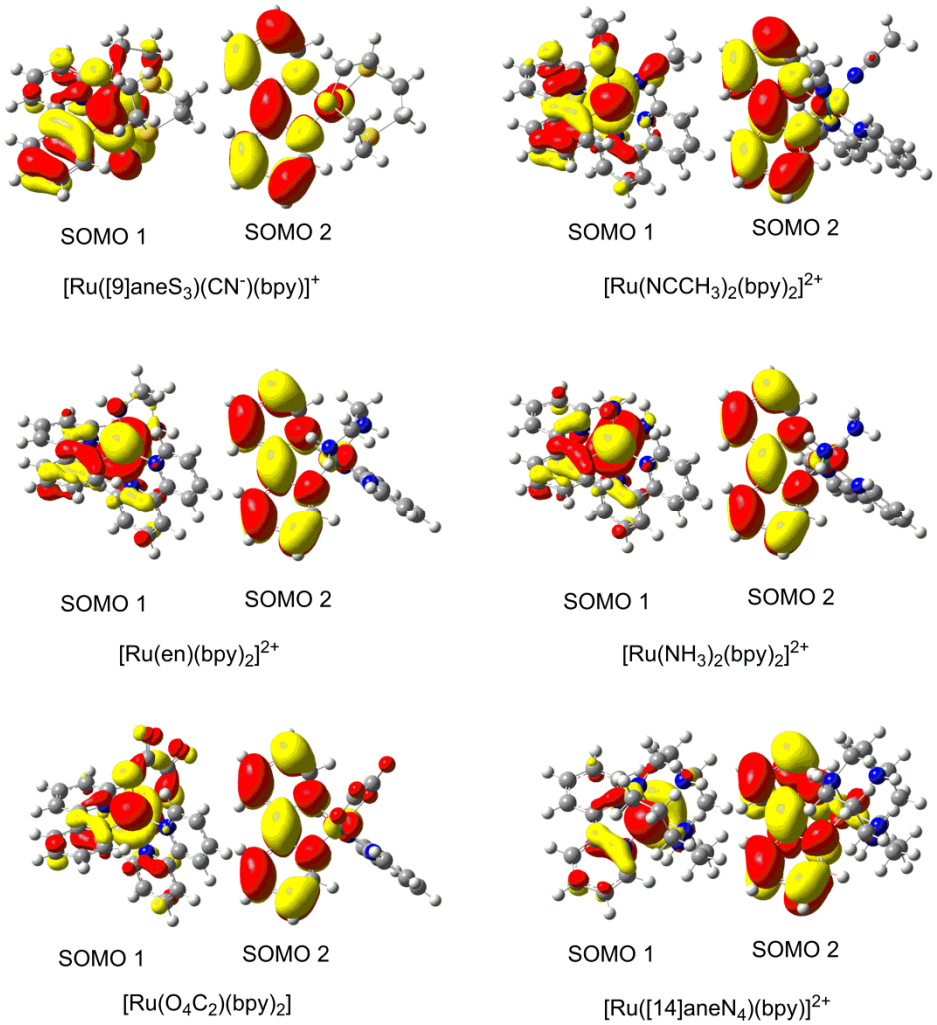

Figure 53. Bi-orthogonalized singly occupied molecular orbitals (SOMOs with an isosurface value of 0.02 a.u.) of the ^{3}MLCT states for selected complexes. The "metal-centered" SOMO (SOMO 1) has contribution from the π-orbital of bpy for all the complexes which illustrates that the emissive triplet state is not a pure metal-to-ligand charge transfer state; instead it has a component from one of the higher energy bpy-based excited states.[7] (Modeled by Dr. Shivnath Mazumder)

The "metal-centered" SOMO 1 has a contribution from the π-orbital of bpy ligand for all the complexes. SOMO 1 of $[Ru([14]aneN_4)(bpy)]^{2+}$, $[Ru(NH_3)_2(bpy)_2]^{2+}$ and $[Ru(en)(bpy)_2]^{2+}$ species has 89%, 87% and 86% $Ru(d_\pi)$ contribution, respectively. These observations illustrate that SOMO 1 is not a pure metal-centered orbital but has contributions from the bpy ligand. The corresponding SOMO for $[Ru(ox)(bpy)_2]$ species is 81% and 6% in $Ru(d_\pi)$ and $ox(p_\pi)$ character,

respectively, while the rest is contributed by the bpy ligand. Ru(d_π) character calculated for SOMO 1 of $[Ru(MeCN)_2(bpy)_2]^{2+}$ and $[Ru([9]aneS_3)(CN)(bpy)]^{+}$ species is considerably lower 77% and 70%, respectively, compared to those of the other complexes. These calculations are consistent with the experimental observation that the emissive state in not a "pure" diabatic unmixed ^{3}MLCT excited state and the mixing is occuring with a higher energy bpy-based excited state. Additionally, the calculated contribution for the bpy is increasing with the experimental $h\nu_{ave}$.

5. Conclusions

The observations in this project support the implications of recent studies from our group[21] that the emission bandshapes of Ru-bpy chromophores are strong functions of configurational mixing between ^{3}MLCT and $\pi\pi^*$ excited states of the bpy ligand. A few inferences from the current project are: a) a "pure" diabatic unmixed Ru-bpy ^{3}MLCT excited state is not greatly distorted and that its emission has weak vibronic contributions in the region of bpy-ligand vibrational modes, b) a "pure" diabatic unmixed Ru-bpy ^{3}MLCT emission has a very small radiative rate constant and c) there is no real evidence that a "pure" diabatic unmixed Ru-bpy ^{3}MLCT emission has ever been observed.

Many aspects of the proposed mixing are yet uncertain, but the apparent decay of a "pure" diabatic unmixed Ru-bpy ^{3}MLCT excited state (T_0) to the singlet (S_0) ground state is a spin forbidden transition. The excited state/excited state mixing suggested in this project is possibly promoted by spin-orbit coupling which would have the effect of relaxing the overall forbidden nature of the ^{3}MLCT/S_0 transition and generate most of the observed vibronic structure.

C. Macrocyclic Effects on Excited-States and Distortions

Excited state electron transfer processes by transition metal excited states have proven to be useful in applications such as photodynamic therapy,[77] dye-sensitized solar cells,[4] and artificial photosynthesis.[1] The efficiency of excited state electron transfer for the above applications is directly correlated to the lowest energy excited states, the structural differences of the electronic states of a donor (D)/acceptor (A) system from their respective ground states and their lifetimes. Metal-centered ligand-field excited states (^{3}MC) offer significant deactivation pathways in some ruthenium charge transfer (^{3}MLCT) complexes.[16] In developing a system that may be useful for water oxidation via solar energy conversion, much consideration must be given to the physical properties of these low lying excited states of the metal complexes because the properties of these states generally determine the overall electron transfer reactivity. Some reasonable approaches to manipulating the photophysical properties of complexes with low lying metal centered excited states are pertubations that alters the energy of the metal-centered states relative to the charge transfer states.[78] The current work investigates thiaether ligands [9]aneS_3 and [15]dieneS_3bpy (figure 54).

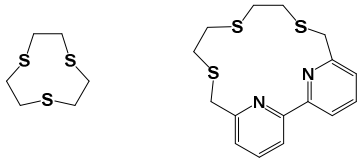

[9]aneS_3 [15]dieneS_3

Figure 54: Thiaether Ligands Investigated 1,4,7- trithiacyclononane ([9]aneS_3) and cyclo-6,6'-[1,9-(2,5,8-trithianonane)]-2,2'-bipyridine ([15]dieneS_3)

The ruthenium-bipyridine (Ru-bpy) complexes using these ligands leaves a sixth coordinated atom (X) that can be changed to generate relative energy differences between the ^{3}MLCT and

^{3}MC excited states. Other authors have examined these energy differences with some of the [9]aneS_3 complexes with a variety of (X) atoms[29, 31, 78], but the current work also allows for a comparison of the effect of having bipyridine synthesized into the macrocycle ([15]dieneS_3bpy). Additionally, in this project, the 77 K radiative properties (spectra, quantum yields and lifetimes) of these complexes are probed to gain more critical insight into the effects of ^{3}MC states on ^{3}MLCT excited states.

1. Redox Calculations

The computed redox potentials, oxidized species, reduced species and the ground state singlet were optimized. These optimizations included an implicit solvation with acetonitrile as the model. The free energy difference associated with an oxidation or reduction was obtained using eq. 22, and converted to an absolute potential using eq. 23:

$$\Delta G(sol)^{redox} = G(sol)^{n} - G(sol)^{n+1} \quad (22)$$

$$E^{o}_{comp} = - \Delta G(sol)^{redox}/nF \quad (23)$$

where $G(sol)^n$ is the solution-phase free energy for the given charged species, $\Delta G(sol)^{redox}$ is the solution-phase free energy difference for a given redox process, E^{o}_{comp} is the calculated absolute potential related with that redox process. The results from these calculations can be found in Fig. 46 and Table 9.

2. Some observations regarding [Ru([15]dieneS$_3$bpy)X]$^{m+}$ and [Ru([9]aneS$_3$)(bpy)X]$^{m+}$ complexes

In this project, [Ru([15]dieneS$_3$bpy)X]$^{m+}$ and [Ru([9]aneS$_3$)(bpy)X]$^{m+}$ complexes offer two significant comparisons: 1) Generation of energy differences between ^{3}MLCT and ^{3}MC

excited states when one atom is changed and 2) Differences in donor-acceptor properties when the acceptor (bipyridine) is linked to the macrocycle. Recently our group investigated the computational modeling, photochemistry and photophysics of $[Ru(MeCN)_4bpy]^{2+}$ and $[Ru([14]aneS_4)bpy]^{2+}$.[6] The computational modeling of these compounds confirmed that the lowest energy excited state is metal centered and that the contrasts in the size of the coordination sphere displacements and the calculated excited state stabilities between the complexes are derived from the stereochemical constraints introduced by the $[14]aneS_4$ macrocyclic ligand.[6] Macrocyclic constraint has the effect of manipulating the excited state ^{3}MLCT/^{3}MC crossing energies by restricting the extent of metal-ligand distortions. Consequently, the ^{3}MC state(s) of constrained complexes are more distorted than the ^{3}MLCT states but less distorted than the ammine analogs.[6, 21] It is calculated that $[Ru([9]aneS_3)(bpy)CN]^+$ has a ^{3}MC state ~1360 cm^{-1} lower in energy than the ^{3}MLCT state. Additionally, the 77 K lifetime of this complex is found to be ~ 15 μs and a quantum yield of 0.361 ± 0.105. The usual assumption, "Kasha's Rule" [63], is that the emitting state is the lowest energy excited state. At present time, there are some examples[6] of Ru-bpy complexes that have relatively strong emissions from ^{3}MLCT excited states that are direct violations of Kasha's rule.

The differences between $[Ru([15]dieneS_3bpy)X]^{m+}$ and $[Ru([9]aneS_3)(bpy)X]^{m+}$ complexes seem most apparent when analyzing the low temperature quantum yields and radiative rates found in table 7. $[Ru([9]aneS_3)(bpy)CN]^+$has a quantum yield and radiative rate constant that is ~ 3 times larger than that of $[Ru([15]dieneS_3bpy)CN]^+$ while the non-radiative rate constant (k_{nr}) is ~ 30% greater than the former. $[Ru([9]aneS_3)(bpy)Cl]^+$ has a quantum yield and radiative rate constant that is just under 2.5 times smaller than that of

$[Ru([15]dieneS_3bpy)Cl]^+$ with seemingly identical non-radiative rate constants. At this point we have the triplet state calculations for $[Ru([9]aneS_3)(bpy)CN]^+$ (^{3}MC state ~1360 cm^{-1} lower in energy than the ^{3}MLCT state), but given that the observed rate constant (k_{obs}) is the same for both of the cyanide complexes and the k_{nr} being larger, $[Ru([15]dieneS_3bpy)CN]^+$ may also have a lower energy ^{3}MC state. This is bit intriguing since the distortions generated from the [15]dieneS$_3$bpy ligand would inevitably be different from that of the [9]aneS$_3$ ligand. Based on the constraint imposed by the [14]aneS$_4$ macrocycle[6], it may be expected that the macrocyclic constraint is greater for the $[Ru([15]dieneS_3bpy)CN]^+$ complex, thus possibly resulting in a more distorted ^{3}MC state.

The observations for the $[Ru([9]aneS_3)(bpy)Cl]^+$ and $[Ru([15]dieneS_3bpy)Cl]^+$ complexes are somewhat interesting since the general macrocyclic constraint argument above is somewhat different for these complexes. A possible explanation for the chloro complexes is that the elongation for the Ru-Cl bond is the main difference and finds its origin in the overall constraint in the macrocycles. If the energies of the ^{3}MC states are somewhat constant in these complexes (inferred from the constant k_{nr}), then the Ru-Cl elongation may be more prominent for the $[Ru([15]dieneS_3bpy)Cl]^+$ complex. It is not obvious why this elongation would result in a 2.5 times larger quantum yield and radiative rate constant.

The comparisons in this section have been between the different trithia ligands with the same sixth coordinated ligand. When comparing the $[Ru([9]aneS_3)(bpy)CN]^+$ to the $[Ru([9]aneS_3)(bpy)Cl]^+$ complex the quantum yield is ~ 6 times larger for the former than for the latter. Furthermore, the averaged emission energy is 2800 cm^{-1} lower for $[Ru([9]aneS_3)(bpy)Cl]^+$. $[Ru([15]dieneS_3bpy)CN]^+$ compared to $[Ru([15]dieneS_3bpy)Cl]^+$ is somewhat puzzling in that the quantum yields are very similar, but the radiative rate is again much larger for the chloro-

substituted complex than for the cyanide. Based on the previous radiative rate constant project for Ru-bpy systems[7], the current work seems unusual for Ru-bpy chromophores (see table 6 compared to table 7) in that for similarly averaged energy ranges the radiative rate constants for the trithia complexes are much different when compared than other Ru-bpy systems. Moreover, the quantum yields for the current work are in the same range for other Ru-bpy chromophores with respect to similar averaged energy ranges.

3. Biexponential decays for $[Ru([9]aneS_3)(bpy)MeCN]^{2+}$ and $[Ru([15]dieneS_3bpy)MeCN]^{2+}$

The acetonitrile versions of both the macrocyclic complexes in this project exhibit at least biexponential decays. The usual assumption with decay behavior that is not monoexponetial is that there may be some type of impurity that is contributing to the overall decay that has a lifetime that is different (longer or shorter) than the actual compound of interest. Current efforts are being made to resynthesize the $[Ru([9]aneS_3)(bpy)MeCN]^{2+}$ complex and characterize for possible impure contributions. In the case that the compound actually has an at least biexponential decay, a possible explanation would be similar to the one proposed for the $[Ru(MeCN)_4(bpy)]^{2+}$ complex[6] due to the acetonitrile lignd being a poor σ bond donor, thus any bond that it makes in the excited state (Ru(III)) will be weak. Therefore, there may be an overall distribution of ^{3}MLCT species in the frozen solvent glass that have slightly different Ru-Acetonitrile (ligand) bond lengths and decay lifetimes.

4. Conclusions

Our current work implicates that the differences in excited state distortions can significantly depend on the coordination sphere around the transition metal. In particular, when

a sterically hindered ligand is coordinated to the metal, the overall distortions will be different. This difference may give rise to different radiative rate behavior. Additionally, changing one coordinated atom in the mentioned class of complexes has the effect of greatly varying the absorption and emission profiles. Modeling for $[Ru([9]aneS_3)(bpy)CN]^+$ suggests that a ^3MC state is lowest in energy. Based on k_{nr} values of $[Ru([15]dieneS_3bpy)CN]^+$ and the calculated ^3MC state for its direct comparison $[Ru([9]aneS_3)(bpy)CN]^+$, it would not be surprising if a ^3MC state is the lowest energy excited state for the $[Ru([15]dieneS_3bpy)CN]^+$ complex. If this is in fact the case, then inefficient population of the emitting state may be a reasonable argument for why the k_r values do not fit with other Ru-bpy chromophores in the same energy range but the quantum yield values do.

D. Developing Photosensitizers with Long-lived Excited-States

Long-lived excited states can offer advantages as photo-catalytic processes, photoactive drugs and dyes for solar energy conversion.[1, 4, 79] The longer excited-state lifetimes for charge transfer complexes can cause improved process efficiencies of the mentioned applications. Ruthenium(II) complexes with polypridine based acceptors have been used extensively as photosensitizers in many photo-catalytic and energy conversion processes.[4-5] Some relevant studies have attempted to optimize ambient lifetimes the Ru-bpy class of photosensitizers using tridentate ligands.[57-58]

In this project, a new class of ruthenium photosensitizers based on the chromophore Ru(TQA) (synthesized in Professor Kodanko's lab by Rajgopal Sharma), where TQA (tris(isoquinolin-1-ylmethyl)amine) is a tetradentate ligand have been spectroscopically observed. These complexes compared to Ru(bpy) chromophores consistently have longer lived ^{3}MLCT excited states at 77 K and calculated lower energy ^{3}MC excited states. Additionally, the TQA based complexes exhibit relatively high emission quantum yields with several ancillary ligands. These observations suggest that the long-lived excited state decays are functions of the TQA chromophore. Furthermore, the results indicate that optimizing long-lived excited states depends on excited state electronic properties of the individual complexes and <u>not only modulating relative ^{3}MLCT and ^{3}MC energies</u>. The 77 K emission spectra of $[RuTQA(X)_2]^{m+}$ complexes where X = MeCN, CN and NCS differ from the Ru-bpy analogs in that the dominant vibronic feature in the spectra is relatively more intense. This observation is indicative of more configurational mixing between the ^{3}MLCT and the $\pi\pi^*$ of the acceptor ligand-based excited state.

My role in this collaborative project was as the lead spectroscopist. This involved low temperature absorption, emission and corresponding lifetime measurements and quantum yield determinations and comparisons to the bipyridine analogs. Triplet state modeling of the mentioned complexes were done with a collaboration with Professor Schlegel's group.

1. $[RuTQA(X)_2]^{m+}$ vs $[Ru(bpy)_2(X)_2]^{m+}$ complexes

Table 8 compares the spectroscopic properties of the newly synthesized $[RuTQA(X)_2]^{m+}$ complexes to the $[Ru(bpy)_2(X)_2]^{m+}$ complexes and other relevant ruthenium based complexes . The derivatives of Ru(TQA) with X = MeCN, CN and NCS exhibit longer lived excited-state lifetimes and relatively high emission quantum yields when compared to $[Ru(bpy)_2(X)_2]^{m+}$ at low temperature and shown in Table 10.[8] This observation demonstrates that Ru(TQA) based complexes have a chromophoric effect with consistent low temperature intrinsic spectroscopic properties. These low temperature lifetimes are present even when calculations suggest that a ^{3}MC is lower in energy than the ^{3}MLCT excited state (violation of Kasha's rule[63]) which may be due to large barriers to crossing to the ^{3}MC surface as the case for the $[Ru(MeCN)_4(bpy)]^{2+}$ and $[Ru([14]aneS_4)(bpy)]^{2+}$ complexes.[6]

Table 10: Excited state lifetimes (τ) and emission quantum yields (Φ_{em}) of some $[RuL(X)_2]^{m+}$ complexes at 77K[a8]

Ligands **L**$(X)_2$	$h\nu_{max}$ $cm^{-1}/10^3$	τ_{in}, μs	Φ_{em}	τ_{TQA}/τ_{bpy}
TQA$(MeCN)_2$	18.3	145	0.45	17
(bpy)$_2$ $(MeCN)_2$	18.5	8.3	0.6	
TQA$(CN)_2$	17.3	78	0.26	22
(bpy)$_2$ $(CN)_2$	15.9	3.4	0.27	
TQA$(NCS)_2$[b]	16.0	17.6	0.50	31
(bpy)$_2$ $(NCS)_2$[b]	14.9	0.57	0.084	

[a] Determined in ethanol/methanol (v/v' = 4/1) solvent except as indicated. [b] Butyronitrile

The emission spectra of $[RuTQA(X)_2]^{m+}$ complexes shown in Fig. 44 are uniquely different from those for the $[Ru(bpy)_2(X)_2]^{m+}$ complexes. The second highest energy peak is more intense for the TQAs than for the $(bpy)_2$ complexes. This observation has been interpreted from our previous publication[21] as more configurational mixing of the TQA complexes between the ππ* of the ligand with the ^{3}MLCT excited state.

2. DFT on the ^{3}MLCT excited states

To try and explain the nature of the long-lived excited states, DFT calculations (performed in Professor Schlegel's lab) were done on the Ru(TQA) complexes and compared to $Ru(bpy)_2$ complexes.

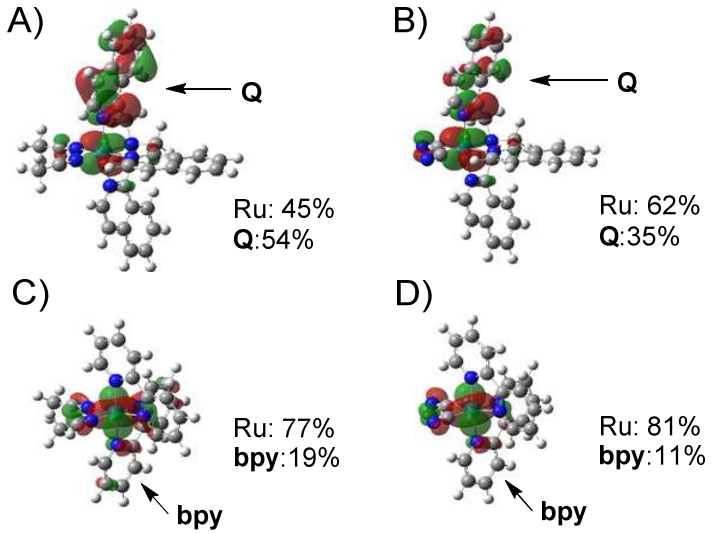

Figure 55: Metal-based SOMOs (isovalue=0.03 a.u.) and orbital contributions (%) of Ru and ligands for A) $[Ru(TQA)(MeCN)_2]^{2+}$; B) $[Ru(TQA)(CN)_2]$; C) $[Ru(bpy)_2(MeCN)_2]^{2+}$; D) $[Ru(bpy)_2(CN)_2]$ in the ^{3}MLCT optimized geometries[8] (Modeled by Yi-Jung Tu)

The metal-based singly occupied MOs or SOMOs of the Ru(TQA) complexes has 35 - 54% (as illustrated in Fig. 55) contribution from the π based orbital of a particular quinoline (Q) structure. This compares to 11 - 19% contribution observed from the π based orbital of the bipyridine ligand in the $Ru(bpy)_2$ complexes. These observations implicate that the emitting state of the Ru(TQA) complexes are not pure ^{3}MLCT excited states but have a great deal of contributions form the $^3\pi\pi^*$ state from the quinoline moiety. These implications are somewhat similar to the

Ru-bpy complexes[7] in that as the energy of the ^{3}MLCT excited state increases, the amount of mixing with the $\pi\pi^*$ is also increasing.

3. Conclusions

The chromophore Ru(TQA) offer remarkably long-lived excited states only at 77 K. These complexes used in applications such as photosensitizers for solar energy conversion or photo-catalytic processes will not be useful unless the similar behavior is revealed at ambient temperature. The ambient lifetimes of the mentioned complexes are short (if at all) due to internal conversion of the ^{3}MLCT excited state to a lower energy ^{3}MC state. The values of k_{NRD} will depend on the differences in excited state molecular geometries based on the reorganizational energy for crossing between the ^{3}MLCT and ^{3}MC states.[6] The significance of this project is to develop complexes with ^{3}MLCT excited states lower in energy than the ^{3}MC excited states. Some implications from this work are: a) Transition metal complexes with ^{3}MLCT excited state lifetimes much longer than those found for $[Ru(bpy)_3]^{2+}$ can be developed, b) Low temperature values for k_{RAD} offer a useful probe for ambient values, c) Based on DFT results compared to experimental lifetime measurements, relative energies of ^{3}MLCT and ^{3}MC excited states is not the only parameter for optimizing long-lived excited states and d) Configurational mixing between the ^{3}MLCT excited state with an acceptor ligand localized excited state of donor and acceptor complexes may be a relavant approach in developing extended lifetimes.

CHAPTER VI: Overall Conclusions

1. The role of metal-centered excited states in affecting the properties of Ru photosensitzers

In developing ruthenium-polypyridyl complexes that may be useful as photosensitzers, much attention is given to the metal-to-ligand charge transfer (^{3}MLCT) excited state.[16] However, the role of metal-centered (^{3}MC) excited states can have the affect of decreasing the overall efficiency of the charge transfer process in Ru photosensitizers. These metal-centered excited states act as deactivation pathways that diminishes the usefulness of the charge transfer state. In general, the reorganizational energy for crossing between the ^{3}MLCT and ^{3}MC states will act as a direct probe to the extent of quenching the ^{3}MLCT will experience at 77 K.[6] This quenching can be detected in the observed lifetime, quantum yield and k_{RAD} of potential photosensitizers at 77 K.[6-8, 12] At ambient temperature, when the ^{3}MC state is lower in energy than the ^{3}MLCT, the lifetime of the emission is diminished within our detection limits.

2. General implications from photochemistry

The 77 K photochemistry found for the $[Ru(MeCN)_4(bpy)]^{2+}$ complex[6] brings up an overall concern about photochemistry for ruthenium-polypyridyl complexes especially at ambient temperature. Furthermore, Tarnovsky (et. al) studied $[Ru(bpy)_3]^{2+}$ at ambient temperature using a high-intensity 400 nm femtosecond transient absorption setup and found solvated electrons produced as a two-photon photoproduct.[61] The general implication from the apparent photochemistry found for these ruthenium-polypyridyl complexes is that there is intrinsic behavior detected at either low temperature or using ultrafast spectroscopy that may be give rise to decreased efficiencies of some photosensitizers.

3. Designing high energy photosensitizers.

The radiative lifetime of a complex is the longest possible lifetime for that given complex based on $\tau^{-1} \approx k_{RAD} + k_{NRD} + k_{IC}$ and that the excited state will relax via an emission specific to the chromophore when all competing relaxation channels are blocked. Additionally, k_{RAD} is expected to increase very minimally (if at all) as the temperature is increased as the case with k_{RAD} values found for $[Ru(bpy)_3]^{2+}$ at ambient and low temperature (see Table 8). Thus, k_{RAD} can be easily probed at low temperatures because the emission decay lifetimes are usually longer (when compared to ambient lifetimes) and possibly determined more accurately in the frozen rigid matrix. A general trend is that k_{RAD} should increase as the excited state energy increases while k_{NRD} should decrease as the excited state energy decreases.[17, 62] An approach to unlocking the similar lifetimes at ambient temperature that are found at low temperature is to "tune" the k_{NRD} and k_{IC} by the incorporation of ancillary ligands. By probing k_{RAD} at low temperatures, unique classes of chromophores with exceptionally long-lived excited state lifetimes can be recognized and then the competing relaxation channels, such as k_{NRD} and k_{IC}, can be reduced. A possible example would be to decrease the amplitudes of acceptor ligand distortions by incorporating an acceptor with delocalized electron density in the ^{3}MLCT excited state. Increasing the delocalization of the electron density in the acceptor ligand may have the effect spreading out the distortions and result in smaller amplitude ligand distortions and giving a desired smaller value of k_{NRD}.

The likely issues in designing high energy photosensitizers are found in excited state/excited state mixing, lower energy ^{3}MC excited states and undesirable photochemistry. Designing high energy photosensitizers for ambient applications will continue to be a struggle.

REFERENCES

1. Lewis, N. S.; Nocera, D. G., *Proc. Natl. Acad. Sci.* **2006,** *103*, 15729.
2. Balzani, V.; Credi, A.; Venturi, M., *Coord. Chem. Rev.* **1998,** *171*, 3.
3. Bignozzi, C. A.; Argazzi, R.; Boaretto, E.; Carli, S.; Ronconi, F.; Caramori, S., *Coordination Chem. Reviews* **2013,** *257*, 1427.
4. Graetzel, M., *Inorg. Chem.* **2005,** *44*, 6841.
5. Graetzel, M.; Moser, J.-E., Solar energy conversion. In *Electron Transfer in Chemistry*, Balzani, V., Ed. Wiley-VCH: Weinheim, 2001; Vol. 5, p 589.
6. Mazumder, S.; Thomas, R. A.; Lord, R. L.; Schlegel, H. B.; Endicott, J. F., *Can. J. Chem.* **2014,** *92*, 996.
7. Thomas, R. A.; Tsai, C. N.; Mazumder, S.; Lu, I. C.; Lord, R. L.; Schlegel, H. B.; Chen, Y. J.; Endicott, J. F., *J. Phys. Chem.* **2014,** (submitted).
8. Sharma, R.; Thomas, R., A.; Tu, Y. J.; Mazumder, S.; Alnaed, M.; Schlegel, H. B.; Endicott, J. F.; Kodanko, J. J., in progress.
9. Balzani, V., *Electron Transfer in Chemistry*. Wiley-VCH: Weinheim, Germany, 2001; Vol. 1-5.
10. Marcus, R. A., *Discuss. Faraday Soc.* **1960,** *29*, 21.
11. Newton, M. D., Electronic coupling elements and electron transfer theory. In *Comprehensive Coordination Chemistry II*, McCleverty, J. A.; Meyer, T. J., Eds. 2004; Vol. 2, p 573.
12. Chen, Y.-J.; Xie, P.; Endicott, J. F., *J. Phys. Chem. A* **2004,** *108*, 5041.
13. Hupp, J. T.; Williams, R. T., *Acc. Chem. Res.* **2001,** *34*, 808.

14. Tsai, C. N.; Tian, Y.-H.; Shi, X.; Lord, R. L.; Schlegel, H. B.; Chen, Y. J.; Endicott, J. F., *Inorg. Chem.* **2013,** *52*, 9774-9790.

15. Coppens, P.; Benedict, J.; Messerschmidt, M.; Novozhilova, I.; Graber, T.; Chen, Y.-S.; Vorontsov, I.; Scheins, S.; Zheng, S.-L., *Acta Cryst.* **2010,** *A66*, 179.

16. Wagenknecht, P. S.; Ford, P. C., *Coord. Chem. Rev.* **2011,** *255*, 591.

17. Birks, J. B., *Photophysics of Aromatic Molecules*. Wiley-Interscience: New York, 1970.

18. Endicott, J. F., Transition metal photochemistry. In *Electronic Structure and Spectroscopy of Inorganic Compounds Vol. 2*, Solomon, E. I.; Lever, A. B. P., Eds. Wiley: New York, 1999; p 291.

19. Endicott, J. F., Charge transfer excited states of transition metal complexes. In *Electron Transfer in Chemistry.*, Balzani, V., Ed. Wiley-VCH: New York, 2001; Vol. 1, p 238.

20. Lever, A. B. P.; Dodsworth, E. S., Echem and CT. In *Electronic Structure and Spectroscopy of Inorganic Compounds, Vol. II*, Lever, A. B. P.; Solomon, E. I., Eds. Wiley: New York, 1999; p 227.

21. Lord, R. L.; Allard, M. M.; Thomas, R., A.; Odongo, O. S.; Schlegel, H. B.; Chen, Y.-J.; Endicott, J. F., *Inorg. Chem.* **2013,** *52*, 1185.

22. Mulliken, R., *J. Am. Chem. Soc.* **1950,** *72*, 600.

23. Mulliken, R., *J. Phys. Chem.* **1952,** *56*, 801.

24. Mulliken, R., *J. Am. Chem. Soc.* **1952,** *74*, 811.

25. Marcus, R. A., *Journal of Chemical Physics* **1956,** *24*, 5.

26. Hush, N. S., *Progress in Inorganic Chemistry* **1967,** *8*, 391.

27. Mulliken, R. S.; Person, W. B., *Molecular Complexes*. Wiley-Interscience: New York, 1967.

28. Krause, R. A., *Inorg. Chim. Acta* **1977,** *22*, 209.

29. Goodfellow, B. J.; Felix, V.; Pacheco, S. M. D.; Jesus, J. P. d.; Drew, M. G. B., *Polyhedron* **1997,** *16* (3), 393 - 401

30. Adams, H.; Amado, A. M.; Felix, V.; Mann, B. E.; Antelo-Martinez, J.; Newell, M.; Ribeiro-Claro, P. J. A.; Spey, S. E.; Thomas, J. A., *Chem. Eur. J.* **2005,** *11*, 2031.

31. De, P.; Maji, S.; Chowdhury, A. D.; Mobin, S. M.; Mondal, T. K.; Paretzki, A.; Lahiri, G. K., *Dalton Transactions* **2011,** *40*, 12527.

32. Demas, J. N.; Crosby, G. A., *J. Am. Chem. Soc.* **1971,** *93*, 2841.

33. Parr, R. G.; Yang, W., *Density-functional theory of atoms and molecules*. Oxford University Press: New York, 1989.

34. Frisch, M. J. T., G. W.; Schlegel, H. B.; Scuseria, G. E.; and M.A.C. Robb, J. R.; Scalmani, G.; Barone, V.; Mennucci, B.; Nakatsuji, G. A. P. H.; Caricato, M. L., X.; Hratchian, H. P.; Izmaylov, A. F.; Bloino, J. Z.,G.; Sonnenberg, J. L.; Hada, M.; Ehara, M.; Toyota, K.; Fukuda, R.; Hasegawa, J.; Ishida, M.; Nakajima, T.; Honda, Y.; Kitao, O.; Nakai, H.; Vreven, T. J. A.; Montgomery, J.; Peralta, J. E.; Ogliaro, F.; Bearpark, M.; Heyd, J. J.; Brothers, E.; Kudin, K. N.; Staroverov, V. N.; Keith, T.; Kobayashi, R.; Normand, J.; Raghavachari, K.; Rendell, A.; Burant, J. C.; Iyengar, S. S.; Tomasi, J.; Cossi, M.; Rega, N.; Millam, J. M.; Klene, M.; Knox, J. E.; Cross, J. B.; Bakken, V.; Adamo, C.; Jaramillo, J.; Gomperts, R.; Stratmann, R. E.; Yazyev, O.; Austin, A. J.; Cammi, R.; Pomelli, C.; Ochterski, J. W.; Martin, R. L.; Morokuma, K.; Zakrzewski, V. G.; Voth, G. A.; Salvador, P.; Dannenberg, J. J.; Dapprich, S.; Parandekar, P. V.; Mayhall, N. J.; Daniels, A. D.; Farkas, O.; Foresman, J. B.; Ortiz, J. V.; Cioslowski, J.; Fox, D. J. Gaussian Development Version, 2012; Gaussian Inc.: Wallingford, CT, 2012.

35. Allard, M. M.; Odongo, O. S.; Lee, M. M.; Chen, Y.-J.; Endicott, J. F.; Schlegel, H. B., *Inorg. Chem.* **2010,** *49*, 6840-6852.

36. Becke, A. D., *J. Chem. Phys.* **1993,** *98*, 5648.

37. Krishnan, R. B.; Binkley, J. S.; Seeger, R.; Pople, J. A., *J. Chem. Phys.* **1980,** *72*, 650.

38. Perdew, J. P., *Phys. Rev. B* **1986,** *33*, 8822.

39. Perdew, J. P.; Burke, K.; Wang, Y., *Phys. Rev.* **1996,** *54*, 16533.

40. Andrae, D.; Haussermann, U.; Dolg, M.; Stoll, H.; Preuss, H., *Theor. Chim. Acta* **1990,** *77*, 123.

41. Dunning, T. H., Jr.; Hay, P. J., In *Modern Theoretical Chemistry*, Schaefer, H. F., III, Ed. Plenum: New York, 1976; Vol. 3, p 1.

42. Igelmann, G.; Stoll, H.; Preuss, H., *Mole. Physics* **1988,** *65*, 1321.

43. Schlegel, H. B.; McDouall, J. J., In *Computational Advances in Organic Chemistry*, Ögretir, C.; Csizmadia, I. G., Eds. Kluwer Academic: Amsterdam, The Netherlands, 1991.

44. Bauernschmitt, R.; Ahlrichs, R., *J. Chem. Phys.* **1996,** *104*, 9047.

45. Schlegel, H. B., *J. Comput. Chem.* **1982,** *3*, 214.

46. Miertuš, S.; Scrocco, E.; Tomasi, J., *J. Chem. Phys.* **1981,** *55*, 117.

47. Scalmani, G.; Frisch, M. J., *J. Chem. Phys.* **2010,** *132*, 114110.

48. Scalmani, G.; Frisch, M. J.; Mennucci, B.; Tomasi, J.; Cammi, R.; Barone, V., *J. Chem. Phys.* **2006,** *124*, 9410.

49. Tomasi, J.; Mennucci, B.; Cammi, R., *Chem. Rev.* **2005,** *105*, 2999.

50. Petit, L.; Maldivi, P.; Adamo, C., *J. Chem. Theory Comput.* **2005,** *1*, 953.

51. Runge, E.; Gross, E. K. U., *Phys. Rev. Lett.* **1984,** *52* (997).

52. Stratmann, R. E.; Scuseria, G. E.; Frisch, M. J., *J. Chem. Phys.* **1998,** *109*, 8218.

53. Xie, P.; Chen, Y.-J.; Uddin, M. J.; Endicott, J. F., *J. Phys. Chem. A* **2005,** *109*, 4671.

54. Chen, Y.-J.; Xie, P.; Heeg, M. J.; Endicott, J. F., *Inorg. Chem.* **2006,** *45*, 6282.

55. Demas, J. N.; Crosby, G. A., *J. Am. Chem. Soc.* **1970,** *92,* , 7262.

56. Tsai, C.-N.; Allard, M. M.; Lord, R. L.; Luo, D.-W.; Schlegel, H. B.; Endicott, J. F.; Chen, Y.-J., **2013,** *52*, 9774.

57. Ragazzon, G.; Verwilst, P.; Denisov, S. A.; Credi, A.; Jonusauskas, G.; McClenaghan, N. D., *Chem. Commun.* **2013,** *49*, 9110.

58. Pal, A. K.; Serroni, S.; Zaccheroni, N.; Campagna, S.; Hanan, G. S., *Chem. Sci.* **2014**, DOI: 10.1039/c4sc01604a.

59. Petroni, A.; Slep, L. D.; Etchenique, R., *Inorg. Chem.* **2008,** *47*, 951.

60. Creutz, C.; Chou, M.; Netzel, T. L.; Okumura, M.; Sutin, N., *J. Am. Chem. Soc.* **1980,** *102*, 1309.

61. Tarnovsky, A. N.; Gawelda, W.; Johnson, M.; Bressler, C.; Chergui, M., *J. Phys. Chem. B* **2006,** *110* (51), 26497 - 26505.

62. Englman, R.; Jortner, J., *J. Mol. Phys.* **1970,** *18*, 145.

63. Kasha, M., *Discuss. Faraday Soc.* **1950,** *9*, 14.

64. Sun, Q.; Mosquera-Vazquez, S.; Daku, L. M. L.; Guenee, L.; Goodwin, H. A.; Vauthey, E.; Hauser, A., *J. Am. Chem. Soc. 135* (37), 13660.

65. Fabian, R. H.; Klassen, D. M.; Sonntag, R. W., *Inorg. Chem.* **1980,** *19*, 1977.

66. Balzani, V.; Juris, A.; Venturi, M.; Campagna, S.; Serroni, S., *Chem. Rev.* **1996,** *96*, 759.

67. Balzani, V.; Scandola, F., *Supramolecular Photochemistry*. Horwood: Chichester, U. K., 1991.

68. Barbara, P. F.; Meyer, T. J.; Ratner, M., *J. Phys. Chem.* **1996,** *100*, 13148.

69. Lewis, N. S., *Inorg. Chem.* **2005,** *44*, 6900.

70. Englman, R.; Jortner, J., *Mol. Phys.* **1970,** *18*, 145.

71. Hush, N. S., *Electrochim. Acta* **1968,** *13*, 1005.

72. Maruszewski, K.; Bajdor, K.; Strommen, D. P.; Kincaid, J. R., *J. Phys. Chem.* **1995,** *99*, 6286.

73. Odongo, O. S.; Heeg, M. J.; Chen, Y.-J.; Xie, P.; Endicott, J. F., *Inorg. Chem.* **2008,** *47*, 7493.

74. Demas , J. N.; Taylor, D. G., *Inorg. Chem.* **1979,** *18*, 3177.

75. Bixon, M.; Jortner, J.; Verhoeven, J. W., *J. Am. Chem. Soc.* **1994,** *116*, 7349.

76. Nozaki, K.; Takamori, K.; Nakatsugawa, Y.; Ohno, T., *Inorg. Chem.* **2006,** *45*, 6161.

77. Albani, B. A.; Pena, B.; Dunbar, K. R.; Turro, C., *Photochem. Photobiol. Sci.* **2014,** (13), 272.

78. Wong, C.-Y.; Lai, L.-M.; Chan, S.-C.; Tai, L.-H., *Organometallics* **2010,** (29), 6259-6266.

79. Burya, S. J.; Palmer, A. M.; Gallucci, J. C.; Turro, C., *Inorg. Chem.* **2012,** *51*, 11882.

ABSTRACT

ON THE NATURE OF EXCITED STATES IN RUTHENIUM COMPLEXES: TOWARDS RENEWABLE ENERGY

by

RYAN ANTONIO THOMAS

August 2015

Advisors: Prof. John F. Endicott and Prof. Cláudio N. Verani

Major: Chemistry (Analytical)

Degree: Doctor of Philosophy

The 77 K radiative properties (spectra, quantum yields and lifetimes) of ruthenium-polypyridyl complexes are investigated to better understand the effects of electronic mixing on metal-to-ligand-charge-transfer (^{3}MLCT) excited state properties and how metal-centered (^{3}MC) excited states affect the properties of potential ruthenium photosensitizers.The radiative rate of relaxation (k_{RAD}) determines the maximum possible excited state lifetime when all other relaxation pathways are blocked ($k_n = 0$ for all $n \neq$ RAD). Thus, the excited state will relax only by means of an emission characteristic of the polypyridyl chromophore. k_{RAD} is expected to increase as the excited state energy increases while the value of the non-radiative decay (k_{NRD}) should decrease. Given this relationship in the decay kinetics, the radiative rate constant can be an important factor in determining the lifetimes of high energy photosensitizers. Additionally, the formalisms used in discussions are based on Einsteinian rate constants for atomic fluorescence spectra and not that of phosphorescent donor-acceptor complexes. Other factors should be considered such as difference in spin multiplicity and molecular distortions in

vibrational modes that are coupled to electronic transitions (evident from vibronic side band features in emission spectra). Density functional theory (DFT) has indicated that the excited state distortions for these systems are due to electronic mixing of Ru-bpy ^{3}MLCT excited state with the bpy ligand π and π^* orbitals, or alternatively from the electronic mixing between the ^{3}MLCT and $\pi\pi^*$ excited states. The spectroscopic and computational results suggests that a "pure" diabatic ^{3}MLCT excited state is not greatly distorted and that its emission has weak vibronic contributions in the region of bpy-ligand vibrational modes in addition to a very small radiative rate constant. Furthermore, there is no evidence that a "pure" ^{3}MLCT emission has ever been observed. Additionally, some of the observed spectroscopic properties will depend on the differences in excited state molecular geometries based on the reorganizational energy for crossing between the ^{3}MLCT and ^{3}MC states.

AUTOBIOGRAPHICAL STATEMENT

Ryan A. Thomas

Professional Preparation

Graduate -Wayne State University, Detroit, MI

-Ph.D. in Analytical Chemistry (emphasis on inorganic spectroscopy), 2015

Undergraduate -University of Michigan, Dearborn, MI

-B.S. Chemistry, 2010

Presentations

"77K Emission Studies and Computational Modeling of Triplet Metal-to-Ligand-Charge-Transfer Excited States" *Poster* -The 43rd ACS Central Regional Meeting, Dearborn, MI, June **2012**

"Photophysics of a Series of Ruthenium-Sulfur Macrocycles towards Water Oxidation" *Poster*- Ohio Inorganic Weekend, Detroit, MI, October **2012**

"Investigations of Ruthenium-Sulfur Macrocyclic Complexes: Possible Higher Energy Excited State 77K Emission" *Poster*- 20th International Symposium on the Photophysics and Photochemistry of Coordination Compounds, Traverse City, MI, July **2013**

"Spectroscopic and DFT Comparisons of Ruthenium-Sulfur Macrocycles" *Talk* - 246th ACS National Meeting & Exposition, Indianapolis, IN, September **2013**

Publications

Lord, R., Allard, M., **Thomas, R.**, Odongo, O., Schlegel, H., Chen, Y., Endicott, J. "*Computational Modeling of the Triplet Metal-to-Ligand Charge-Transfer Excited State Structures of Mono-Bipyridine - Ruthenium(II) Complexes and Comparisons to their 77 K Emission Band Shapes", Inorganic Chemistry*, **2013**, 52 (3), 1185.

Mazumder, S., **Thomas, R.**, Lord, R., Schlegel, H., Endicott, J. *"A DFT and Spectroscopic study of Intramolecular Quenching of Metal to Ligand Charge Transfer Excited states in some mono-Bipyridine Ruthenium(II) Complexes", Canadian Journal of Chemistry*, ***2014*** in press *(Invited Manuscript for A.B.P. Lever Edition).*

Thomas, R., Tsai, C., Mazumder, S. Lord, R., Schlegel, H., Chen, Y. and Endicott, J.*,"Energy Dependence of Metal-to-Ligand Charge Transfer Excited State Radiative Lifetimes for Ruthenium(II) - Bipyridine Chromophores: Effects of ππ*(bipyridine)Mixing", Journal of Physical Chemistry B*, **2015, DOI:** 10.1021/jp510949x.

Sharma, R.,**Thomas, R., A**.,Tu, Y. J.,Mazumder, S., Alnaed, M., Schlegel, H.,Endicott, J. ; Kodanko, J., in progress.